Landscape Position Impacts on the Water Balance in the Chihuahuan Desert: Insights from Cosmic-Ray Neutron Sensing at Upland Watershed and Downstream Playa Sites

by

Ruby Yaritza Hurtado

A Thesis Presented in Partial Fulfillment
of the Requirements for the Degree
Master of Science

Approved June 2024 by the
Graduate Supervisory Committee:

Enrique R. Vivoni, Chair
Trenton E. Franz
Craig Hargrove
Jiwei Li

ARIZONA STATE UNIVERSITY

August 2024

ABSTRACT

In the semiarid, water-limited deserts of the Southwest United States, soil moisture is a crucial factor influencing atmospheric, hydrologic, and ecological processes. These dynamics are driven by infrequent yet significant precipitation events that redistribute moisture and establish hydrologic connectivity across the landscape. The Chihuahuan Desert, particularly within its endorheic basins, exemplifies these large-scale interactions where a complex balance of hydrological fluxes is maintained within a closed system. These basins receive most of their precipitation in upland regions, from which surface runoff can lead to downstream connectivity. This connectivity is influenced by the local water balance, including interactions among precipitation, leakage, and evapotranspiration, which are essential for understanding soil moisture variability. Additionally, soil moisture is affected by soil profile characteristics, vegetation, and atmospheric conditions. Field-scale methods like Cosmic-Ray Neutron Sensing (CRNS) are more appropriate than point-scale in situ sensors for quantifying hydrologic connectivity between upland and downstream regions, as CRNS reliably captures soil moisture temporal dynamics over several hectares. This study examines these dynamics within the endorheic Jornada Basin of the Chihuahuan Desert, focusing on two contrasting sites: an Upland Watershed (UW) on a piedmont slope and a Downstream Playa (DP) in a valley bottom. Using CRNS and complementary water balance instrumentation, I compared soil moisture dynamics at these two sites from July 2022 to February 2024. My analysis centered on a significant precipitation event early in the study period that generated surface runoff and playa inundation, followed by an

extended dry period. Although temporal variations in leakage and evapotranspiration are similar at both sites, their rates differ significantly. The UW experienced a higher drying rate, necessitating greater plant water uptake from the subsurface. This led to an increased upward leakage to sustain vegetation, resulting in a leakage value of -205 mm, indicating vertical plant water uptake. Conversely, at the DP, the inundation event was formed by 228 mm of surface runoff, supplementing water inputs from precipitation. This additional water reduced the need for upward soil water movement to sustain plant water uptake, resulting in a leakage value of -97 mm. These findings enhance our understanding of hydrologic fluxes within endorheic basins and improve the applicability of hydrological models and the downscaling of remotely sensed soil moisture products.

ACKNOWLEDGMENTS

First and foremost, I would like to express my deepest gratitude to my advisor, Dr. Enrique Vivoni. His guidance throughout my research has been invaluable, and his unwavering commitment to hard work, discipline, and excellence has been a constant source of inspiration for me. The exponential growth in my research skills and work ethic is a direct reflection of his dedication and leadership. I am deeply grateful for his mentorship and plan to carry the invaluable skills and lessons he has imparted into my own career. Thank you to my committee member, Dr. Trenton Franz, for generously giving his precious time to help me navigate the complex problems of my research. His constant fountain of knowledge and support has been indispensable throughout this work. I would like to extend my heartfelt thanks to Dr. Craig Hardgrove and Dr. Jiwei Li for their constant feedback and support throughout my research. Their insights and fresh perspectives have continually helped me refine and expand my work, fostering my growth and encouraging me to see my research from new angles. I would also like to extend my deepest gratitude to the many professors and friends who made this work possible in countless ways: Agustin Robles, Adam Schreiner-McGraw, Eli Perez, Charles Kimsal, Jose Becerra, Luisa Orci, Sara Alonso, Mary Ferguson, Zhaocheng Wang, and many others who have supported me over these past two years. Your guidance, encouragement, and camaraderie have been invaluable. I am also immensely grateful to all the incredible researchers and staff at the Jornada Basin LTER, especially John Anderson, for their unwavering support and collaboration. This work was made possible with funding from the Jornada Basin LTER in the form of a graduate summer fellowship, for which I am profoundly thankful.

TABLE OF CONTENTS

Page

LIST OF TABLES

Table Page

LIST OF FIGURES

Figure Page

Figure Page

Figure Page

CHAPTER 1

INTRODUCTION

Stretching across Arizona, New Mexico, and southwest Texas, the Chihuahuan Desert is a landscape defined by extremes. In this semiarid region, every drop of rain helps alleviate the palpable water scarcity, affecting vital processes such as infiltration (*I*), evapotranspiration (*ET*), and surface runoff (*Q*). These processes encompass the dryland water balance, which hinges on the dynamic interplay between soil moisture and the surrounding vegetation. Although precipitation events are the primary water source, understanding hydrological connectivity solely based on precipitation can be too limiting due to differences in rainfall frequency, timing and magnitude, landscape position and feedback loops between vegetation and hydrologic processes (Williams and Bonnell, 1988). Soil water availability offers a better lens for understanding hydrological connectivity, considering its various states within a landscape, such as shallow soil water, deep soil water, and groundwater (Ehleringer and Dawson, 1992, as cited in Snyder, Mitchell, and Herrick, 2006). This perspective is further enhanced by examining how soil water availability influences the rate of infiltration, which can vary significantly with soil type and vegetation cover (Snyder and Williams, 2000). These variations impact how quickly water transitions from surface runoff to deeper groundwater supplies (Schwinning and Ehleringer, 2001). Therefore, maintaining connectivity between these hydrological processes is essential for predicting and managing water sustainability in response to both natural and human-induced changes.

In endorheic basins, measuring soil moisture dynamics is complicated by the lack of natural outlets such as rivers or oceans. Within these basins, soil water storage is affected by the fluxes of precipitation (*P*), evaporation, and groundwater exchange (Wang, 2018). In semiarid endorheic basins, deep soil recharge occurs infrequently in most years, but certain rainfall patterns can facilitate this process (Phillips, 1994; Small, 2005). Even yet, recharge rates can exhibit significant spatial variability due to differences in local geomorphology (Scanlon et al., 1999). Specific features like playas, fissures, channels, or burrow pits can enhance recharge rates; however, these features constitute only a small fraction of the surface area of semiarid endorheic basins (Scanlon and Goldsmith, 1997).

As a result, the majority of precipitation is lost through evaporation from the soil and transpiration by plants (Scanlon and Goldsmith, 1997). Approximately 95% of precipitation is lost via evapotranspiration (*ET*); however, whether it occurs through soil evaporation or plant transpiration has significant implications for ecosystem processes (Dugas et al., 1996). Evaporation primarily affects soil processes, such as soil respiration and water recharge, while transpiration drives plant productivity (Huxman et al., 2005). These processes occur within the Jornada Basin, a semiarid endorheic basin located on the northern edge of the Chihuahuan Desert and bounded by the San Andres Mountains (Nichols et al., 2011). The basin geological features are composed of mountain blocks, piedmont slopes, and the basin floor, thus ensuring the hydrological connectivity across the region is maintained within these features (Gile et al., 1981; Wondzel et al., 1977).

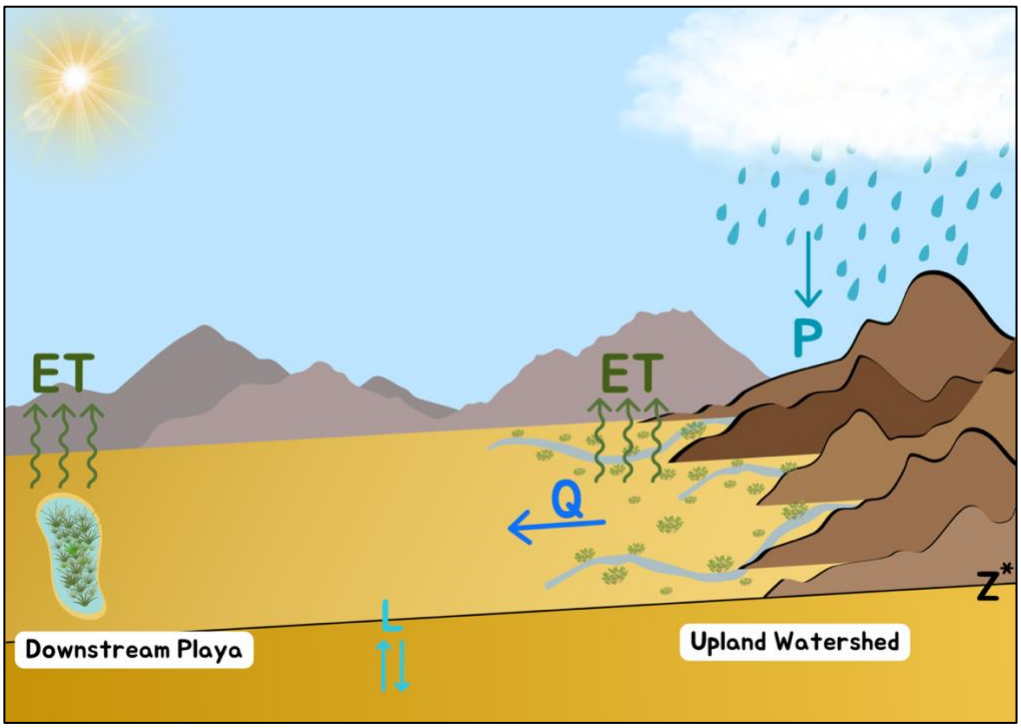

Figure 1. Illustration of the water cycle within an internally draining (endorheic) basin.

In the piedmont slope region of the Jornada Basin, upland watersheds act as first-order water recipients, generating runoff only when precipitation exceeds the soil infiltration capacity, as shown in Figure 1 through the transport of surface runoff (Q) (Horton, 1933; Schreiner-McGraw, 2017). During significant rainfall events, water and sediments from the mountain block flow through channels to the basin floor, accumulating in recharge playas (Rosen, 1994). These low points collect not only runoff and sediment but also soil organic carbon and nutrients, crucial for enhancing playa plant productivity (McKenna and Sala, 2018). The movement of water and sediment from higher elevations to these topographic depressions plays a vital role in the hydrologic and sediment transport dynamics of the area, supporting both water storage and soil fertility (Rosen 1994; Cohen, 2016; McKenna and Sala, 2016).

In their investigations of dryland ecosystems, Schreiner-McGraw et al. (2016), Perez-Ruiz et al. (2022), and Keller et al. (2023) explored soil moisture dynamics, water availability, and hydrologic connectivity in the Chihuahuan Desert, specifically in the Upland Watershed. Schreiner-McGraw et al. (2016) validated the Cosmic-Ray Neutron Sensing (CRNS) method for soil moisture estimation, demonstrating its utility in closing the water balance. Their results linked soil moisture dynamics to hydrological processes and plant water uptake, finding that drier conditions promoted deeper soil moisture usage at the Upland Watershed. Perez-Ruiz et al. (2022) identified that seasonal rainfall and subsurface water storage during wet periods sustained net primary productivity during dry periods, causing the shrubland to act as an annual net carbon sink. Most recently, Keller et al. (2023) examined the thresholds and controls of hillslope-to-channel connectivity, highlighting that intense short-term rainfall primarily drove runoff at the Upland Watershed. Collectively, these studies underscore the critical roles of soil moisture measurement, water storage, and hydrologic connectivity in understanding and managing dryland ecosystem productivity and water dynamics.

Previous studies focused on the biogeochemical functions linking upland ecosystems and recharge playas, particularly in terms of Aboveground Net Primary Production (ANPP) (McKenna and Sala, 2016; McKenna and Sala, 2018). The findings indicate that during dry years with less than 200 mm of rainfall, playa ecosystems were as productive as upland ecosystems (McKenna and Sala, 2018). In moderately wet years, with precipitation between 200 and 300 mm, playa ecosystems showed higher productivity than surrounding upland ecosystems (McKenna and Sala, 2018). However, this elevated productivity at playa ecosystems significantly decreases during wetter years

with over 300 mm of rain, aligning once again with the productivity levels of upland ecosystems (McKenna and Sala, 2018). A key finding of this study is how McKenna and Sala (2018) characterized recharge playas. They described these areas as 'active controlled points that support high process rates under the right conditions,' a concept introduced by Bernhardt et al. (2017). The term refers to regions where statistically higher rates or distinct dominant processes are observed. This finding is significant for the framework of this study as it highlights the potential for recharge plays to function hydrologically differently from their surrounding upland regions in endorheic basins.

Kimsal (2023) investigated the hydrologic dynamics of eighteen playas in the Jornada Basin, emphasizing the connection between the surrounding catchments and the playas during precipitation events. This study, covering June 2016 to October 2022, used water level observations and gauge-corrected radar precipitation estimates to analyze playa inundation drivers and variability. Inundation events were all linked to precipitation, with 70% occurring during the North American monsoon season. Inundation thresholds for precipitation depth and intensity varied, influenced by upland catchment area and the spatial rainfall variability within the catchments. The study revealed that larger catchment areas were associated with lower inundation likelihood and higher rainfall thresholds. This research highlights the intricate relationship between rainfall and playa hydrology, demonstrating how landscape conditions affect water connectivity and ecosystem processes in the surrounding areas.

Furthermore, additional studies have demonstrated that topography significantly influences soil moisture dynamics in semiarid regions extending beyond the variations between upland ecosystems and recharge playas. Gutiérrez-Jurado et al. (2013)

demonstrated that variations in topography can create distinct microclimates thereby affecting the water and energy balances of landscapes. In their study, a semiarid watershed featured sharply contrasting vegetation on opposing hillslopes. Vegetation differences influenced the water balance and runoff production within the hillslopes (Gutiérrez-Jurado et al., 2013). Notably, these variations were found to impact not only runoff but also evapotranspiration and soil moisture residence times. This evidence of the intricate interplay between topography, plant species and hydrological processes is particularly relevant to this study, as it supports the expectation that upland ecosystems will behave differently from recharge plays due to their environmental surroundings.

Research Motivation

This study aims to examine the soil moisture dynamics within an Upland Watershed (UW) and a Downstream Playa (DP), within the context of the hydrologic connectivity in a semiarid endorheic basin. The primary method for capturing soil moisture dynamics at the two sites is the Cosmic-Ray Neutron Sensing (CRNS) method, which measures soil moisture by detecting galactically sourced neutrons that enter the Earth's atmosphere and are moderated by hydrogen (Zreda, 2008). This technique provides soil moisture measurements over an aerial footprint of about 250 meters (Desilets, 2010). The effectiveness of evaluating soil moisture dynamics over a larger aerial footprint, rather than at point scale as with in-situ sensors, is underscored by previous studies (Franz et al., 2012; McJannet et al., 2014; Dong et al., 2014). The study conducted by Schreiner-McGraw et al. (2016) is pivotal, demonstrating the effectiveness of the CRNS method for capturing spatial soil moisture dynamics within a

heterogeneous, semiarid watershed. A good agreement was found with a distributed sensor network at the Upland Watershed, as evidenced by a root mean square error (RMSE) of 0.013 m^3/m^3. Similarly, comparisons between CRNS and watershed water balance methods revealed a low RMSE of 0.082 m^3/m^3, underscoring the reliability of CRNS for quantifying soil moisture dynamics (Schreiner-McGraw et al., 2016).

However, Schreiner-McGraw et al. (2016) also identified limitations with the CRNS method at the Upland Watershed, particularly its inability to detect leakage or percolation beneath the time-variable sensor measurement depth due to rapid bypassing of the measurement depth during wetting events. To address this, Schreiner-McGraw et al. (2016) recommended implementing deeper soil moisture sensor profiles to detect such leakage events—a recommendation that this study has considered by installing deeper profiles at the Upland Watershed (UW) and Downstream Playa (DP). Furthermore, the findings from Schreiner-McGraw et al. (2016) align with observations that during wetter-than-average summer periods, wet surface soils promote leakage into the deeper vadose zone, reducing water availability for runoff (Q) and evapotranspiration (ET) losses. This aspect of water balance is crucial, as more recent studies, such as those by Perez-Ruiz et al. (2022), have noted how seasonal water retention from a wet season carries over, providing water for vegetation in the subsurface for use during subsequent seasons, significantly influencing plant growth in the semiarid landscape.

Building on these insights, this study aims to explore soil moisture dynamics at two distinct sites over a 19-month period, from July 1, 2022, to January 31, 2024. A significant precipitation event from August 18 to 20, 2022, at the start of the study period, provides an opportunity to examine McKenna and Sala (2018) concept of recharge playas

as 'active control points'. This event will allow us to further investigate these dynamics through the lens of soil moisture and its impact on the water balance. By employing field-scale methods, this study seeks to better understand how water is distributed and utilized across seasons in the Upland Watershed and Downstream Playa. The following are the study objectives:

Objective 1: Calibrate and validate the CRNS sites at the Upland Watershed and Downstream Playa using gravimetric sampling along with vertical and horizontal assessments of the sensor networks.

Objective 2: Characterize and analyze the changes in soil moisture at the Upland Watershed and Downstream Playa following precipitation events and compare these behaviors to understand their implications.

Objective 3: Quantify the impact of soil moisture dynamics on water balance partitioning at both sites, comparing leakage estimates derived from the water balance formula and a theoretical leakage model.

To achieve the research objectives, a comprehensive data collection and analysis strategy was implemented at both study sites. For **objective 1**, 108 gravimetric samples were collected at specified intervals and depths, ensuring thorough spatial representation of soil moisture around the Cosmic-Ray Neutron Sensors (CRNS). These gravimetric soil moisture data were used to calibrate the CRNS measurements. To validate the CRNS soil

moisture measurements, a vertical and horizontal weighting method was applied to Time Domain Reflectometry (TDR) soil sensor networks, enabling a direct comparison between the CRNS measurements and the weighted sensor network. For **objective 2**, precipitation events and the resulting soil moisture pulses were categorized to quantify relevant time frames, allowing for meaningful comparisons between the Upland Watershed and Downstream Playa. Finally, for **objective 3**, water balance variables were quantified using two observational formulas: the water balance formula and the CRNS flux formula. These were used to characterize the response to significant precipitation events and the entire study period. Additionally, a theoretical formula was employed to quantify the leakage observed during significant precipitation events.

CHAPTER 2

METHODS

Regional Setting

The Chihuahuan Desert stretches from southern New Mexico and southwest Texas and into the Central Mexican Highlands. On its northern edge, just east of Las Cruces, New Mexico, sits the Jornada Basin. The regional context of this basin hosts the Jornada Basin Long Term Ecological Research (LTER), a program which is rooted in the historical context of the 19th century Jornada Basin. During this time, the Jornada Basin was undergoing intense levels of cattle grazing, which led to a significant ecological transition from perennial grasslands to desert woody shrubs (Gibbens et al., 2003). To better understand the desertification occurring in the Jornada Basin, two research programs were established, forming what is now known as the Jornada Basin LTER program, covering a total area of 1042 square kilometers. The first component of the Jornada Basin LTER is the US Department of Agriculture's Jornada Experimental Range (JER). This section begins at the northwestern part of the San Andres Mountain block and spans southwest to the basin floor as shown in Figure 2. The second component is the Chihuahuan Desert Rangeland Research Center (CDRRC), owned and operated by New Mexico State University. The CDRRC shares the southwestern boundary starting at the basin floor and extends beyond Mount Summerford reaching all the way to the Rio Grande, as illustrated in Figure 2. The early establishment of these two sites has fostered a rich repository of ecological and hydrological data in past and present centuries.

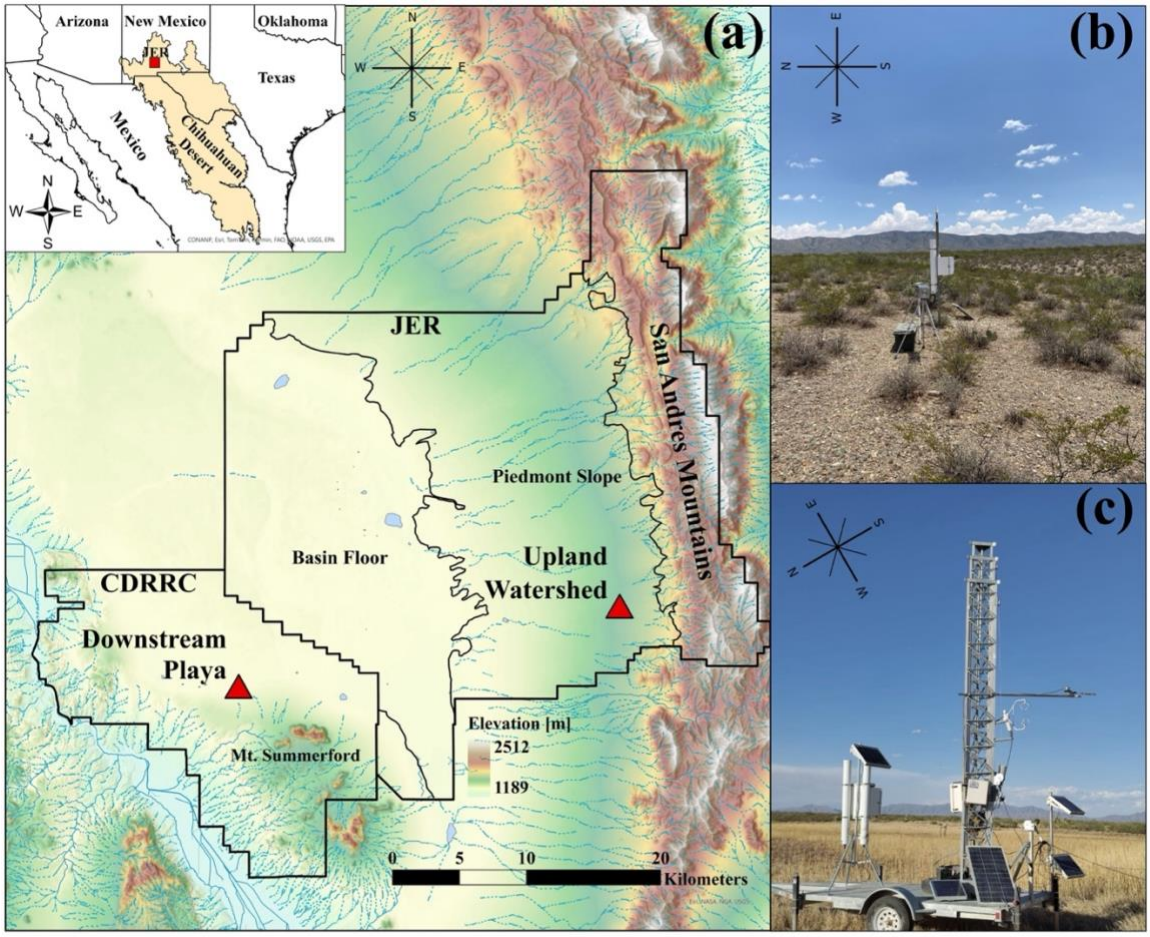

Figure 2. (a) Study site located in the Jornada Long Term Experimental Range (JER) in the Chihuahuan Desert of New Mexico, USA. (b) CRNS at the Upland Watershed (UW). (c) CRNS (left) and eddy covariance tower (right) at Downstream Playa (DP).

Geological Setting

The genesis of the Jornada Basin began in the Precambrian eon with the development of the crystalline basement (Seager 1981; Mack et al. 1998a, 1998b). In areas such as the base of the San Andres mountains, remnants of these metamorphic rocks are exposed (Seager 1981; Mack et al. 1998a, 1998b). Following the Paleozoic eon, the formation of the Ancestral Rocky Mountains began across the Jornada Basin region consisting of sedimentary mountains and thick alluvial deposited basins (Kottlowski et al.

1956; Kottlowski 1965; Mack and Sugio 1991; Mack et al. 1995). Yet the most significant orographic effects culminate during the latest Cretaceous and early Paleogene period, known as the Laramide Orogeny (Cather, 2004). The most significant byproduct of the Laramide Orogeny in the Jornada Basin is the Rio Grande uplift (Seager and Mack 1986; Seager et al. 1986, 1997; Seager and Mayer 1988). During this epoch (Oligocene), volcanic activity related to the Rio Grande rift brought regional uplift and basin development, creating the remnants of the modern Doña Ana Mountains (Seager et al. 1976; Seager 1981; McIntosh et al.1991). Further orographic development was followed in the Miocene epoch with the increase of regional block lifts and basin subsidence that delineate the modern San Andres Mountains (Seager, 1975; Seager et al., 1984; Ingersoll, 2001). This period also brought the Ancestral Rio Grande which contributed to further incision of the basin floor, resulting in fluvial deposits in the basin. The silhouette of the Ancestral Rio Grande can faintly be seen in Figure 2 near the ephemeral playas (light blue polygons). The combination of ancient rifting, basin floor incision, and ongoing tectonic activity has shaped the Jornada Basin, which is characterized by mountain blocks, piedmont slopes, the basin floor, and the Rio Grande Valley (Gile et al., 1981).

Upland Watershed Study Site

At the foot of the San Andres Mountain block, the piedmont slope serves as a transitional area that transports water and alluvial deposits from the base of the mountain to the basin floor through ephemeral drainage channels. The Upland Watershed (UW) is located on the southeastern part of this slope. As a first-order watershed, this site is the initial recipient of storms, yet loses the majority of its water through transmission losses

and evapotranspiration (Schreiner-McGraw and Vivoni, 2018). Typical annual precipitation at the Upland Watershed is an estimated 250 mm per year, with 60 to 80% of the precipitation arriving during July through September during the North American Monsoon (NAM) (Peters et al., 2010). Soil characteristics at the Upland Watershed are dominated by the alluvial deposits from the nearby San Andres Mountains and are formally known as the Middle Tank Gravelly Soils, characterized as a sandy loam with high gravel content (Veatch, 1918; Gile et al., 1981). The sandy loam with high gravel content found at the watershed is further defined by its course rock fragments, with only the top 25 to 80 centimeters containing the gravelly sandy loam type and beneath that a thick caliche layer (Gile et al., 1981). In areas with regular erosion, such as the ephemeral channels, the thick caliche layer is fully exposed with a mixture of alluvial deposits and igneous rocks (Gile et al., 1981). Due to the coarse and indurated caliche layer at the Upland Watershed, the common vegetation types are creosote bush (*Larrea tridentata*) and honey mesquite (*Prosopis glandulosa*) due to their robust rooting systems allowing them to navigate through the dry gravelly soil (Gibbens and Lenz, 2001).

The Upland Watershed is equipped with an extensive array of instrumentation that has been capturing hydrological data for over a decade (Templeton et al., 2014). This robust instrumentation includes an eddy covariance (EC) tower for measuring evapotranspiration (ET), rain gauges (P), soil sensor transects (θ_{SN}), outlet flume (Q), and a Cosmic-Ray Neutron Sensor (θ_{CRNS}).

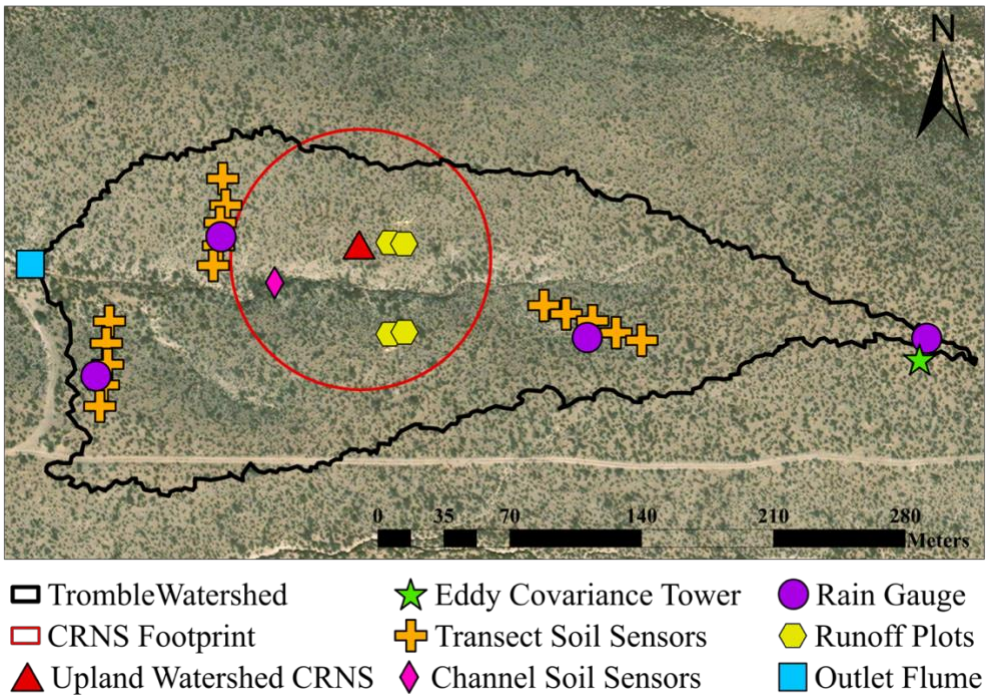

Figure 3. Sensor locations at the Upland Watershed, including the watershed boundary, Eddy Covariance Tower, and a CRNS (Cosmic-Ray Neutron Sensor) footprint.

Table 1 provides an overview of the sensors deployed in the Upland Watershed. A Hydroinnova CRS-1000/B, CRNS sensor operates with a 1-hour time resolution and an accuracy of ± 0.01 m^3/m^3 and a sensor network is comprised of Stevens Hydraprobe II soil moisture sensors which offer a 30-minute resolution with an accuracy range of ± 0.01 to 0.03 m^3/m^3. Rainfall is measured using Texas Electronics TR-525I rain gauges, which have a 1-second resolution and ± 1% accuracy. Four rain gauges are weighted using the Thiessen polygon method to produce a spatially weighted rainfall amount throughout the watershed. Water level fluctuations are captured by the Campbell Scientific CS451 pressure transducer in the outlet flume, with a 1-minute resolution and ± 0.1% accuracy. Additionally, EC measurements are conducted using Campbell Scientific CSAT3 Sonic Anemometer and LI-COR LI-7500 IRGA Open Path CO_2 and H_2O gas analyzer, with a 30-minute resolution and accuracy ranges of 0.015 to 0.04 mm/30-min.

Sensor Type	Model	Time Resolution	Sensor Accuracy	No.	WB
Upstream Watershed					
CRNS Sensor	Hydroinnova CRS-1000/B	1-hr	± 0.01 [m^3/m^3]	1	θ_{CRNS}
Soil Moisture Sensors	Stevens Hydraprobe II	30-min	± 0.01 to 0.03 [m^3/m^3]	50	θ_{SN}
Rain Gauges	Texas Elect. TR-525I	1-sec	± 1%	3	P
Water Level Sensor	Campbell Sci. CS451 Pressure Trans. in Flume	1-min	± 0.1%	4	Q
Eddy Covariance	Campbell Sci. CSAT3 LiCOR LI-7500 IRGA	30-min	0.015 to 0.04 mm/30-min	1	ET
Downstream Playa					
CRNS Sensor	Hydroinnova CRS-1000/B	1-hr	± 0.01 [m^3/m^3]	1	θ_{CRNS}
Soil Moisture Sensors	Stevens Hydraprobe II	30-min	± 0.01 to 0.03 [m^3/m^3]	18	θ_{SN}
Rain Gauges	Texas Elect. TR-525I	1-sec	± 1%	1	P
Water Level Sensor	HOBO U20L Water Level Sensor	1-min	± 0.1%	1	Q
Eddy Covariance	Campbell Sci. CSAT3 LiCOR LI-7500 IRGA	30-min	0.015 to 0.04 mm/30-min	1	ET

Table 1. Description of water balance (*WB*) instrumentation at the upland watershed and downstream playa sites, including model types, time resolution, sensor accuracy, quantity (No.), and *WB* component measured.

Downstream Playa Study Site

Due to its closed and internally draining nature, the Jornada Basin maintains its hydrological connectivity as water moves from the upland areas across the basin floor to the lowest endpoint in playas (Dorsaz et al., 2013). In this study, the Downstream Playa (DP) is characterized as an ephemeral recharge playa that periodically floods due to large precipitation events and surface runoff from upland areas (Smith, 2003). Although the Downstream Playa is not directly connected to the Upland Watershed, it is linked to the nearby Mount Summerford (Snyder et al., 2006). Moreover, comparisons between the two study sites are applicable to playas located downstream of the Upland Watershed. A defining feature of recharge playas is their function as depositories that collect fine-grained sediment during surface runoff events (Snyder et al., 2006). Consequently, most playas in the Jornada Basin have an abundance of clay-like soils in contrast to their surrounding areas (McKenna and Sala, 2018). At the Downstream Playa, extensive soil surveys have classified the soil as ranging from a fine sandy loam to a silty clay loam, yet the key finding is that the soil at the Downstream Playa exhibits a high porosity paired with low infiltration rates (Bulloch and Neher, 1980; Bergametti and Gillette, 2010). Due to consistent fine sediment deposition at these topographic low points and the absence of caliche-like layers, such as those found at the Upland Watershed, playas serve as repositories of soil organic carbon and nutrients that accumulate at rates five times greater than upland areas (Scanlon et al., 2012; Peters and Gibbens, 2006). The common vegetation type found at the Downstream Playa are a variety of perennial grasses such as *Panicum obtusum* (Vine Mesquite Grass), *Cirsium ochrocentrum* (Yellow Spine Thistle), and *Asclepias suberticillata* (Horsetail Milkweed) (Huenneke et al., 2002).

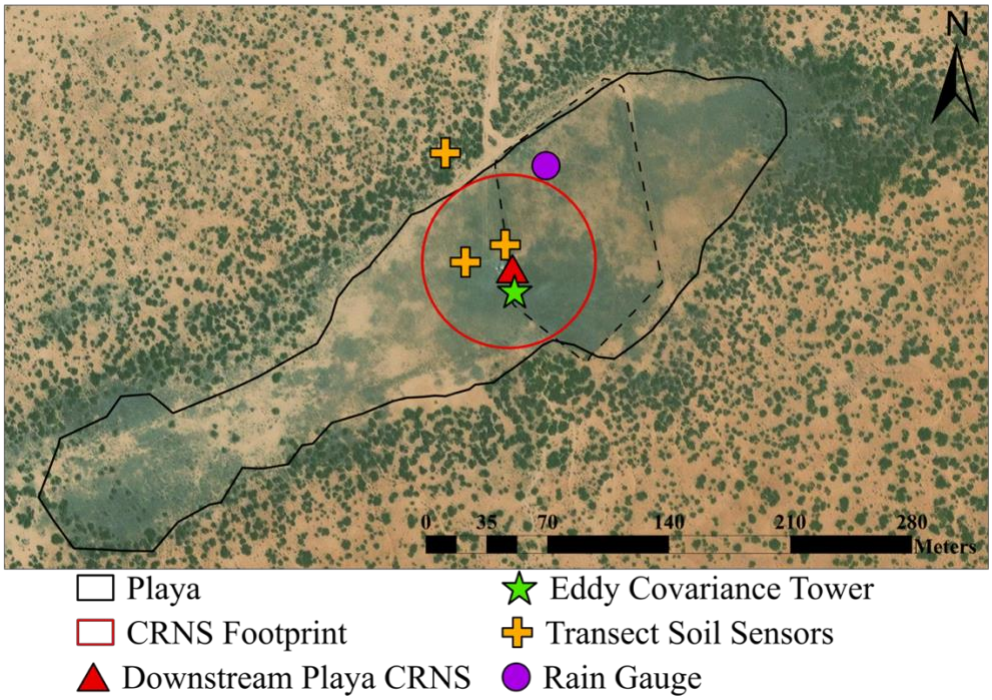

Figure 4. Sensor locations at the Downstream Playa including the playa boundary, location of CRNS and the CRNS footprint (red triangle and red circle), EC tower (green star), soil transects (orange cross), and rain gauge (purple circle).

Field instrumentation was deployed at the Downstream Playa in June 2022 for this study, as shown in Figure 4. The field installation includes an eddy covariance tower for measuring evapotranspiration (*ET*), as well as the deployment of a Cosmic-Ray Neutron Sensor (θ_{CRNS}) and a weighted soil moisture sensor network (θ_{SN}). A Hydroinnova CRS-1000/B CRNS Sensor, similar to the one used at the Upland Watershed, is utilized at the Downstream Playa with a 1-hour time resolution and accuracy ± 0.01 [m^3/m^3]. Additionally, the weighted sensor network (θ_{SN}) at the Downstream Playa utilizes Stevens Hydraprobe II soil moisture sensors, offering a 30-minute resolution and an accuracy ranging from ± 0.01 to 0.03 [m^3/m^3]. Rainfall data is collected using one Texas Electronics TR-525I rain gauge, with a 1-second resolution and a ± 1% accuracy. Water levels within the playa are monitored using HOBO U20L

water level data logger with a 1-minute resolution and ± 0.1% accuracy. These water level measurements contribute to the Jornada Long-Term Ecological Research (LTER) project's Net Primary Production (NPP) data collection efforts, as noted by Anderson (2023). EC measurements at the Downstream Playa are performed using Campbell Scientific CSAT3 Sonic Anemometer and LI-COR LI-75000 IRGA CO_2 and H_2O gas analyzer, similar to those used in the Upstream Watershed. The eddy-covariance tower operates with a 30-minute resolution and have an accuracy range of 0.015 to 0.04 mm/30 minutes, allowing for precise measurements of evapotranspiration (*ET*) rates.

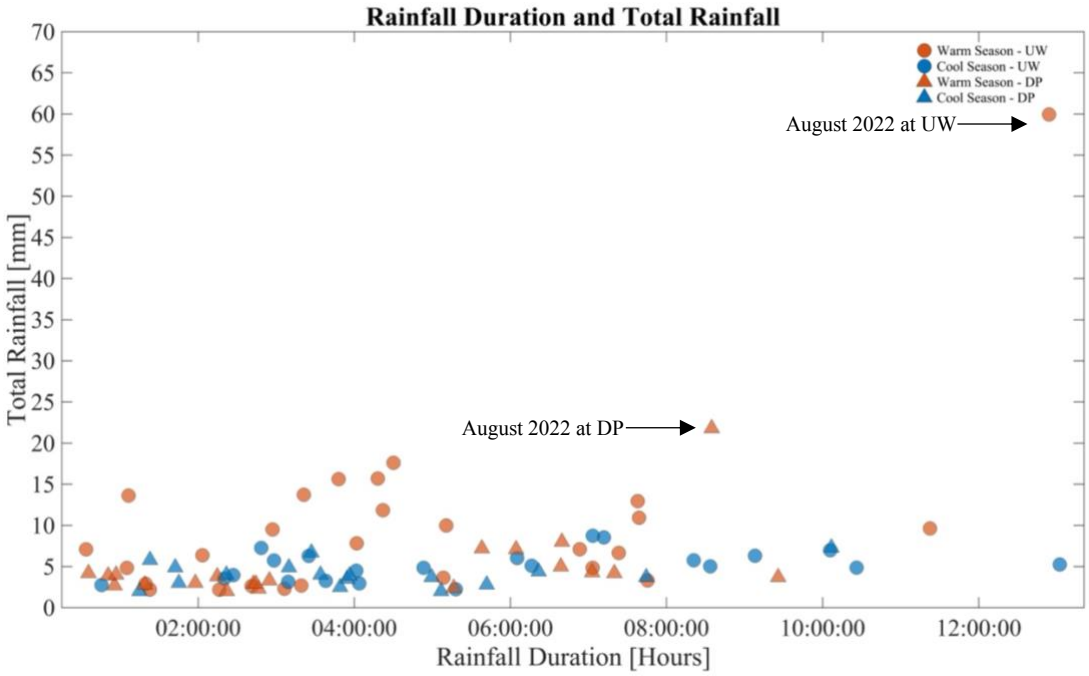

Figure 5. Precipitation events larger than 2 mm of rain at the Upland Watershed and Downstream Playa during the 19-month study period divided between two seasons.

Precipitation Analysis

A notable precipitation event in the Jornada Basin occurred from August 19 to 20, 2022, leading to the flooding of the Downstream Playa, an infrequent occurrence. To provide context on this event size, all rainfall events larger than 2 mm were analyzed from the 19-month study period, spanning from July 1, 2022, to January 31, 2024. Two distinct seasons were also defined: (a) the warm season from April to September and (b) the cool season from October to March. Figure 5 shows that during the study period, the Upland Watershed experienced a total of 49 significant precipitation events exceeding 2 mm, while the Downstream Playa recorded 38 such events. These findings highlight the variability in rainfall patterns between the two locations over the 19-month duration.

The most significant precipitation event occurred from August 19, 2022, at 11:00 AM to August 20, 2022, at 12:00 AM in the Upland Watershed, lasting 13 hours and delivering 59.94 mm of rain. At the Downstream Playa, this event took place on August 19, 2022, from 2:30 PM to 10:30 PM, lasting 8 hours and delivering 21.8 mm of rain. The significance of this event lies in its impact on the Downstream Playa, causing an infrequent flooding event that allowed for the analysis of soil moisture dynamics under inundation conditions. Analyzing this significant precipitation event provided valuable insights into the behavior of soil moisture in response to heavy rainfall at both sites. By examining soil moisture dynamics during and after the event, the soil response to the influx of water can be tracked. This included changes in soil moisture content, the rate of infiltration, and the subsequent redistribution of water within the soil profile.

In addition to soil moisture dynamics, this significant precipitation event had implications for the overall water balance of the two study sites. By analyzing the event

impact on both the Upland Watershed and the Downstream Playa, it was possible to assess the flow of water through the system, including the rates of evapotranspiration, surface runoff, and leakage. A comparison of the Upland Watershed and Downstream Playa during this event can be used to highlight the differences in their hydrological responses. As described subsequently, the Upland Watershed, with its steeper slopes and coarser soils, experienced a more intense runoff response to the large 60 mm precipitation event, leading to discharge. In contrast, the Downstream Playa, with its flatter terrain and more muted 22 mm precipitation event, received surface runoff arising from the surrounding area which led to a short period of inundation.

Lastly, the significant precipitation event of August 19-20, 2022, provided a case study for understanding soil moisture dynamics and hydrological responses to extreme rainfall. The flooding of the Downstream Playa, although rare, offered valuable data for analyzing water movement and retention in the soil system. Kimsal (2023) analyzed the hydrological thresholds of 30 instrumented playas in the Jornada LTER, focusing on precipitation thresholds, inundation characteristics, and precipitation intensities. In this study, the Downstream Playa is classified as an "Uplifted Plain Playa" due to its proximity to a fault running through the CDRRC, resulting in an uplifted alluvial plain (Kimsal, 2023). Kimsal identifies four main types of inundation classifications. The Downstream Playa was categorized under response type C: rapid deep events. This classification indicates that inundation events occur infrequently, with a short duration, but maintain high water levels during these events. For such type C inundation events to occur at the Downstream Playa, a precipitation threshold of 17.5 mm must be met (Kimsal, 2023).

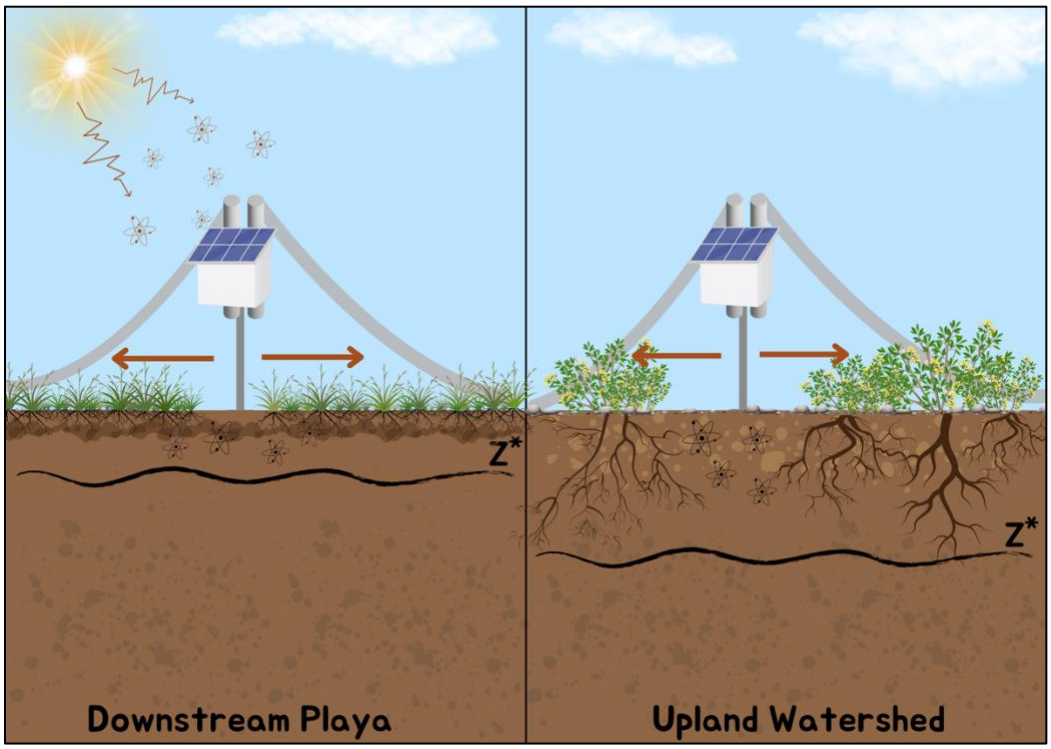

Figure 6. CRNS method at the Upland Watershed and Downstream Playa.

Cosmic-Ray Neutron Sensing Method

Cosmic-Ray Neutron Sensing (CRNS) is a method that converts galactically sourced fast neutrons that are continuously entering the Earth's atmosphere into soil moisture values (Desilets and Zreda, 2008). This technique is based neutron particle physics. In 1966, physicists Hendrick and Edge demonstrated that the intensity of fast neutrons correlates with the water content in the ground (Hendrick and Edge, 1966). This discovery paved the way for the modern CRNS method, which relies on the ability of hydrogen found in the surface and the atmosphere to moderate fast neutrons (Zreda et al., 2008; Zreda et al., 2012; Desilets and Zreda, 2013). A typical Cosmic Ray Neutron Sensor features two key components as illustrated in Figure 6: a fast neutron detector and a thermal neutron detector, represented by two gray cylinders. In this study, the deployed

model at both research sites is CRS-1000/B, manufactured by Hydroinnova in Albuquerque, New Mexico. These detectors are strategically positioned above the surface to capture neutron mixing in the atmosphere, which spans several meters, thus creating a spatial footprint. This footprint is sensitive to variations in atmospheric conditions, including pressure and water vapor, enabling it to dynamically respond to the surrounding environment as detailed in seminal studies (Zreda et al., 2008; Desilets et al., 2010; Zreda et al., 2012; Rosolem et al., 2013; Franz et al., 2013).

Calibration of CRNS for Soil Moisture Estimates

The Cosmic Ray Neutron Sensor not only records the counts of raw moderated and non-moderated neutrons but also measures key integral atmospheric variables: air temperature (T_a), barometric pressure (p), and relative humidity (r). These variables are essential for converting the raw moderated neutron counts into corrected neutron counts (Ncorr) using the formula detailed in Equation 1.

$$N_{corr} = N f_w f_p f_i f_s \quad (1)$$

This equation introduces f_w, a correction factor for atmospheric water vapor under reference conditions. Here, ρ_v represents the absolute humidity (g/cm^3), averaged over the duration of raw neutron measurements and derived from relative humidity and air temperature:

$$f_w = 1 + 0.0054\rho_v \quad (2)$$

The primary goal of this correction is to differentiate hydrogen sources affecting soil moisture measurements. Since the CRNS technique quantifies soil moisture by detecting

neutrons moderated by hydrogen atoms, atmospheric hydrogen present in water vapor must be distinguished to ensure precise soil moisture readings.

Additionally, Equation 1 includes a barometric pressure correction factor (f_p), outlined in Equation 3. In which, p is the measured barometric pressure, and p_o is a reference pressure specific to each site in g/cm^2 and L is the mass attenuation length for high energy neutrons (L = 130 g/cm2) applicable across North America (Desilets et al., 2006). This exponential model accounts for the exponential decrease in air density with altitude, adjusting the neutron counts to a standard reference level.

$$f_p = \exp\left(\frac{p - p_o}{L}\right) \tag{3}$$

The next subset of corrections in Equation 1, is a neutron intensity correction (f_i) for the time-varying neutron intensity (I_m) (Zreda et al., 2012). This factor adjusts for variations in the cosmic ray flux, which can affect the base level of neutrons detected by the sensor. Changes in solar activity and other cosmic phenomena can influence the intensity of cosmic rays entering the atmosphere, which in turn affects neutron production, thus the correction is represented as:

$$f_i = \frac{I_0}{I_m} \tag{4}$$

where I_0 is the reference neutron intensity obtained from the Neutron Monitor Database from the Jungfraujoch NM64 station in Bern, Switzerland (McJannet and Desilets, 2023). I_m is the measured neutron intensity during the study period for each given site, which in return this ration ensures that the neutron counts are normalized to standard cosmic ray conditions. Finally, the scaling factor adjusts for geographical and environmental conditions such as latitude and altitude. High latitudes and sea levels can influence

neutron moderated due to varying magnetic and atmospheric pressures, which affect cosmic-ray interactions. This constant factor is detailed in Table 2 for the Upland Watershed and Downstream Playa.

Desilets et al. (2010) established an empirical relationship linking the corrected neutron counts (N_{corr}) with the soil water content (θ_p in g/g) through the use of Monte Carlo simulations. This relationship was later expanded by Franz et al. (2013) to incorporate additional water-related parameters within the soil matrix. These parameters include lattice water (θ_{LW} in g/g) and the water equivalent of soil organic carbon (θ_{SOCeq} in g/g), as illustrated in Equation 5. This extension provides a more comprehensive model for understanding moisture dynamics in soil systems by integrating various forms of water content.

$$(\theta_p + \theta_{LW} + \theta_{SOCeq}) = \frac{a_0}{\left(\frac{N_{corr}}{N_0}\right) - a_1} - a_2 \quad (5)$$

Franz et al. (2012) describe N_0 as the counting rate over dry soil, measured under the same reference conditions used during gravimetric soil collection. Furthermore, the constants a_0, a_1, and a_2 originate from Desilets et al. (2010) as part of the initial theoretical model, with values of 0.0808, 0.372, and 0.115 respectively. Moreover, the values for lattice water (θ_{LW}) and water equivalent of soil organic carbon (θ_{SOCeq}) are obtained from soil chemistry samples collected on June 29th, 2023, for both the Upland Watershed and June 28th, 2023, for the Downstream Playa. The soil chemistry samples for both sites, were collected over 18 evenly spaced locations following the same schematic layout utilized in the gravimetric soil sample collections. The soil chemistry samples were collected from 5cm to 30cm at each location, then placed in a cumulative

container for each site. Thus, creating a cumulative soil chemistry sample for the Upland Watershed and Downstream Playa. These results from this collection suggest that both lattice water and soil organic carbon levels are substantially higher at the Downstream Playa compared to the Upland Watershed, as detailed in Table 2.

In 2012, Franz et al. pioneered a field validation method for Cosmic Ray Neutron Sensors at the Santa Rita Experimental Range, a semiarid ecosystem in southern Arizona. This method was designed to refine the area-average soil moisture estimations within the CRNS's spatial footprint, thereby enhancing the original formula proposed by Desilets et al. (2010), now encapsulated in Equation 5. The method uses gravimetric soil measurements to convert into volumetric soil moisture values (θ_p) through Equation 6:

$$\theta_{CRNS} = \frac{\rho_{bd}}{\rho_w}\theta_p \tag{6}$$

in which ρ_{bd} represents the dry soil bulk density (g/cm³), and ρ_w, the density of water, is standardized at 1 g/cm³. This conversion is essential for accurately translating the gravimetric soil samples into the volumetric soil moisture values required by Equation 5. To estimate the variable N_0 for Equation 5, soil samples were collected from both the Upland Watershed and the Downstream Playa. The sampling protocol involved collecting samples at six angular intervals of 60 degrees and at distances of 25, 75, and 200 meters from the sensor. At each location, samples were taken from six different depths—5, 10, 15, 20, 25, and 30 centimeters—yielding a total of 108 gravimetric soil samples per calibration at each site. These samples were then oven-dried for 48 hours at 105°C and subsequently analyzed to determine their volumetric water content (m³/m³), following the protocols outlined in the "Soil Science Society of America: Methods of Soil Analysis,

Site Characteristics	*Upland Watershed*	*Downstream Playa*
Corrected Neutron Count [N_{corr}]	1352	885
Neutron Count [N_0]	1511	1367
Lattice Water [g/g]	0.03	0.060
Soil Organic Carbon [g/g]	0.01	0.004
Bulk Density [g/cm^3]	1.30	1.23
Porosity [m^3/m^3]	0.51	0.53
Gravimetric Water Content [g/g]	0.05	0.14
Pressure Correction Factor [-]	1.06	1.05
Elevation [m]	1458	1325
Atmospheric Water Vapor [g/m^3]	1.03	1.03
Scaling Factor	3.13	3.19

Table 2. Site characteristics used as inputs for CRNS calibration procedures at the Upland Watershed and Downstream Playa.

Part 4: Physical Methods" (Dane and Topp, 2002, p. 422). The gravimetric soil samples and soil chemistry results for both the Upland Watershed and Downstream Playa can also be found in Appendix D.

On July 11th, 2022, an initial gravimetric soil collection was conducted at the Upland Watershed, lasting a total of 8 hours. During this period, the average corrected neutron counting rate (N_{corr}) was recorded at 1,352 counts per hour, while the counting rate over dry soil (N_0) used in Equation 5 was 1,511 counts per hour. The results from the gravimetric soil samples, which provided data on bulk density, porosity, and volumetric water content (θp), are detailed in Table 2. Additionally, a subsequent gravimetric soil sample collection occurred on February 10th, 2013, as part of the Schreiner-McGraw study conducted in 2016 at the same watershed. The bulk density values reported in

Table 2 for the Upland Watershed originate from the gravimetric soil sample collection on February 10th, 2013. The other necessary variables, such as porosity and volumetric water content (θ_p), were derived from the soil samples collected on July 11th, 2022.

At the Downstream Playa, gravimetric samples were collected on July 1st, 2022, and December 5th, 2022. The need for the second gravimetric soil sample collection on December 5th, 2022, is due to a wetting front in the beginning of the study period caused by significant precipitation events affecting the gravimetric soil samples collected on July 1st, 2022. Thus, the values reported for the Downstream Playa in Table 2 reflect the December 5th, 2022, gravimetric soil samples, which lasted a total of 7 hours. The corrected neutron count (N_{corr}) rate during this gravimetric soil sample collected yielded a value of 885, and the neutron count rate over dry soil (N_0) is equal to 1367 counts per hour shown in Table 2.

The Cosmic-Ray Neutron Sensing method typically employs a single gravimetric soil sample collection to derive the site-specific calibration factor N_0. This approach is considered sufficient due to the integrated nature of CRNS, which provides an averaged soil moisture measurement over a large footprint. The effectiveness of this single sampling strategy is supported by studies showing strong correlations between neutron counts and gravimetric soil moisture within the sensor footprint. For example, Vieira Lima et al. (2023) validated CRNS using multiple gravimetric soil samples at different agricultural sites, demonstrating the method's reliability with just a single sample collection under certain conditions. Similarly, Schrön et al. (2023) emphasized the importance of sampling soil bulk density and moisture content at least once for calibration but did not find significant improvements with multiple samplings. Rivera

Villarreyes et al. (2013) evaluated different calibration approaches in cropped fields and highlighted that a single set of parameters could accurately estimate soil moisture, though adjustments might be needed for seasonal vegetation changes. Xie and Rosolem (2017) found that while additional calibration days can reduce uncertainty, the improvements are marginal beyond two days, making single-day calibration generally sufficient. Schrön et al. (2017) also demonstrated the robustness of the CRNS signal with single, well-placed gravimetric sampling, especially when using a physically based weighting approach for sample locations. Iwema et al. (2015) noted that while more than one calibration day can be beneficial, the gains in accuracy diminish after six days, reinforcing the practicality of single sampling for most applications. This differs from other fields where at least two sampling activities are needed to establish a reliable relationship due to higher variability in conditions. The inherent averaging characteristic of CRNS over large areas reduces the need for multiple samplings, making a single gravimetric sampling a standard approach.

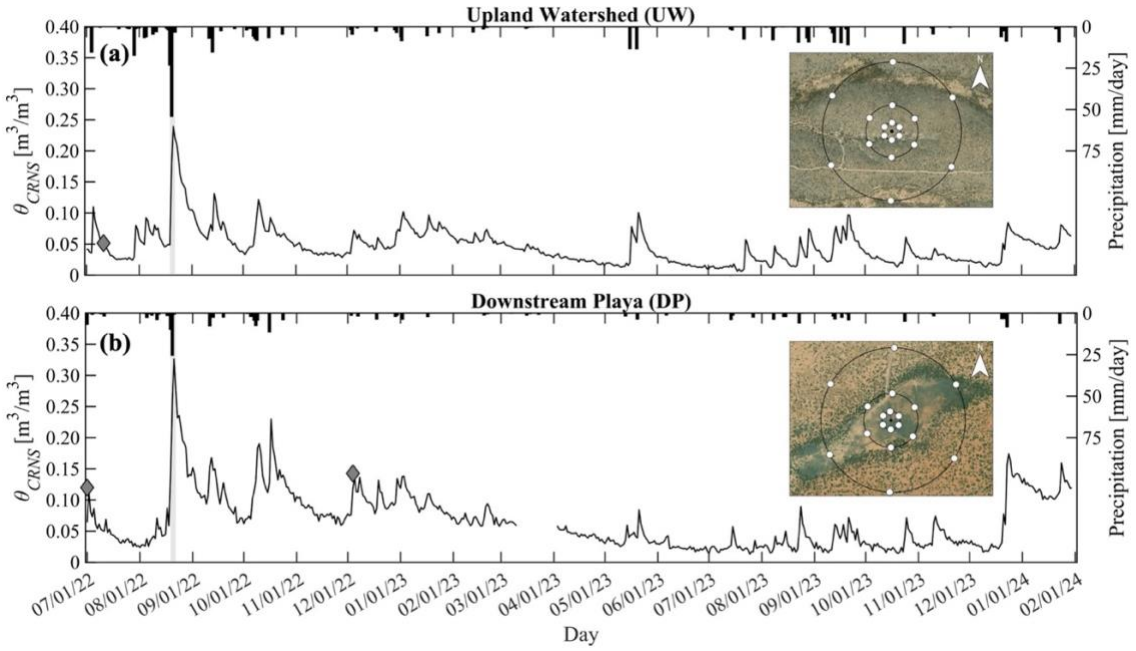

Figure 7. (a) UW soil moisture (θ_{CRNS}, black line), with gravimetric sampling on July 11, 2022 (gray diamond). (b) DP soil moisture (θ_{CRNS}, black line) with gravimetric sampling on July 1 and December 5, 2022 (gray diamond). The study period is from July 1, 2022, to January 31, 2024. Daily precipitation at each site is shown for reference. Insets shows the radial sampling pattern at 25, 75, and 200 m intervals (white circles).

Figure 7 illustrates the calibration at the Upland Watershed and Downstream Playa, including the spatial distribution of the gravimetric soil collections, shown in the insets. The gray diamonds represent the gravimetric soil collections, which have been converted to volumetric water content values. At the Upland Watershed, the gray diamond symbol aligns with the soil moisture recession limb, indicating the decline in soil moisture that was captured from the gravimetric soil collections. Conversely, at the Downstream Playa, the gray diamond symbol accurately captures the peaks in soil moisture values on July 1st, 2022, and December 5th, 2022.

Validation of CRNS Soil Moisture Estimates

After calibrating the Cosmic Ray Neutron Sensor (CRNS), validating its soil moisture estimates with in-situ soil sensor measurements is essential. These in-situ sensors, organized into a "Sensor Network" for each site, are strategically placed and weighted both vertically and horizontally to optimize the comparisons with CRNS soil moisture values. This network configuration ensures spatial coverage and accurate cross-referencing of soil moisture data across different soil depths and horizontal planes.

The CRNS sensor's vertically averaged sampling depth (Z^*), as shown in Equation 7, represents the CRNS penetration depth. This depth is a critical parameter, calculated based on the soil water content (θ_{CRNS}), lattice water (θ_{LW}), and the water equivalent of soil organic carbon (θ_{SOCeq}) (Franz et al., 2012):

$$Z^* = \frac{b_0}{\frac{\rho_{bd}}{\rho_W}\left(\theta_{LW} + \theta_{SOCeq}\right) + \theta_{CRNS} + b_1} \quad (7)$$

In this equation, ρ_{bd} is the dry bulk density of the soil, and ρ_w is the density of water. The parameters b_0 and b_1 are empirical constants set at 5.8 and 0.0829, respectively. These parameters were determined through extensive field calibration and testing to accurately reflect the relationship between neutron counts and soil moisture content (Franz et al., 2012). The inclusion of θ_{LW} and θ_{SOCeq} in the equation highlights the importance of accounting for the bound water in soil minerals and the water content associated with soil organic matter. These factors are critical in heterogeneous soils where organic content and mineral composition can significantly influence the CRNS soil moisture readings (Franz et al., 2012).

To accurately represent the soil moisture profile measured by the Cosmic Ray Neutron Sensor, a vertical weighting depth is applied to the sensor network. This vertical weighting accounts for the averaging depth produced by the CRNS, ensuring that the sensor network's measurements align with the CRNS's penetration depth (Z^*). The vertical weighting of the sensor network is calculated using the following formula (Franz et al., 2012):

$$wt(z) = \left(\frac{2}{z^*}\right)\left(1 - \frac{z}{z^*}\right) \tag{8}$$

In this equation, $wt(Z)$ represents the weight at depth Z to be applied to the sensor network. This weight function is designed to ensure that the soil moisture measurements from different depths are integrated in a manner that reflects the CRNS's penetration depth (Z^*). The constant factor $2/Z^*$ is defined to normalize the profile so that the total integrated weight equals unity, ensuring that the sum of the weighted measurements provides an accurate representation of the average soil moisture derived from the sensor network. The parameter Z^* is the penetration depth of the CRNS, which is a function of the soil's water content and other factors such as lattice water (θ_{LW}) and soil organic carbon (θ_{SOCeq}), as described earlier. This penetration depth indicates the effective range within which the CRNS is sensitive to changes in soil moisture. By applying the vertical weighting function, each sensor in the network contributes to the overall soil moisture estimate proportionally to its depth and the CRNS's sensitivity at that depth. The vertical weighting depth is crucial for aligning the sensor network's soil moisture estimates with the CRNS measurements, particularly in heterogeneous soil environments where moisture content can vary significantly with depth. By weighting the sensor readings

according to their depth, the integrated soil moisture profile becomes more representative of the actual conditions measured by the CRNS, enhancing the accuracy and reliability of the soil moisture data.

A horizontal weighting function is applied to account for the high sensitivity of the neutron signal to the first few meters around the CRNS. This function gives greater weight to soil profiles closer to the CRNS, reflecting the exponential nature of the CRNS footprint, where the nearest region contains the most significant portion of soil moisture values (Khöli et al., 2015; Schrön et al., 2017). The horizontal weighting formula is defined as follows:

$$W_r(h,\theta,p,H_{veg}) = \begin{cases} (F_1 e^{-F_{2r*}} + F_3 e^{-F_{4r*}})(1 - e^{-F_{0r*}}), & 0m < r \leq 1m \\ F_1 e^{-F_{2r*}} + F_3 e^{-F_{4r*}}, & 1m < r \leq 50m \\ F_5 e^{-F_{6r*}} + F_7 e^{-F_{8r*}}, & 50m < r < 600m \end{cases} \quad (9)$$

W_r is the weighted horizontal value to be given to each soil profile, r is the radial distance from the CRNS in meters, h is the air humidity in g/m³, θ is the volumetric soil moisture, p is the air pressure, and H_{veg} is the vegetation height. The formula consists of different exponential terms with coefficients (F_1, F_2, F_3, F_4, F_5, F_6, F_7, F_8) that adjust the rate at which the weight decreases with distance from the CRNS (*r*). These coefficients are determined empirically based on field data and specific site conditions from the gravimetric soil sample collection days for the Upland Watershed and Downstream Playa. The horizontal weighting function ensures that soil profiles closer to the CRNS receive higher weights, reflecting the higher sensitivity of the neutron signal in these regions. This weighting is crucial for accurately estimating soil moisture over the footprint of the CRNS, which extends several hundred meters but has an exponentially decreasing sensitivity with distance. By incorporating variables such as air humidity (*h*),

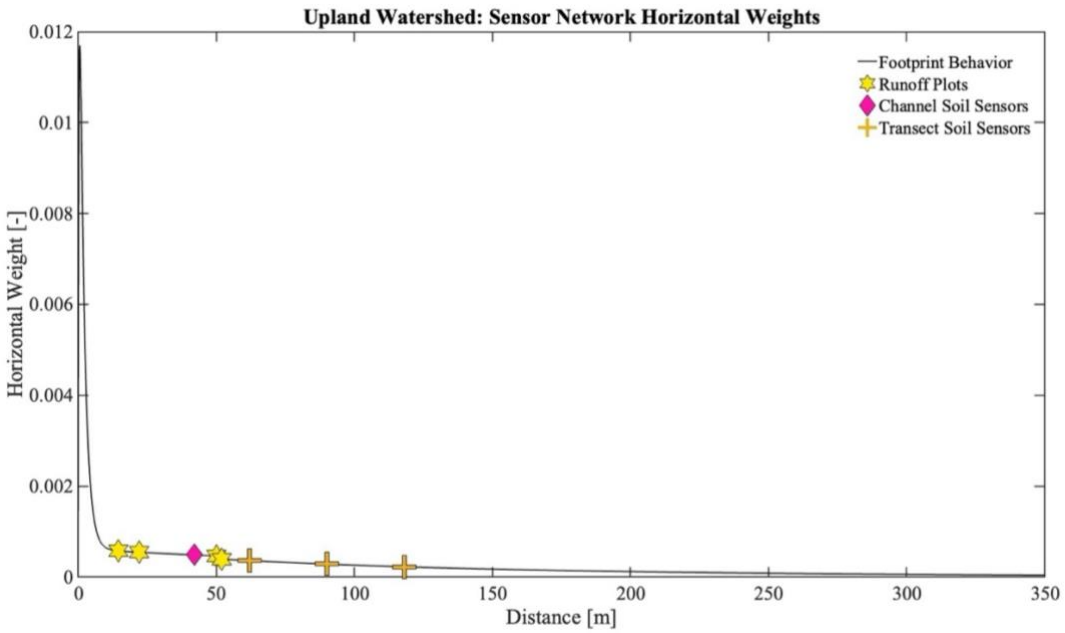

Figure 8. Horizontal weighting scheme at the Upland Watershed with each sensor network location indicated.

volumetric soil moisture (θ), air pressure (p), and vegetation height (H_{veg}), the function accounts for environmental factors that influence the neutron signal and, consequently, the soil moisture estimates.

Figure 8 presents the results of the horizontal weighting function at the Upland Watershed, illustrating how proximity influences the significance of soil profile locations for the gravimetric soil collection date of July 11th, 2022. On this date, the volumetric soil moisture measurement was recorded at 0.0515 m^3/m^3. The horizontal weighting function is crucial because it accounts for the high sensitivity of the neutron signal to the first few meters around the CRNS.

In this figure, the soil profiles within the runoff plots at the Upland Watershed are assigned the highest weighting due to their close proximity to the CRNS. This means that these nearest regions have the most substantial influence on the soil moisture values

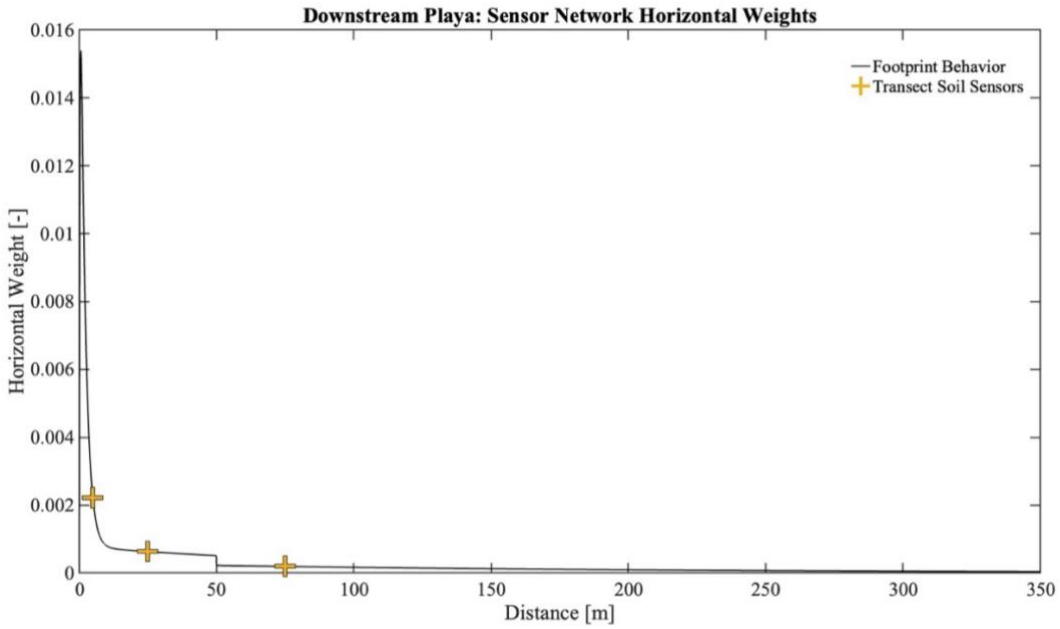

Figure 9. Horizontal weighting scheme of transect soil sensors at the Downstream Playa.

captured by the CRNS. As the distance from the CRNS increases, the weighting function exponentially decreases, reducing the impact of more distant measurements. This reflects the physical principle that the neutron sensor's sensitivity diminishes with distance, ensuring that the soil moisture estimates are more representative of the conditions near the sensor.

In contrast, Figure 9 shows the horizontal weighting function applied at the Downstream Playa for the gravimetric soil sample collection date of December 5th, 2022. Here, the soil profiles are positioned significantly closer to the CRNS, with one location being less than 5 meters away. This closer positioning results in higher weights assigned to these profiles, indicating that the soil moisture measurements are more aligned with the CRNS signal.

The differences between the two sites highlight the importance of sensor placement and environmental conditions in interpreting CRNS data. At the Upland

Watershed, the more dispersed positioning of the sensors requires a careful application of the horizontal weighting function to accurately reflect the soil moisture profile. Meanwhile, the Downstream Playa benefits from a more concentrated arrangement of sensors, enhancing the alignment and reliability of the CRNS measurements.

Overall, these figures underscore the significance of the horizontal weighting function in optimizing soil moisture estimates by emphasizing measurements closer to the CRNS and appropriately reducing the influence of those further away. This approach ensures that the resulting data accurately represents the soil moisture conditions within the CRNS footprint.

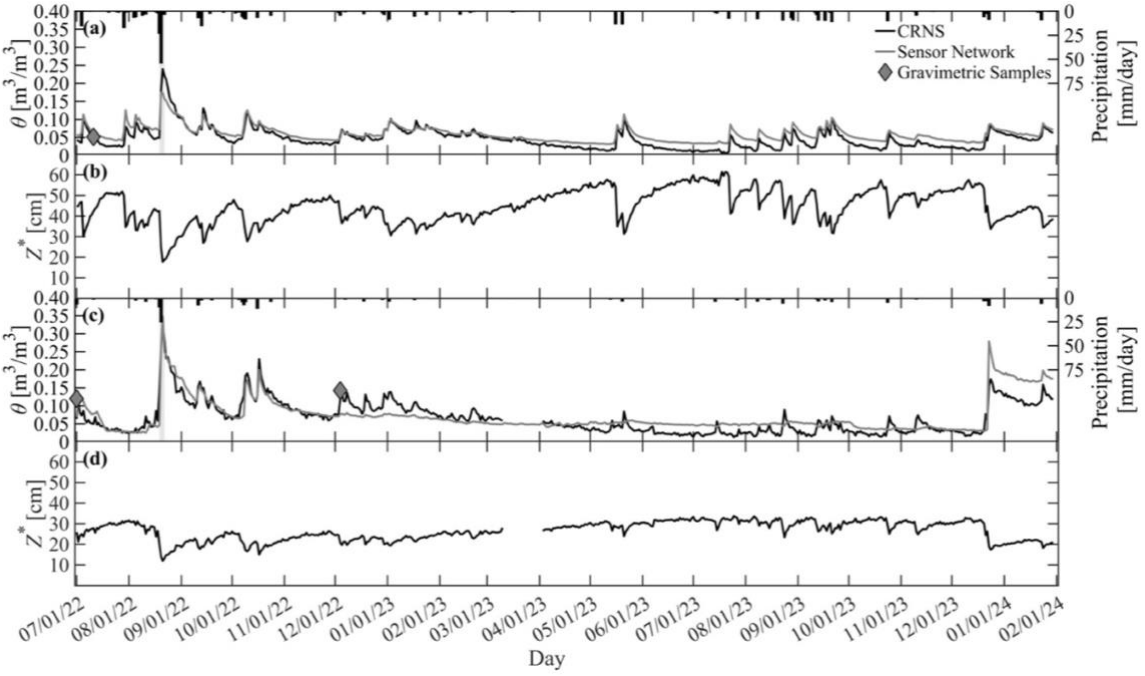

Figure 10. Comparison of daily, spatially averaged θ_{SN} and θ_{CRNS} at (a) UW and (c) DP. Daily sampling depth, Z*, for the CRNS sensor is shown in (b) UW and (d) DP. Daily precipitation at each site is shown for reference.

Figure 10 shows the comparison of CRNS soil moisture measurements θ_{CRNS} (black line) and the weighted sensor network θ_{SN} (gray line) at the Upland Watershed and Downstream Playa. These results accounts for the spatial footprint of the soil moisture measurement from the CRNS and the vertically and horizontally weighted measurements from the sensor network. Additionally, the sampling depth (Z^*) from CRNS is shown during the study period, from July 1st, 2022, to January 31st, 2024. It can be appreciated that the watershed has a deeper sampling depth, averaging from 30 cm to 60 cm, while the Downstream Playa exhibits a shallower depth, from 10 cm to 30 cm. This variation is primarily due to the fact that penetration depth is influenced by the presence of lattice water, and the soil moisture tends to be wetter at the playa compared to the watershed.

To further evaluate the correlation between θ_{CRNS} and θ_{SN} at both the Upland Watershed and Downstream Playa, a linear regression was conducted at both sites. This analysis compared θ_{CRNS} and θ_{SN} across two temporal scales: daily and hourly. The results are presented in Figure 11 and Table 3. At both sites, the daily temporal scale proves to be the most effective for comparing θ_{CRNS} and θ_{SN}. At this scale, the relationship between θ_{CRNS} and θ_{SN} at the Upland Watershed yields an R^2 value of 0.90. However, at the more granular hourly scale, the R^2 value decreases to 0.83. This indicates a statistically significant comparison between the two-soil moisture estimates across these scales. Unlike the Upland Watershed, which is heavily instrumented with multiple soil profile transects, the Downstream Playa features only three such profiles.

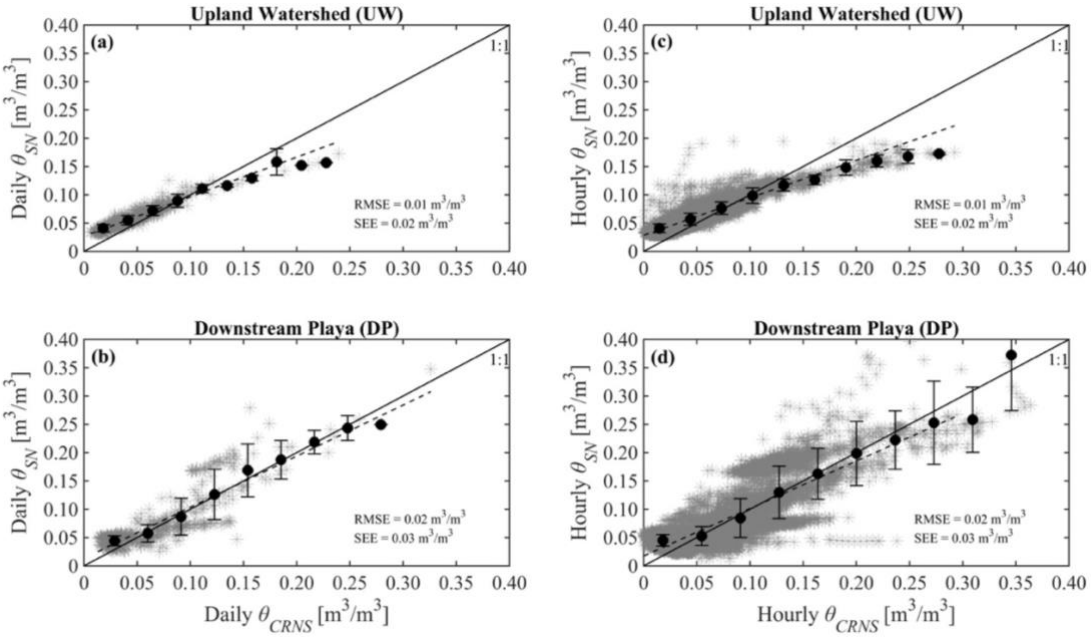

Figure 11. Comparison of spatially averaged soil moisture from the weighted sensor network, θ_{SN}, and CRNS, θ_{CRNS}, at daily (a, b) and hourly (c, d) resolution (gray asterisks) at UW (top row) and DP (bottom row). 1:1 line are shown for comparison. Black circles and error bars depict bin averages and ±1 bin standard deviations. Dashed black lines represent linear regressions: (a) y = 0.70x + 0.03, (b) y = 0.90x + 0.01, (c) y = 0.66x + 0.03, and (d) y = 0.83x + 0.02.

Statistical Metric	*Upland Watershed*	*Downstream Playa*
Daily Comparisons		
R^2 [-]	0.900	0.731
Root Mean Squared Error [RMSE, m^3/m^3]	0.010	0.025
Correlation Coefficient [CC, -]	0.950	0.855
Bias [B, m^3/m^3]	0.012	0.007
Standard Error of Estimates [SEE, m^3/m^3]	0.007	0.025
Hourly Comparisons		
R^2 [-]	0.833	0.660
Root Mean Squared Error [RMSE, m^3/m^3]	0.009	0.030
Correlation Coefficient [CC, -]	0.912	0.820
Bias [B, m^3/m^3]	0.012	0.007
Standard Error of Estimates [SEE, m^3/m^3]	0.010	0.030

Table 3. Statistical comparisons of CRNS and sensor networks at daily and hourly time scales for upland watershed and downstream playa.

This difference in instrumentation is evident in the results of the statistical comparison conducted across the two temporal scales. At the daily scale, the comparison of θ_{CRNS} and θ_{SN} at the playa yields an R^2 value of 0.73. Although this is still statistically significant, it is not as robust as the R^2 value of 0.90 observed at the watershed. Similarly, the robustness decreases at the hourly scale at the playa, just as it does at the watershed, where the R^2 value drops to 0.66. The overall trend observed at both the Upland Watershed and Downstream Playa indicates that the θ_{CRNS} shows both overestimations and underestimations of soil moisture wetness compared to θ_{SN}, with the discrepancies being more pronounced at the Upland Watershed. These contrasting behaviors highlight the influence of local conditions and sensor distribution on the accuracy of moisture measurements.

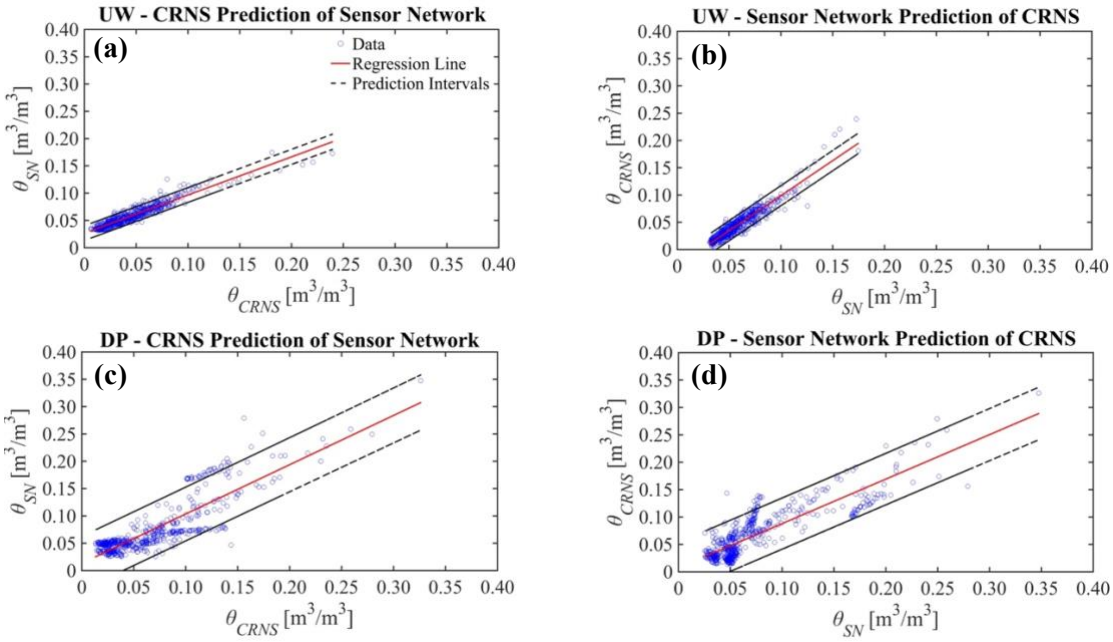

Figure 12. Prediction and confidence intervals of daily soil moisture at the Upland Watershed and Downstream Playa. Daily soil moisture values (blue dots), regression line (red line), prediction intervals (black dashed lines).

To better understand the uncertainty bounds between the CRNS and Sensor Network daily soil moisture values, a comparative analysis of the uncertainty bounds was analyzed conducted at the Upland Watershed and Downstream Playa. Figure 12 is comprised of four subplots, each illustrating prediction intervals for different scenarios. At the Upland Watershed, CRNS soil moisture values predict Sensor Network soil moisture values with a strong linear correlation and narrow prediction intervals, indicating high predictive accuracy and low uncertainty. Conversely, the prediction of CRNS soil moisture values using Sensor Network soil moisture values at the Upland Watershed also demonstrates minimal uncertainty, as evidenced by the close fit of the regression line to the data points and tight prediction intervals. In contrast, the Downstream Playa site exhibits slightly wider prediction intervals when CRNS soil moisture values predict Sensor Network values, indicating marginally increased prediction uncertainty. The reverse scenario, where Sensor Network soil moisture values predict CRNS soil moisture values, shows a reasonable fit but with noticeably wider prediction intervals, reflecting greater variability and higher uncertainty. Overall, while both predictive methods are effective, the degree of uncertainty varies between sites, with the Upland Watershed demonstrating more robust predictive capabilities compared to the Downstream Playa.

	Upland Watershed		*Downstream Playa*	
Confidence Intervals	**CRNS**	**Sensor Network**	**CRNS**	**Sensor Network**
Mean [m^3/m^3]	0.045	0.06	0.065	0.075
25^{th} Percentile [m^3/m^3]	0.04	0.06	0.06	0.07
95^{th} Percentile [m^3/m^3]	0.05	0.06	0.07	0.08

Table 4. Statistical confidence intervals from the daily CRNS and Sensor Network soil moisture values at the mean, lower bound and upper bound intervals.

To enhance the understanding of the predictive relationship between CRNS and sensor network soil moisture values, an analysis of the confidence intervals for the Upland Watershed and Downstream Playa sites is essential. Table 4 provides statistical confidence intervals for daily CRNS and Sensor Network soil moisture values at the mean, 25th percentile, and 95th percentile. This analysis aims to pair these confidence intervals with the prediction intervals illustrated in Figure 12 to offer deeper insights into the two systems' accuracy and variability.

At the Upland Watershed, the narrow range between the 25th and 95th percentiles indicate a relatively low variability in CRNS soil moisture values at this site. This low variability aligns with the tight prediction intervals observed in Figure 12, reinforcing the high predictive accuracy and low uncertainty of CRNS data for the sensor network values. Moreover, the Sensor Network at the Upland Watershed, yields identical values across the percentiles suggest extremely low variability in sensor network measurements. This consistency contributes to the narrow prediction intervals seen in the regression analysis, further supporting the robust predictive relationship at the Upland Watershed. However, at the Downstream Playa, the broader range between the 25th and 95th percentiles compared to the Upland Watershed indicates higher variability in CRNS measurements at the Downstream Playa. This increased variability is reflected in the wider prediction intervals shown in Figure 12, suggesting a higher degree of uncertainty in predicting Sensor Network values using CRNS soil moisture values at this site. Whereas, the Sensor Network at the Downstream Playa has a wider percentile range compared to the Upland Watershed also points to increased variability in the Sensor

Network measurements. This variability contributes to the wider prediction intervals observed in the regression analysis, indicating a less reliable predictive relationship at the Downstream Playa. The confidence intervals for soil moisture values at the Upland Watershed exhibit minimal variability for both CRNS and Sensor Network soil moisture values, which corresponds to the tight prediction intervals and high predictive accuracy shown in Figure 12. In contrast, the Downstream Playa demonstrates higher variability in soil moisture measurements for both CRNS and Sensor Network soil moisture values, resulting in wider prediction intervals and greater predictive uncertainty. This analysis underscores the more robust and reliable predictive relationship between CRNS and Sensor Network soil moisture values at the Upland Watershed compared to the Downstream Playa.

Sensor Network Placement at the Upland Watershed and Downstream Playa

Figure 13 provides a detailed analysis of soil moisture values across the various soil transects that compose the Sensor Network at the Upland Watershed, which include the hillslopes and a channel, comparing the CRNS soil moisture values and the overall weighted Sensor Network measurements. Although, the figures (13a-13d) do not show all of the soil transects at the Upland Watershed, only the soil transects that have the highest impact of topographical features within the CRNS footprint are shown. At the hillslopes of the Upland Watershed (Figures 13a and 13b), the soil moisture values from sensors placed on the southeast (SE) and northeast (NE) hillslopes show a similar overall trend to those observed in the CRNS and weighted sensor network soil moisture values (Figure

13d). Additionally, at the hillslope locations, sensors placed at 30 cm depth typically record higher soil moisture values compared to those at 5 cm and 15 cm depths. This is

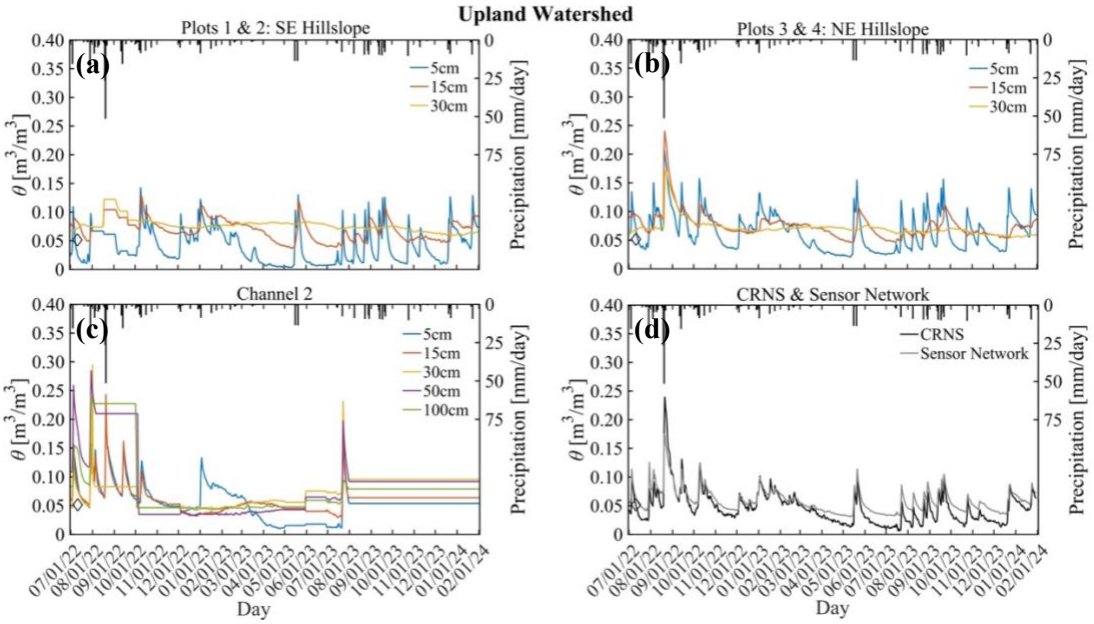

Figure 13. Sensor Network placement and comparison of the Upland Watershed hillslopes and channels.

likely due to the presence of a caliche layer, a hard layer of calcium carbonate found at around 30 cm depth, which can retain moisture more effectively. However, the channel's soil moisture values at 5 cm depth are significantly lower than those recorded at the hillslopes and by the overall CRNS and sensor network. This difference could be attributed to the channel's role in directing surface runoff, which might limit the infiltration at shallow depths while deeper soil layers might be less affected. These observations suggest that factors such as inundation, caliche layers, and topographical differences are critical in understanding and comparing soil moisture values. Improvements in sensor placement, accounting for these factors, can enhance the accuracy and reliability of soil moisture monitoring at the watershed level.

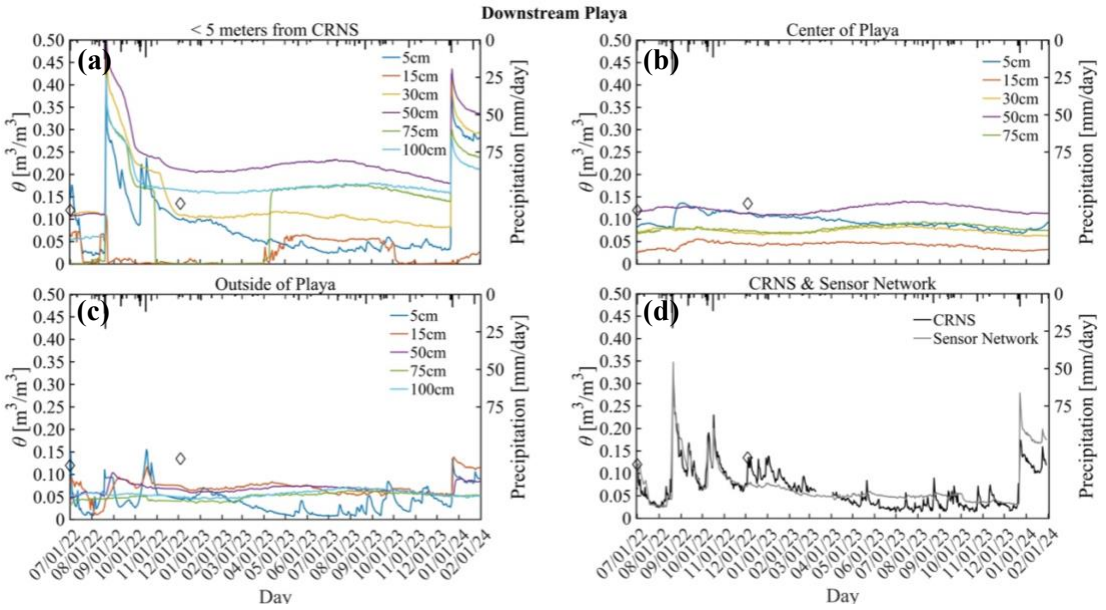

Figure 14. Sensor Network placement and comparison of the Downstream Playa within and outside the playa boundary.

The Downstream Playa has a simpler instrumentation of the soil transects encompassing the Sensor Network, as shown by Figure 14, in which Figure 14a, and Figure 14b represent the soil moisture values within the clay rich playa boundary, and Figure 14c, outside of the playa surrounded by mesquite shrubs and sandy clay loam, with a more of a desert pavement gravel is found. Figure 14a, exhibits an overall higher daily soil moisture value over the 19-month period, with deep soil sensors such as at 30 centimeters and below hardly respond to the soil moistures pulses seen in Figure 14d, that show the CRNS soil moisture values encompassing, the weighted Sensor Network soil moisture values. However, in Figure 14b, the soil transects located within the middle of the playa, hardly experiences any soil moisture pulses despite precipitation events occurring at the Playa. This can possibly be due to the spatial coverage of precipitation events at the Downstream Playa not fully encompassing the playa, suggested by the

subliminal soil moisture peak shown in Figure 14b, at the 5cm sensor depth. Additionally, outside of the playa, in Figure 14c, the sensors at the various depths do have a more relative response to precipitation events in comparison to the soil transect located at the center of the playa. However, neither the transect, at the center of the playa nor the outside of the playa, experience as high magnitudes of soil moisture pulses as compared to the soil transect located right next to the CRNS sensor, and also weighted the heaviest. Possibly suggesting to the reason as to why the CRNS and weighted Sensor Network soil moisture values have more contrasting difference than the CRNS and Sensor Network located at the Upland Watershed. Along with differences in soil moisture recessions specifically at the Downstream Playa, in which each soil transect, has vastly different soil moisture recession limbs to the significant precipitation events such as the August event.

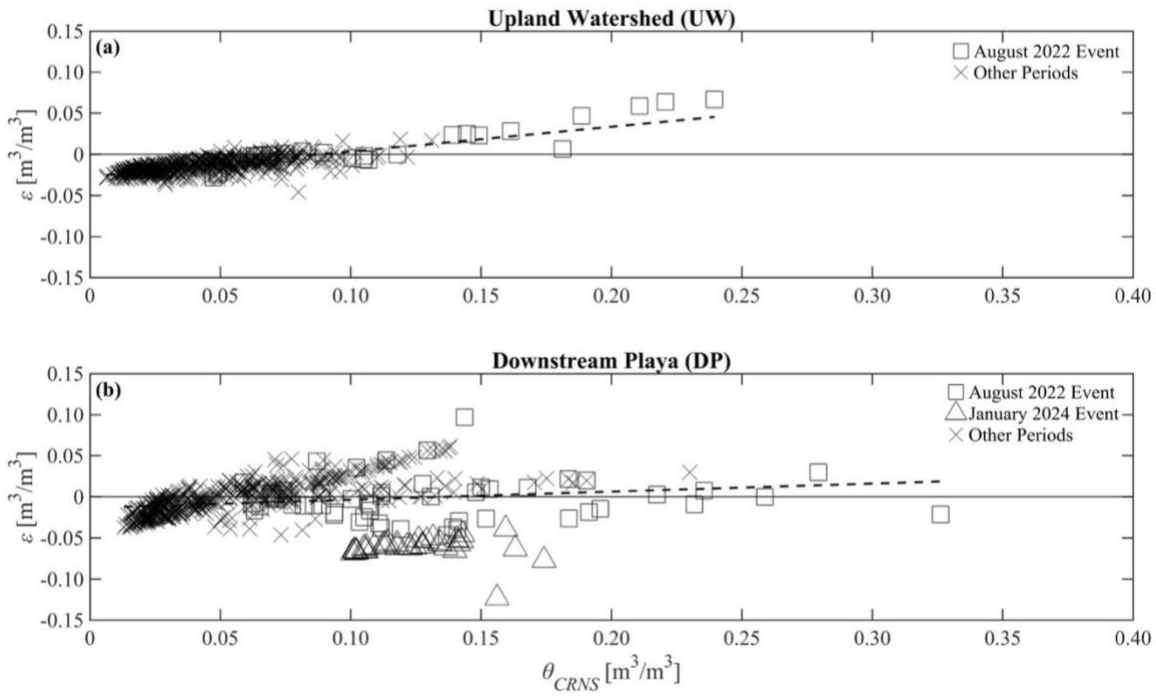

Figure 15. Daily soil moisture difference between θ_{CRNS} and θ_{SN}, $\varepsilon = \theta_{CRNS} - \theta_{SN}$, as a function of θ_{CRNS} at (a) UW and (b) DP for a large precipitation event at both sites in August 2022 (squares), a soil moisture pulse at DP in January 2024 (triangles in b), and all other soil moisture values (x, labelled Other Periods). Dashed black lines are linear regressions.

Inundation Effect at the Upland Watershed and Downstream Playa

An additional biomass correction was evaluated between the CRNS soil moisture measurements (θ_{CRNS}) and the weighted sensor network (θ_{SN}). The purpose of this biomass correction was to determine if vegetation, particularly grasses at the Downstream Playa, impacted the comparisons between CRNS and the sensor network at both sites. The CRNS provides aboveground, non-invasive soil moisture readings, whereas the weighted sensor network involves in-ground measurements (i.e., directly within the soil).

To quantify the differences, the value epsilon (ε) represents the difference between the CRNS soil moisture values and the weighted sensor network soil moisture values ($\varepsilon = \theta_{CRNS} - \theta_{SN}$). An ideal agreement would be when ε is zero, indicating no

difference between the two measurements. If ε is positive, this indicates that the CRNS soil moisture measurements are an overestimate in comparison to the weighted sensor network. Conversely, when ε is negative, the weighted sensor network is an overestimate of the surface average soil moisture measurements. As shown in Figure 15, the reading difference between the two soil sensor systems at the Upland Watershed vary with soil moisture levels. The CRNS measurements(θ_{CRNS}) tend to be lower than the weighted sensor network measurements (θ_{SN}) when the soil is dry and higher when the soil is wet.

However, at the Downstream Playa, the scenario differs. During large precipitation events, the difference between the CRNS soil moisture measurements (θ_{CRNS}) and the weighted sensor network (θ_{SN}) shows less agreement, indicated by more variable ε values. This discrepancy is likely influenced by surface inundation rather than vegetation, as evidenced by the pronounced variations during the large inundation event and the significant January event, as shown in Figure 15b. The black squares representing the surface inundation and the black triangles for the January event highlight the considerable discrepancies during these periods.

Several factors could contribute to this discrepancy. One factor is the distribution and density of the sensor networks. The Downstream Playa has fewer sensors in the study site compared to the Upland Watershed. This sparse distribution may lead to less accurate representation of the overall soil moisture, especially during large precipitation events. Moreover, the nature of the vegetation at the Downstream Playa could be affecting the CRNS measurements. Wet grasses and other types of vegetation can impact the neutron counts detected by CRNS.

Water Balance Analysis

In this study, two water balance formulas are analyzed to determine soil moisture dynamics. The first formula is the CRNS cumulative daily flux (f_{CRNS}), as outlined by Franz et al. (2012). This equation calculates the daily flux of soil moisture in millimeters per day, measured by CRNS on a 1-day time step scale. It incorporates the minimum penetration depth (Z^*) between two consecutive days to accurately reflect changes in soil moisture over time. This approach allows for a precise measurement of daily soil moisture variations, which is essential for understanding the hydrological processes within the study area:

$$f_{CRNS} = \frac{\left(\theta_{CRNS,t} - \theta_{CRNS,t-1}\right) \min(Z_t^*, Z_{t-1}^*)}{\Delta t} \quad (10)$$

The values of f_{CRNS} are utilized to extrapolate daily values of infiltration and outflow, measured in millimeters (Franz et al., 2012; Schreiner-McGraw, 2016). Specifically: (1) Positive values of f_{CRNS} indicate an increase in soil moisture, representing net infiltration. This is expressed as $f_{CRNS} = I$ (Infiltration) in mm/day. (2) Negative values of f_{CRNS} indicate a reduction in soil moisture, representing net outflow. This relationship is formulated as f_{CRNS} = Outflow (O) in mm/day. The calculation of inflow and outflow is subject to certain conditions to ensure accurate representation of soil moisture dynamics: (1) Inflow (I): Infiltration is only counted when there is a discernible increase in soil moisture caused by a precipitation event ($f_{CRNS} > 0$). This increase must be significant enough to surpass any measurement noise or natural variability, indicating actual water movement into the soil. Outflow (Evaporation and Transpiration): Outflow is considered when there is a measurable decrease in soil

moisture ($f_{CRNS} < 0$). This decrease signifies water loss from the soil, which could be due to evaporation, transpiration, or deeper percolation. Equation 10, was applied throughout the duration of the 19-month study period, thus capturing large soil moisture pulses caused by precipitation events before and after their recession.

Leakage or deep percolation can be estimated from the net outflow values by subtracting daily evapotranspiration (*ET*) from the daily outflow, thereby estimating leakage ($L = O - ET$) (Franz et al., 2012; Schreiner-McGraw et al., 2016). This calculation helps in understanding the interactions between ground and atmospheric processes at both sites, providing insight into the underlying hydrological mechanisms. By considering these conditions, the study ensures that the derived soil moisture fluxes accurately reflect the true hydrological processes occurring in the study area.

The second approach used in this study is the water balance formula:

$$Z^* \frac{\Delta\theta}{\Delta t} = P - ET \pm Q \pm L \tag{11}$$

This formula incorporates several key components essential for understanding the hydrological processes. Z^* represents the effective sampling depth; $\Delta\theta$ denotes the change in volumetric soil moisture within a specified temporal scale Δt; *P*, precipitation, is a primary input that accounts for the total rainfall received; Q symbolizes surface runoff, with its sign indicating the direction and nature of runoff; and leakage, *L*, can occur in both positive and negative values, depending on the direction of water movement.

At the Upland Watershed, negative values of *Q* reflect the process of surface runoff as water exits the watershed. At the Downstream Playa, positive values of *Q* indicate the accumulation or inflow of water. The distinction in runoff ($\pm Q$) between

the two sites highlights the different hydrological responses observed. It provides a nuanced understanding of local water balance dynamics, illustrating how each site interacts with surface water differently.

At both sites, leakage ($\pm L$) can occur in both positive and negative values. Negative values of leakage indicate water being absorbed by plant roots, moving upwards. This upward movement, known as root water uptake, is critical for sustaining vegetation, particularly in arid environments where water is a limiting factor (Kizito et al., 2012; Schreiner-McGraw et al., 2016). Positive values of leakage suggest that water is percolating downward, moving deeper into the vadose zone beneath Z^*. This downward percolation is essential for recharging groundwater and maintaining soil moisture levels below the root zone (Kizito et al., 2012; Schreiner-McGraw et al., 2016).

Understanding the calculation of leakage at these two sites is important for several reasons. Firstly, it allows to quantify the movement of water within the soil profile, which is critical for understanding the overall water balance and the hydrological connectivity between the Upland Watershed and the Downstream Playa. The Upland Watershed, located on a piedmont slope, is expected to exhibit different leakage dynamics compared to the Downstream Playa on the basin floor due to variations in topography, soil composition, and vegetation cover.

Secondly, calculating leakage helps test the hypothesis regarding the differences in soil moisture dynamics between the two landscape positions. At the Upland Watershed anticipated rates of higher upward leakage (negative $-L$) due to root water uptake by vegetation adapted to drier conditions. In contrast, the Downstream Playa is expected to have higher rates of downward leakage (positive $+L$) due to its position on the basin

floor, where water accumulation from runoff and precipitation is more likely to percolate deeper into the soil. By comparing the leakage values between the two sites, a better understanding of the hydrological connectivity and water movement patterns within the Jornada endorheic basin can be achieved. This information is crucial for predicting the impacts of climate variability between upland and lowland sites connectivity.

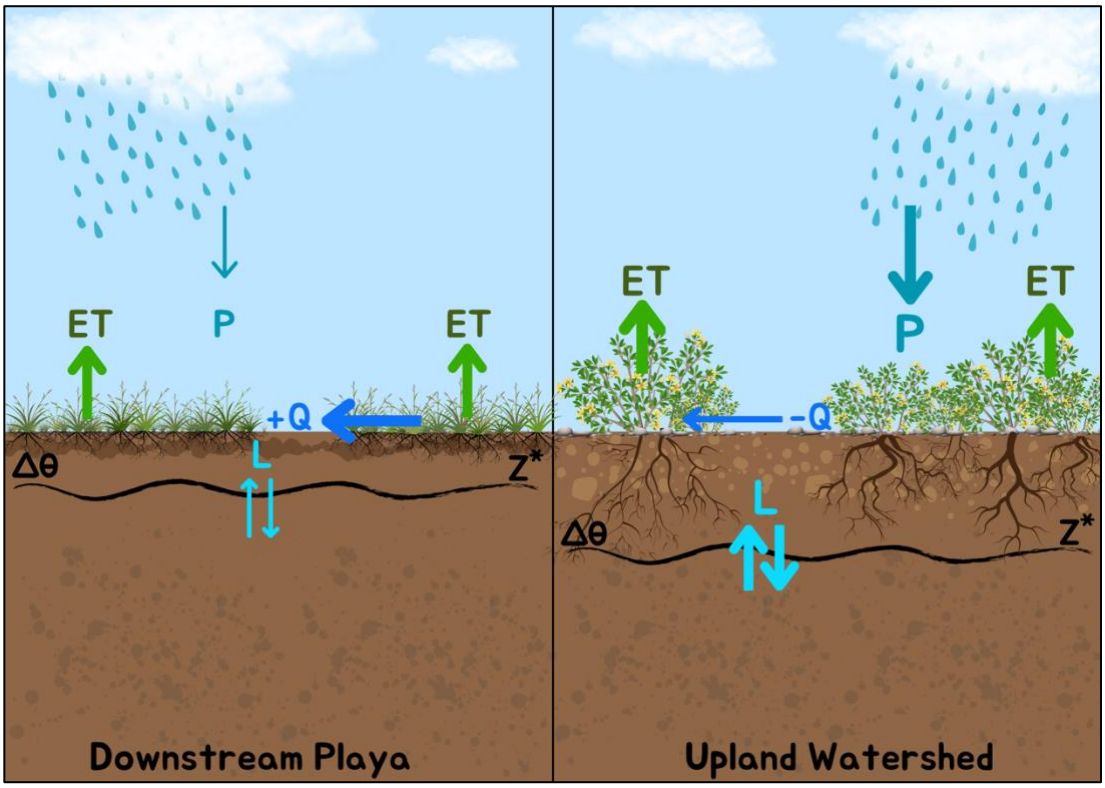

Figure 16. Water balance illustration at the Upland Watershed and Downstream Playa.

Leakage Estimation

The third analysis in this study uses the water balance to determine leakage (L) at each study site. As shown in Figure 16, leakage can occur in two directions; the most common involves saturation in the vadose zone, which allows water to percolate beyond depth Z^*. This behavior is often described by an exponential decay of soil moisture, particularly under conditions that reduce hydraulic conductivity (K_s). This relationship and its underlying assumptions are expressed in Equation 12, as outlined by Rodríguez-Iturbe and Porporato (2004). This formula can be applied when key parameters are known, including hydraulic conductivity (K_s), relative soil moisture (s), a soil coefficient ($\beta = 2b + 4$), and field capacity (s_{fc}). For its use, the Upland Watershed is classified as a sandy loam, while the Downstream Playa is classified as a silty loam.

$$L(s) = \frac{K_s}{e^{\beta(1-s_{fc})} - 1}\left[e^{\beta(s-s_{fc})} - 1\right], \qquad s_{fc} < s \leq 1 \tag{12}$$

Equation 13 is the water balance rearranged to solve for leakage (L), with each variable in millimeters, collected over the entire study period of 19 months. The purpose of using two equations to estimate leakage is to understand water movement within the vadose zone across two different temporal scales. Equation 12 is employed to quantify leakage during large precipitation events, while Equation 13 provides insights into the ongoing water movement in the vadose zone throughout the entire study period.

$$L = P - ET \pm Q \pm Z^* \Delta\theta \tag{13}$$

To understand the leakage estimates, sensitivity scenarios were conducted for both study sites. By adjusting the water balance variables, the influence of these

modifications on the total leakage over the 19-month study period was assessed. Table 5 presents the percentage adjustments for each variable as they relate to Equation 13.

Leakage Estimates, *L* [mm]	
Downstream Playa (DP)	*Upland Watershed (UW)*
P = -10%, ET = -25%, Q = -10%	P = -10%, ET = -25%, Q = -10%
P = -10%, ET = -25%, Q = +10%	P = -10%, ET = -25%, Q = +10%
P = -10%, ET = No Change, Q = -10%	P = -10%, ET = No Change, Q = -10%
P = -10%, ET = No Change, Q = +10%	P = -10%, ET = No Change, Q = +10%
P = -10%, ET = +25%, Q = -10%	P = -10%, ET = +25%, Q = -10%
P = -10%, ET = +25%, Q = +10%	P = -10%, ET = +25%, Q = +10%

Table 5. Leakage estimates derived from CRNS under different assumptions of error in precipitation (P), evapotranspiration (ET), and discharge (Q).

CHAPTER 3

RESULTS

Response to Significant Precipitation Event

A critical aspect of this study involves examining the water balance during a substantial precipitation event from August 19 to 20, 2022, affecting both the Upland Watershed and Downstream Playa, as illustrated in Figure 17. This event is meticulously detailed in Table 6, which itemizes the rainfall during this period. The Upland Watershed received a total of 78.33 mm of rain, with the peak occurring between 17:00 (UTC) on August 19 and 6:00 (UTC) on August 20, amounting to 59.94 mm. Conversely, the Downstream Playa experienced 21.8 mm of precipitation during the peak times from 20:30 (UTC) on August 19 to 4:30 (UTC) on August 20, 2022.

This significant precipitation is crucial as it highlights the hydrological connectivity between the upland and lowland areas within an endorheic basin. The event serves as a key indicator, allowing for an in-depth analysis of hydrological pulses and the subsequent estimation of leakage (L) through various models.

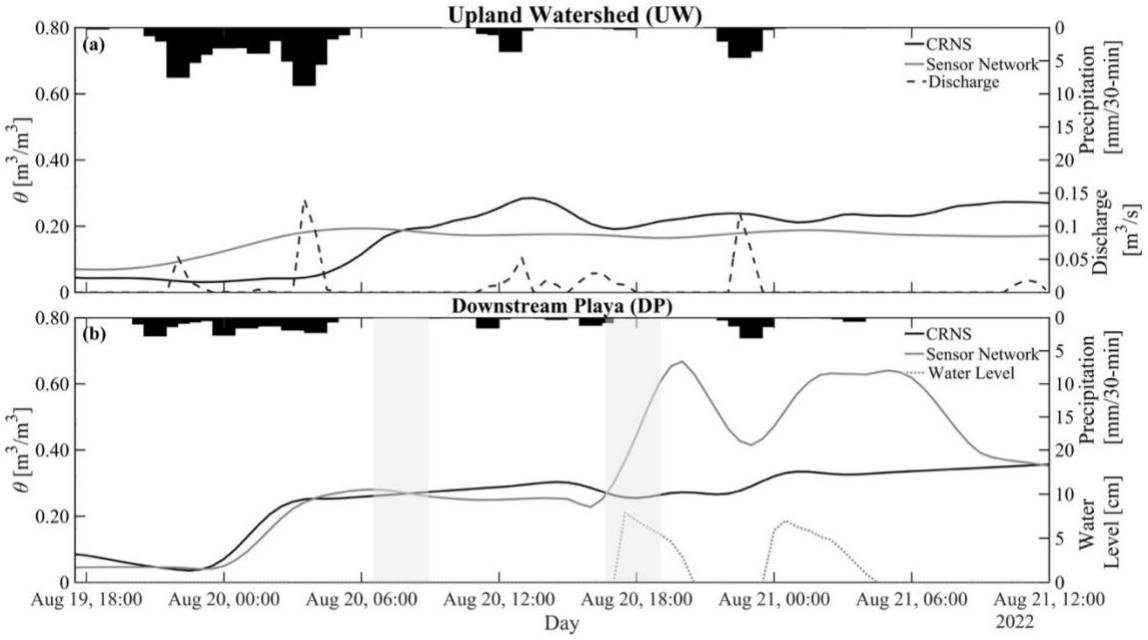

Figure 17. Response of (a) UW and (b) DP to a large precipitation event in August 2022. Precipitation (black bars), θ_{CRNS} (black lines), and θ_{SN} (gray lines) are shown for each site. Discharge from UW (dashed black line) and water level at DP (dashed gray line) are shown. Shaded areas in (b) depict periods of time where CRNS suffered data losses and interpolated values were used. Total precipitation was 78 mm at UW and 34 mm at DP.

Upland Watershed			
Start Time	*End Time*	*Duration*	*Total Rain [mm]*
8/19/22 6:30	8/19/22 8:30	2h 0m 0s	0.37
8/19/22 17:00	8/20/22 6:00	13h 0m 0s	59.94
8/20/22 11:00	8/20/22 17:30	6h 30m 0s	7.10
8/20/22 21:30	8/21/22 4:30	7h 0m 0s	10.92
			78.33
Downstream Playa			
Start Time	*End Time*	*Duration*	*Total Rain [mm]*
08/19/22 07:00:00	08/19/22 07:30:00	0h 30m 0s	0.10
08/19/22 20:30:00	08/20/22 04:30:00	8h 0m 0s	21.8
08/20/22 08:30:00	08/20/22 09:00:00	0h 30m 0s	0.10
08/20/22 11:00:00	08/20/22 18:00:00	7h 0m 0s	4.30
08/20/22 21:30:00	08/21/22 03:30:00	6h 0m 0s	7.20
			33.5

Table 6. Rain event details for the August 19th - August 20th precipitation event at the Upland Watershed and Downstream Playa table.

In Figure 17, hourly precipitation is shown with black bars, while the black and gray lines represent soil moisture measurements from the Cosmic Ray Neutron Sensor (θ_{CRNS}) and the weighted Sensor Network (θ_{SN}), respectively. Notably, the CRNS at the Downstream Playa encountered data gaps due to equipment failure during critical inundation periods, which slightly hindered comprehensive data capture. Nevertheless, the Upland Watershed documented a cumulative surface runoff (Q) of 1.03 m^3 over the two days, and the Downstream Playa saw significant flooding, with water levels rising to 76.1 cm. The impact of this event was particularly pronounced at the Downstream Playa, as depicted in Figure 17b. Two major peaks in soil moisture, recorded by the weighted Sensor Network, matched the timing of the inundation events, the first around 16:00 (UTC) on August 20 and the second near 23:00 (UTC) on August 21. These responses are consistent with the Type C inundation profile defined by Kimsal (2023): infrequent occurrences with short durations but high inundation depths. In contrast, the Upland Watershed showed a gradual increase in soil moisture that plateaued after the initial rainfall, demonstrating a more subdued hydrological response. This divergence in hydrological behavior underlines the unique dynamics at each site. While the Upland Watershed shows a consistent, gradual increase in moisture followed by a plateau, indicative of its robust handling of precipitation events, the Downstream Playa reacts more dramatically, highlighting its vulnerability to flooding. These observations not only reinforce the importance of site-specific calibration in hydrological models but also validate the effectiveness and reliability of the deployed sensor networks in capturing these critical dynamics.

Daily Cumulative Fluxes and Water Balance Dynamics

Figure 18 provides a depiction of daily cumulative CRNS fluxes, derived from Equation 10, and presents these data on a one-day time step. The calculation involves subtracting the CRNS soil moisture values over a 24-hour period, multiplying by the minimum depth (Z^*), and then dividing by the daily time step. The result is referred to as the cumulative daily CRNS flux (f_{CRNS}). Positive values of f_{CRNS} indicate an increase in soil moisture, termed as net infiltration (I), whereas negative values signify a decrease in soil moisture, classified as net outflow (O), measured in millimeters per day. The figure also illustrates cumulative precipitation (P, represented by the gray line) and cumulative evapotranspiration (ET, depicted by the dashed black line) the Upland Watershed (UW) (Figure 18a) and the Downstream Playa (DP) (Figure 18b). By juxtaposing these fluxes, Figure 18 allows for a nuanced understanding of the hydrological processes at these two sites over a 19-month period, from July 1st, 2022, to January 31st, 2024.

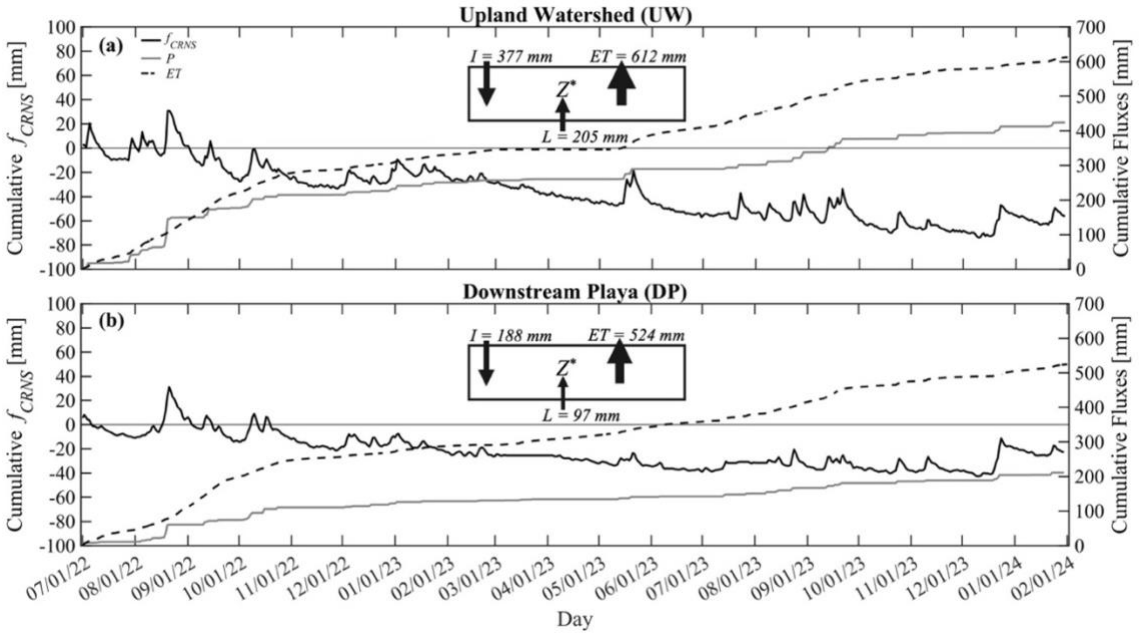

Figure 18. Daily cumulative CRNS flux (f_{CRNS}, black lines), cumulative evapotranspiration (*ET*, dashed black lines), and cumulative precipitation (*P*, gray lines) at (a) UW and (b) DP. Box represents the fluxes into and out from a soil layer of depth Z^* with arrows depicting infiltration (*I*) derived from f_{CRNS}, *ET* derived from the eddy covariance method, and leakage (*L*) derived from the water balance at the site.

The most salient trend observed in Figure 18 is the overarching drying pattern at both the Upland Watershed and the Downstream Playa throughout the study period, with various hydrological forces acting upon each site at a different rate. This drying trend is more pronounced at the Upland Watershed. Initially, on July 1st, 2022, the Upland Watershed exhibited a cumulative flux (f_{CRNS}) of approximately 20 mm, associated with a precipitation event at the start of July. By the end of the study period, the cumulative flux at the Upland Watershed had significantly dropped to around -60 mm, receiving a slight bounce back from the January precipitation events at the end of the study period. Examining the water balance dynamics at the Upland Watershed, the black box in Figure 18a, reveals key insights. The total net infiltration (*I*), derived from positive f_{CRNS} values, is 377 mm. This net infiltration is a result of soil moisture pulses from precipitation

events, aligning closely with the total precipitation (P) received, which is 423 mm for a 19-month study period. The cumulative ET at the Upland Watershed stands at 612 mm, indicating substantial ET losses that exceed the precipitation input. This is common in semiarid ecosystems, where ET often surpasses precipitation due to a high evaporative demand.

A critical aspect of the water balance at the Upland Watershed is the negative cumulative leakage (L), which is -205 mm, as indicated by the black arrow towards the black box in Figure 18a, derived from the water balance formula (Equation 13). In which the total 19-month study period sums, were utilized, such as: precipitation (P), evapotranspiration (ET), total surface runoff (Q), and total soil storage change ($\Delta\theta$).

This negative leakage value indicates that the system is depleting its stored water reserves, as evapotranspiration significantly exceeds precipitation over a two-year period. In the Upland Watershed, evapotranspiration is the primary factor in water loss, reaching a substantial rate of 612 mm. This rate of water extractor surpasses the contributions from precipitation, suggesting reliance on existing water stores within the soil

To understand the implications of this negative leakage, it is essential to consider the interplay of water balance components at the Upland Watershed. The primary water input is precipitation, which contributes to infiltration. However, the high ET demand necessitates the withdrawal of water from deeper soil layers to sustain plant life. This vertical leakage supports plant water uptake, leading to a net negative leakage. The dominant vegetation at the Upland Watershed, primarily woody shrubs with deep taproots, further exacerbates this effect. These plants can access water deep within the vadose zone, thereby intensifying the system reliance on deeper soil moisture reserves.

A fitting an analogy for the Upland Watershed and its hydrological forcings, a pressing system but with slow hydrological forcings. The Upland Watershed receives more rainfall, than lowland areas, releases some as runoff (Q), but stores the rest of the water in the soil, which then most of that water is used for evapotranspiration (ET), either by plants or the atmosphere. To compensate, for this slow hydrological forcing always acting upon the system (Evapotranspiration (ET) and precipitation (P), The Upland Watershed system relies on previous water storage to consume. Due to the fact that the Upland Watershed is always receiving precipitation events (P), due to its proximity to the mountain block, the Upland Watershed is typically able to produce runoff (Q), if permittable by overland flow. Thus, the Upland Watershed is consistently always hydrologically active, and hydrologically connected to its surrounding areas. In other words, the Upland Watershed always has a strategy to keep the constant and slow hydrological presses moving throughout the water balance of its system. Whereas the Upland Watershed, is continuously processing hydrological presses through its system, the Downstream Playa is a hydrological system waiting to be acted upon, such as a pulsing system. The Downstream Playa, depicted in Figure 18b, also exhibits a drying trend, although slightly less intense compared to the Upland Watershed. At the start of the study period, the Downstream Playa showed a cumulative flux (f_{CRNS}) similar to that of the Upland Watershed, but by the end, the cumulative flux was higher, around -20 mm, again being able to slightly re-cooperate its cumulative flux losses through the January precipitation events at the end of the study period. The total net infiltration (I) at the Downstream Playa is 188 mm, which is considerably lower than that at the Upland Watershed, however this low value is also reflected in the total amount of precipitation

received at the Downstream Playa which is equal to 212 mm. The cumulative *ET* at the Downstream Playa is 524 mm, which is also less than that at the Upland Watershed, indicating a lower evapotranspiration rate.

The cumulative leakage (*L*) at the Downstream Playa is -97 mm. While still negative, this leakage is less severe than the corresponding value at the Upland Watershed. Whereas the Upland Watershed can be described as a hydrologically active system, with slow hydrological presses stemming from precipitation (P) and evapotranspiration (ET). The Downstream Playa behaves as a dormant hydrological system waiting to be acted upon through the bridge of hydrological connectivity, allowing for these pulses to occur. Which then the Downstream Playa is able to process the input of hydrological forces such as precipitation (*P*), or the gain of surface runoff (*Q*). Whereas the Upland Watershed does not experience a dormancy period, due to its nature of always receiving precipitation events and generating surface runoff.

Additionally, two key factors distinguish the hydrological behaviors depicted at each site. Firstly, the Upland Watershed is characterized by a sandy loam soil with high gravel content. This type of soil, combined with the presence of woody shrubs such as creosote bush, which possesses extensive and deep rooting systems, significantly influences the soil water balance dynamics. In contrast, the Downstream Playa features a sandy clay loam soil, inhabited primarily by perennial grasses. The rooting depth of these grasses does not exceed 20 centimeters in the vadose zone. This shallow rooting depth limits the ability of the vegetation to access deeper water reserves. Consequently, the Downstream Playa soil properties, including its high clay content, enhance its capacity to store water in the vadose zone. Considering these differences, a similar need to access

vadose zone water exists at both sites. However, due to the playa soil properties and the shallow rooting depth of its vegetation, the vertical water uptake occurs at a weaker scale compared to the Upland Watershed, at which vertical water uptake is needed to support the vegetation found at the Upland Watershed.

Table 7 presents a detailed compilation of the cumulative values derived from Figure 18, along with additional metrics needed to quantify the soil water balance system at each study site. The variables of interest include precipitation (P), evapotranspiration (ET), surface discharge (Q), and soil water storage changes ($\Delta\theta_{CRNS}$). In the 19-month study period at the Upland Watershed, the discharge was calculated to be -5 mm. This measurement is derived using the empirical methods employed at the Santa Rita supercritical flume, located at the watershed's outlet. Here, a piezometer measures the water height (h), which is then converted into millimeters to quantify the volume of surface runoff leaving the Upland Watershed. Given its classification as a primary producer of surface runoff from precipitation events through overland flow, this discharge represents a net loss of water from the system.

Conversely, the Downstream Playa recorded a significant surface runoff gain of +228 mm during two brief inundation events. This figure is based on the playa characteristics outlined in Kimsal (2023), which consider the inundation volume (m^3), calculated from the water heights of 8 centimeters and 7 centimeters observed during the August 19th through the 20th precipitation events. These volumes are then divided by the inundation areas for the respective events: 21,309 m^2 and 20,659 m^2, as specified in Kimsal (2023). Thus, for this study, the +228 mm is the summation of the two brief inundation events, recognized as the net surface inflow during these inundation periods.

Water Balance Component	*Upland Watershed*	*Downstream Playa*
Water Balance Estimates		
Precipitation, P [mm]	423	212
Evapotranspiration, ET [mm]	612	524
Discharge, Q [mm]	-5	+228
Leakage, L [mm]	-205	-97
CRNS Estimates		
Infiltration, I [mm]	377	188
Outflow, O [mm]	560	344
Soil Water Storage, $\Delta\theta_{CRNS}$ [mm]	+11	+13
Water Balance Ratios		
Evapotranspiration Ratio, ET/P [-]	1.44	2.47
Outflow Ratio, O/P [-]	1.32	1.62

Table 7. Comparisons of water balance components and ratios estimated from site instrumentation and CRNS for the Upland Watershed and Downstream Playa.

An additional, important variable reported in Table 6 is the soil water storage change, represented as ($\Delta\theta_{CRNS}$), which can provide insights into the soil moisture dynamics at each site. However, it is important to note how $\Delta\theta_{CRNS}$ is calculated for the entirety of the 19-month study period. To calculate, $\Delta\theta_{CRNS}$ the soil moisture value from the beginning of the study period is utilized for both sites, this would be July 1st, 2022, then this value is subtracted from the soil moisture value of the last day of the study period, for both sites this would again be January 31st, 2024. Although, the Upland Watershed yields a positive change in soil water storage, amounting to +11mm. It is rather difficult to discern the cumulative soil water storage gain from these two dates as they are both dates that occur within the wetting fronts of the study period duration. With the July to August precipitation in 2022 creating a large soil moisture gain at both sites,

and the late January 2024 precipitation events also creating significant soil moisture pulses at the end of the study period. Similarly, the Downstream Playa yields a positive soil water storage of +13 mm, indicative of a net gain in soil moisture levels at the very beginning and end of the study period for both sites. This can be further illustrated when examining Figure 18, in which both the Upland Watershed and Downstream Playa are exhibiting an overall drying trend, and the input of the January 2024 precipitation events gives the Upland Watershed a slight increase in cumulative flux but not enough to overcome the overall drying trend. Conversely, at the Downstream Playa, Figure 18b, the input of the January 2024 precipitation events, does give a slightly increased push towards net gain cumulative fluxes ($f_{CRNS} > 0$) it is not enough to overcome the overall drying trend occurring at the Downstream Playa. Thus, the soil water storage variable is crucial to understand overall net gain or net loss of water stored in the soil matrix of each site, large wetting fronts at the end members of a study period can misrepresent the total value of $\Delta\theta_{CRNS}$. However, further in the results, $\Delta\theta_{CRNS}$ is used at a higher resolution temporal scale, monthly differences in soil water storage gain leading to a better understanding of the true net gain or loss of soil water within each site.

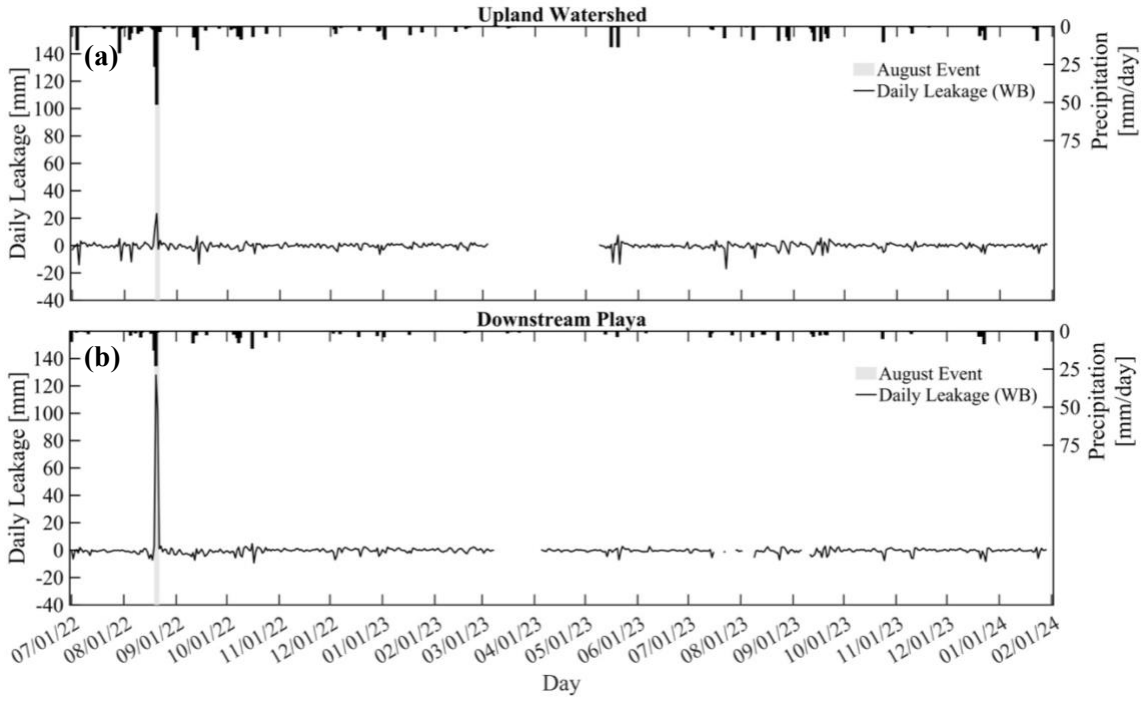

Figure 19. Leakage derived from the water balance formula (Equation 10) at the Upland Watershed and Downstream Playa.

At the Upland Watershed, the cumulative leakage value derived for the 19-month study period is equal to -205mm, calculated based on Equation 13. Figure 19b, shows the daily leakage derived from Equation 13 at the Upland Watershed, and most notably for the August precipitation event which yielded a total of 78 mm of precipitation over a two-day period, this corresponds with the most significant pulse of leakage (L) at this site, with a total of 22 mm of net water gain generated from the precipitation event. The overall trend of daily leakage (L) at the Upland Watershed, is dominated by negative values of leakage (L). This same trend is shared in Figure 19b, in which the daily leakage values derived Equation 13 for the Downstream Playa have the most significant leakage gain during the August precipitation event. In contrast to the 78 mm of precipitation received at the Upland Watershed, the Downstream Playa only received a total of 33.5 mm of precipitation over a two-day period. However, due to the infrequent

inundation event that occurred during this event, the Downstream Playa, received a surplus of surface run off (+Q =228 mm) resulting in the large leakage pulse shown in Figure 19b, yielding a total of 135 mm of water gained to the vadose zone. Overall, for both the Upland Watershed and Downstream Playa, without the input of large precipitation events, the overall trend of daily leakage values at both sites, results in a leakage loss. Further supporting the total leakage values derived respectively at each site, Upland Watershed (L = -205 mm) and the Downstream Playa (L = -97 mm).

Lastly, Table 7 shows the water balance ratios, offering critical insights into the hydrological dynamics at both study sites. The first ratio examined is the evapotranspiration (*ET*) over precipitation (*P*) ratio (*ET/P*). At the Upland Watershed, the *ET/P* ratio is calculated to be 1.44. This value indicates that evapotranspiration exceeds the precipitation received, suggesting a high level of water usage by vegetation and/or significant evaporation rates. Such a ratio underscores the intense demand placed on water resources by the ecosystem, where the vegetation and atmospheric conditions drive substantial water loss through evapotranspiration.

In a similar demand, the Downstream Playa exhibits an even higher *ET/P* ratio of 2.47. The elevated *ET/P* ratio at the Downstream Playa can be partially attributed to the brief inundation events on August 19th, 2022, through August 20th, 2022. During these brief inundation events, evapotranspiration and plant transpiration would be stopped to the layer of water of over the surface. The daily gain in leakage (*L*) shown in Figure 19b, suggest that this inundation event allowed for the Downstream Playa to store the abundance of surface runoff (*Q*) and store it within the soil water matrix to use at a later time. This is further supported by the significantly larger *ET*/*P* ratio found in the

Downstream Playa in comparison to the Upland Watershed. Very much like the Upland Watershed, that is utilizing past water from precipitation events to support the surrounding vegetation the Downstream Playa is behaving similarly. However, the Downstream Playa has two large advantages over the Upland Watershed exacerbating the ET/P ratio, first being its soil type, dominated by a sandy clay loam, that can hold on to water, longer than the sandy loam with high gravel found at the Upland Watershed. Secondly, the Downstream Playa, does not carry the burden of supporting vegetation such as mesquite shrubs, with invasive tap roots that can access water within the soil. The Downstream Playa is dominated by perennial grasses, with shallow rooting systems, that behave in a dormant manner if there is not enough precipitation to support their growth. Thus, The *ET/P* ratios for both sites indicate that the ecosystems are experiencing high evapotranspiration rates relative to their precipitation inputs, utilizing past water from historic precipitation events to support their hydrological systems.

The final water balance ratio presented in Table 7 is the Outflow Ratio (*O/P*), which quantifies the proportion of outflow (*O*) relative to precipitation (*P*) at both the Upland Watershed and the Downstream Playa. This ratio serves to elucidate the extent to which precipitation contributes to the outflow from each site, encompassing both surface processes, such as evapotranspiration (*ET*) and surface runoff (*Q*), and subsurface processes, such as infiltration (*I*). At the Upland Watershed, the *O/P* ratio is calculated to be 1.32. This value indicates that the outflow exceeds the total precipitation received, since the total outflow is calculated from the reduction of soil moisture (θ_{CRNS}) it can be appreciated that this indicates that there is either a loss from evapotranspiration or water moving past the reading depth (Z^*). In contrast, the Downstream Playa exhibits an *O*/*P*

ratio of 1.62, implying that the outflow is greater than the precipitation received. The O/P ratios at both sites are consistent with the previously discussed ET/P ratios, further emphasizing that evapotranspiration is a major component of water loss that exceeds the incoming precipitation. In the case of the Upland Watershed, its sandy loam soil with high gravel content and presence of woody shrubs with deep roots, facilitate significant water movement beyond the local precipitation input. This movement could include both vertical infiltration to deeper soil layers and lateral flow out of the watershed. For the Downstream Playa, its sandy clay loam soil and the presence of perennial grasses with shallow root systems suggest that surface processes dominate water movement. The higher O/P ratio indicates that the site experiences substantial water fluxes, possibly driven by episodic inundation events and subsequent evaporation. This highlights the dynamic nature of the playa water balance, where periods of high-water availability can lead to significant outflows that exceed the direct precipitation input.

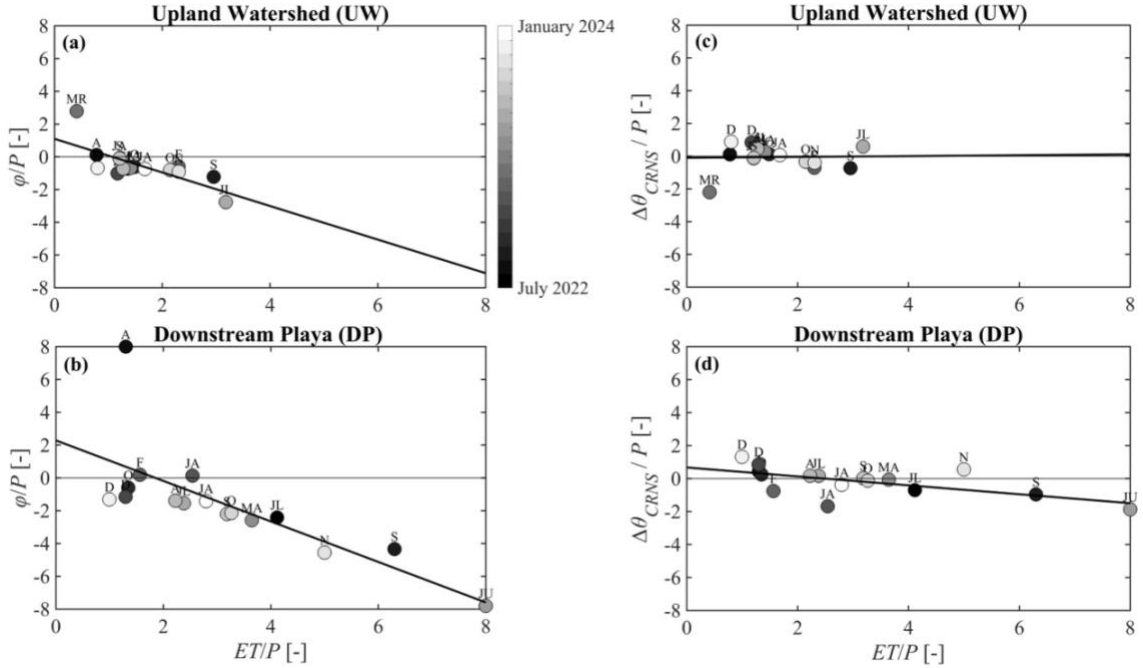

Figure 20. Monthly climographs for (a, c) UW and (b, d) DP. Monthly normalized losses (φ/P) are the ratio of the sum of leakage (L) and discharge (Q) divided by precipitation (P) shown in relation to the normalized evapotranspiration (ET/P). Monthly normalized soil storage change ($\Delta\theta_{CRNS}/P$) shown in relation to ET/P. Black lines show linear regressions in each case. Time evolution during the study period (July 1st, 2022, to January 31st, 2024) shown with the color bar.

Monthly Climographs and Water Balance Analysis

Figure 20 provides a detailed analysis of monthly hydrological dynamics through the use of climographs. The figure is divided into four panels. The left panels (Figures 20a and 20b) illustrate normalized losses (φ), defined as the sum of leakage (L) and discharge (Q) divided by precipitation (P). The color bar adjacent to Figure 20a indicates the study period, with black representing the start (July 1, 2022) and white representing the end (January 31, 2024). The right panels (Figures 20c and 20d) depict the normalized change in soil storage ($\Delta\theta_{CRNS}$) divided by precipitation (P). Each climograph shares the

same x-axis, representing the *ET/P* ratio, which denotes the relationship between evapotranspiration (*ET*) and precipitation (*P*).

The most significant finding presented in Figure 20 is the clear distinction in monthly hydrological behavior between the Upland Watershed and the Downstream Playa. Figure 20a illustrates the normalized losses at the Upland Watershed, which exhibit a consistent negative trend over the 19-month period, with each month showing similar patterns. The sole exception is March 2022, when an absence of precipitation events led to a pronounced drying trend compared to previous months, as depicted in Figure 20c. Despite substantial precipitation and leakage in August 2022, the Upland Watershed failed to sustain its hydrological balance due to insufficient hydrological inputs.

In contrast, the Downstream Playa, although less hydrologically stable in response to environmental forcings than the Upland Watershed, displayed only slight variations in hydrological responses from month to month. Notably, the precipitation event on August 19th-20th, 2022, significantly altered the hydrological pattern, as highlighted by a black circle labeled 'A' in Figure 20b, indicating an anomaly for that month. This event was followed by September 2022, which exhibited a marked shift towards a negative trend line, indicating a substantial increase in evapotranspiration losses relative to precipitation.

This behavioral difference is also evident in the soil storage change climographs (Figures 20c and 20d). The Upland Watershed shows no significant trend in either direction, suggesting a stable maintenance of soil moisture levels despite variations in *ET* and *P*. Conversely, the Downstream Playa shows a negative trend in normalized soil water change ($\Delta\theta_{CRNS}/P$), particularly impacted by the September 2022 data following the

August inundation event. This indicates a significant reduction in soil moisture and a higher evapotranspiration loss in the Downstream Playa during this period.

The results depicted in Figure 20 align closely with those in Figure 18 and Table 6. Both the Upland Watershed and Downstream Playa are characterized by water losses and challenges in retaining soil moisture. However, the rate and consistency of these losses differ significantly. The results presented in Figure 20 are consistent with those in Figure 18 and Table 7, showing how both the Upland Watershed and Downstream Playa face challenges related to water losses and soil moisture retention. However, the rates and consistency of these losses vary markedly between the two sites. The Upland Watershed exhibits a more effective capacity to process hydrological inputs such as precipitation (P) and surface runoff (Q), as indicated by the relatively stable ET/P and soil storage change ratios. This watershed can be characterized as a hydrologically active system, consistently responding to hydrological pressures.

Conversely, the Downstream Playa demonstrates characteristics of a hydrologically passive system, responding to infrequent but significant hydrological pulses that allow for hydrological connectivity with the surrounding environment. The monthly fluctuations in water balance metrics at the Downstream Playa highlight its dynamic role within the ecosystem, particularly during and following inundation events. This intermittent hydrological behavior provides a stark contrast to the more consistent and stable patterns observed in the Upland Watershed, underscoring the critical role that playas play in the regional water balance.

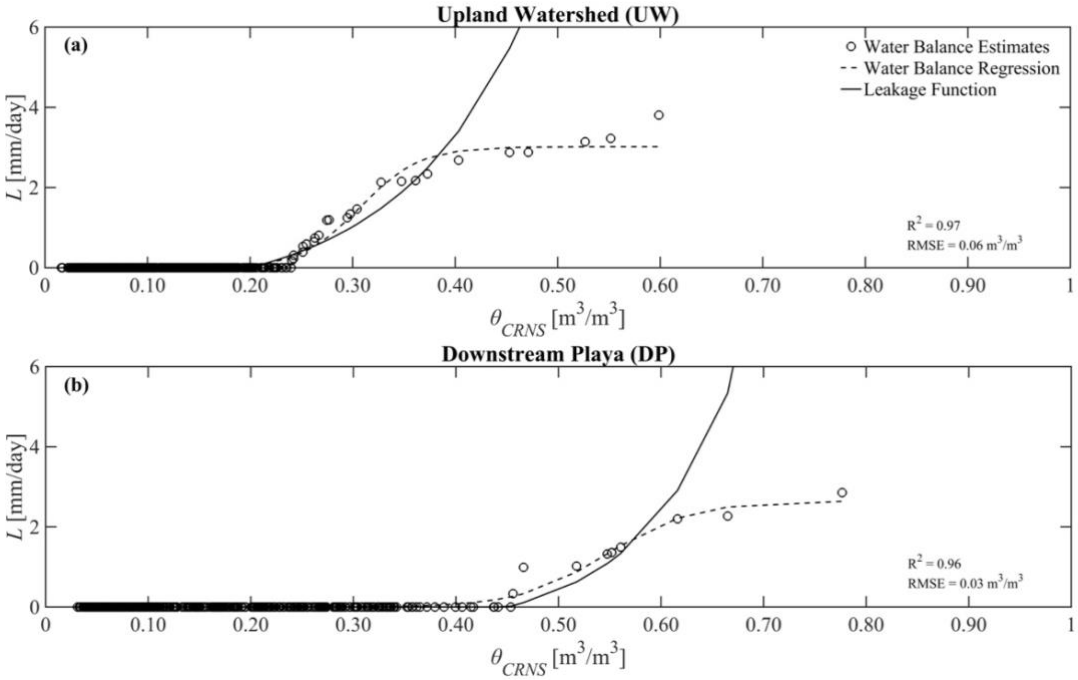

Figure 21. Comparison of leakage functions for (a) UW and (b) DP. Leakage estimates (L, circles) from the water balance for days after the August 2022 event are used to derive logistic regressions (dashed lines). At UW, the logistic regression is*:* y = 3.02 / (1 + exp (-34.22(x – 0.30))) - 0.012. At DP, the logistic regression is: y = 2.65 / (1 + exp (-23.77(x – 0.54))) - 0.003. The formulation of Liao *et al.* (2002) is also shown with best-fit parameters (solid lines).

Comparison of Leakage Functions and Logistic Regressions

The analysis of leakage over the 19-month study period is critical for understanding the hydrological dynamics of the Upland Watershed and Downstream Playa. However, Figure 21 shifts the focus to evaluating leakage in the context of a significant precipitation event over the course of two days August 19th, 2022, to August 20th, 2022, utilizing the Liao et al. (2002) leakage model. This model is depicted by the solid black lines in Figures 21a and 21b. The model uses specific soil parameters, with the saturated hydraulic conductivity (K_s) set at 500 mm/day for the sandy loam of the Upland Watershed and 220 mm/day for the sandy clay loam of the Downstream Playa. In which the soil parameters were obtained from Rodríguez-Iturbe and Porporato (2000).

Leakage Parameters	*Upland Watershed*	*Downstream Playa*
Leakage Parameters and Regression Metrics		
Saturated Hydraulic Conductivity, K_s [mm/day]	500	220
Pore Index, b [-]	2.0	3.40
Relative Field Capacity, s_{fc} [-]	0.20	0.45
Porosity, n [-]	0.40	0.42
R^2 [-]	0.70	0.60
Root Mean Squared Error [RMSE, m^3/m^3]	0.21	0.14
Correlation Coefficient [CC, -]	0.83	0.76
Bias [B, m^3/m^3]	0.06	0.03
Standard Error of Estimates [SEE, m^3/m^3]	0.20	0.13
Logistic Regression Metrics		
R^2 [-]	0.97	0.96
Root Mean Squared Error [RMSE, m^3/m^3]	0.06	0.03
Correlation Coefficient [CC, -]	0.98	0.98
Bias [B, m^3/m^3]	$-1.09e^{-8}$	$-4.25e^{-9}$
Standard Error of Estimates [SEE, m^3/m^3]	0.06	0.03

Table 8. Performance metric for leakage relations from Liao et al. (2002), including best-fit parameters, and logistic regressions derived from water balance estimates.

Additional soil parameters, such as the pore index (b), relative field capacity (s_f), and porosity (η), are detailed in Table 8. The water balance estimates, represented by black circles, illustrate leakage values derived from soil moisture values from the CRNS at both sites during the precipitation event on August 19-20, 2022.

The key finding from Figure 21 is the discrepancy between the water balance estimates and the leakage function predicted by the Liao et al. (2002) model. At both the Upland Watershed and Downstream Playa, the R^2 values for the Liao et al. (2002) model was 0.70 and 0.60, respectively. These values indicate a moderate fit, suggesting that the model does not fully capture the observed leakage behavior. To address this, a logistic regression model was applied, yielding much higher R^2 values of 0.97 at the Upland

Watershed and 0.96 at the Downstream Playa. The regression metrics further reveal that the Liao et al. (2002) model, with RMSE values of 0.21 m^3/m^3 for the Upland Watershed and 0.14 m^3/m^3 for the Downstream Playa, is inadequate in fitting the observed data. In contrast, the logistic regression models show significantly improved fits, with much lower RMSE values of 0.06 m^3/m^3 for the Upland Watershed and 0.03 m^3/m^3 for the Downstream Playa. These high R^2 values and low RMSE values demonstrate that the logistic regression model captures the leakage dynamics far more accurately. These results suggest that the Liao et al. (2002) model may not be sufficient for capturing leakage during significant precipitation events in semiarid environments. The superior fit of the logistic regression model implies that leakage behavior is more complex and requires a model that can accommodate non-linear responses to soil moisture changes.

Additionally, the results from Figure 21 suggest distinct leakage thresholds for both the Upland Watershed and Downstream Playa. The Upland Watershed has a leakage threshold at lower soil moisture values (0.23 m^3/m^3) compared to the Downstream Playa, which has a higher threshold (0.45 m^3/m^3). The Liao et al. (2002) model implies that leakage within the vadose zone increases exponentially with soil moisture. However, the logistic regression model shown in Figure 21 indicates that leakage increases only up to a certain soil moisture threshold, beyond which then asymptotes, forming a horizontal line. This suggests that logistic regression captures the non-linear behavior of soil moisture and leakage more accurately than the exponential model. These findings imply that leakage modeling in such environments should consider models that account for non-linear responses to soil moisture changes, as traditional exponential models may overestimate leakage beyond certain moisture levels, leading to inaccurate predictions.

Lastly, the gap between the water balance approach used to capture the logistic regression and the theoretical leakage formula highlights that the traditional model (Liao et al. (2002), may not adequately capture the actual leakage dynamics in semiarid environments. Since the water balance approach, considers observed soil moisture values, this reveals discrepancies when compared to the theoretical predictions of the theoretical model. Moreover, the transition from exponential to asymptotic behavior in leakage modeling is significant. Exponential models such as the Liao et al. (2002) predict continuous, unbounded increases in leakage with increasing soil moisture, implying that leakage rates would escalate indefinitely as soil moisture rises. However, the logistic regression model suggests that leakage rates increase up to a certain threshold of soil moisture and then plateau. This asymptotic behavior indicates that beyond a certain soil moisture, additional increases do not result in proportional increases in leakage.

Leakage Estimates, *L* [mm]	*Upland Watershed*	*Downstream Playa*
P = -10%, ET = -25%, Q = -10%	-93	-10
P = -10%, ET = -25%, Q = +10%	-94	35
P = -10%, ET = No Change, Q = -10%	-246	-141
P = -10%, ET = No Change, Q = +10%	-247	-95
P = -10%, ET = +25%, Q = -10%	-399	-272
P = -10%, ET = +25%, Q = +10%	-400	-226
P = +10%, ET = -25%, Q = -10%	-8	32
P = +10%, ET = -25%, Q = +10%	-9	78
P = +10%, ET = No Change, Q = -10%	-161	-98
P = +10%, ET = No Change, Q = +10%	-162	-53
P = +10%, ET = +25%, Q = -10%	-314	-229
P = +10%, ET = +25%, Q = +10%	-315	-184

Table 9. Leakage derived from CRNS and other site instruments under different scenarios in precipitation (P), evapotranspiration (ET), and discharge (Q).

Leakage Estimates from CRNS and Site Instrumentation

Table 9 shows leakage estimates (L) derived from CRNS soil moisture values (θ_{CRNS}) under various error scenarios in precipitation (P), evapotranspiration (ET), and discharge (Q). These errors, expressed as percentages, reflect deviations from actual values in Table 4. The analysis reveals significant variability in leakage estimates for both the Upland Watershed and Downstream Playa across different scenarios.

For the Upland Watershed, leakage estimates range from -93 mm to -400 mm. For example, a -10% error in P, -25% error in ET, and -10% error in Q results in a leakage estimate of -93 mm, whereas a +10% error in P, +25% error in ET, and +10% error in Q results in a leakage estimate of -315 mm. Similarly, for the Downstream Playa, leakage estimates range from -10 mm to -272 mm. A scenario with -10% error in P, -25% error in ET, and -10% error in Q results in a leakage estimate of -10 mm, while a +10% error in P, +25% error in ET, and +10% error in Q results in -184 mm.

The most significant finding from Table 6 is the considerable impact that errors in P, ET, and Q have on leakage estimates. Two important factors need to be considered: (1) the changes in ET are higher (25% vs. 10%) than those in P and Q, and (2) ET magnitudes are much higher ($ET > P > Q$). Therefore, combining a higher percent change with a flux that has a higher magnitude naturally leads to more sensitivity in leakage estimates. Changes in precipitation influence leakage estimates, but their impact is less pronounced compared to ET. For instance, in the Upland Watershed, a -10% error in P with no change in ET and Q results in -246 mm of leakage, whereas a +10% error in P under the same conditions results in -161 mm of leakage. In the Downstream Playa, these

values are -141 mm and -98 mm, respectively. Errors in *ET* have the most substantial effect on leakage estimates. At the Upland Watershed, a -25% error in *ET* with no changes in *P* and *Q* results in -93 mm of leakage, while a +25% error results in -399 mm. Similarly, in the Downstream Playa, a -25% error in *ET* results in -10 mm of leakage, and a +25% error leads to -272 mm. The larger impact of *ET* changes is partly due to the higher percent change applied (25%) and the higher magnitude of *ET* compared to *P* and *Q*. Changes in discharge also affect leakage estimates, though to a lesser extent than *ET*. For the Upland Watershed, a -10% error in *Q* with no changes in *P* and *ET* results in -246 mm of leakage, while a +10% error results in -247 mm. In the Downstream Playa, these values are -141 mm and -95 mm, respectively.

In summary, the error estimates indicate that evapotranspiration (*ET*) has the most significant impact on leakage estimates for both the Upland Watershed and Downstream Playa, primarily due to the higher magnitude of *ET* and the larger percent changes applied. While precipitation (*P*) and discharge (*Q*) also influence leakage values, the changes induced by *ET* adjustments are more pronounced and consistent. This finding underscores the critical role of accurate ET measurement in hydrological studies and water balance assessments, particularly in semiarid environments where ET represents a major component of water loss.

CHAPTER 4

CONCLUSIONS AND FUTURE WORK

Summary

The Jornada Basin is characterized as an endorheic basin, composed of three distinct topographical regions, the mountain block, piedmont slope, and the basin floor. Due to the Jornada Basin being an internally draining basin, hydrologic fluxes are maintained within the three topographical regions. However, the hydrological fluxes received at location differ. At the mountain block, this region receives frequent precipitation events due to their proximity to the mountain range. As a byproduct of this, the region below the mountain block, the piedmont slope, is also within the region of the endorheic basin that is more frequently hydrologically active. However, in regions such as the basin floor, hydrological fluxes such as precipitation events are infrequent. Additionally, ephemeral playas located within the basin floor are hydrologically dormant in comparison to the regions of the endorheic basin with continuous hydrological presses. The water balance partitioning in areas such as the Upland Watershed have been thoroughly investigated to understand the hydrological connectivity occurring within this system. However, lowland regions such as the Downstream Playa, the hydrologically connectivity and its water balance partitioning to upland neighbors serves as an investigation gap needing to be filled. Thus, the purpose of this study was to be able to quantify the soil moisture dynamics within an upland region represented by the Upland Watershed and hydrologically active lowland region represented by the Downstream Playa. Additionally, the Downstream Playa is of particular interest due to its ability to inundate during large precipitation events allowing for the hydrological forcing within

each system to be analyzed, within the parameters of soil moisture dynamics. The objectives of this study were analyzed amongst three goals. The first being the calibration and validation of the Cosmic-Ray Neutron Sensor at the Upland Watershed and Downstream Playa utilizing various atmospheric correction factors and soil sample analysis. The second to characterize and analyze the changes in soil moisture between these two sites, amongst the backdrop of significant precipitation events, and lastly quantifying the impact of soil moisture dynamics on the water balance partitioning between both sites. These three objectives were accomplished over the 19-month study period, in which key findings highlighted the significant differences in how each site responds to water inputs and losses.

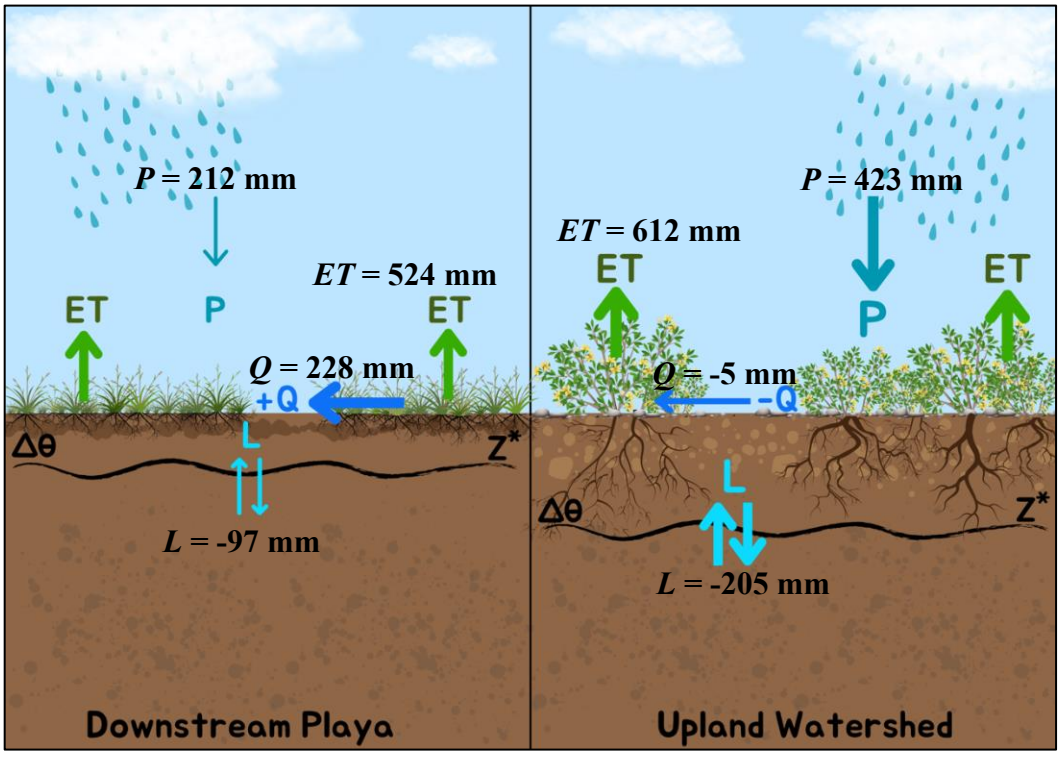

Figure 22. Cumulative Results of the Upland Watershed and Downstream Playa.

The cumulative results of each hydrological variable over the 19-month study period are summarized in Figure 22, with the most significant values being the total leakage derived at each site. At the Upland Watershed, for the 19-month study a negative value of leakage was produced (-205 mm), highlighting the extensive root plant water uptake occurring within this system over a 19-month drying period. In the Downstream Playa, a negative value for leakage is also, -97 mm. However, the distinct magnitudes of leakage derived from the soil water balance formula at both sites highlight their overall hydrological system. The Upland Watershed demonstrates a remarkable ability to continuously process hydrological pulses, as evidenced by the consistent patterns observed in cumulative CRNS fluxes, evapotranspiration (*ET*), and soil moisture changes. Additionally, the *ET/P* ratio of 1.44 for the Upland Watershed indicates that evapotranspiration (ET) exceeds precipitation, suggesting that during the study period, the watershed relied on subsurface water sources stored within the soil. Typically, in semiarid ecosystems without access to groundwater, *ET* is below *P*, indicating that precipitation generally exceeds evapotranspiration. Despite the high *ET* rate, the relatively stable soil water storage change ($\Delta\theta_{CRNS}/P$) and outflow ratio (*O/P*) suggest that the Upland Watershed effectively maintains its water resources. The watershed exhibits a water balance without extreme fluctuations, indicating a continuous working system capable of buffering against variable climatic conditions. This stability is likely attributed to a combination of factors, including soil properties, vegetation with deep root systems, and geomorphological features that facilitate efficient water infiltration and retention.

In contrast, the Downstream Playa displays a more dormant hydrological system processing monthly water balance variations, such as infrequent hydrological pulses like

inundation events. The sensitivity of the Downstream Playa to process hydrological pulses is also further supported cumulative daily CRNS (f_{CRNS}) fluxes and soil moisture changes, in which influxes such as the January 2024 precipitation events are to be fully captured within the soil water of the Downstream Playa. The *ET/P* ratio of 2.47 at the Downstream Playa points towards the systems to process only the significant hydrological pulses such as large precipitation events and inundations events and store them within the system. This is evident by the significantly large ET/P ratio, in which water from past precipitation events is being utilized to surplus the lack of precipitation naturally going within the system.

Although the Upland Watershed and Downstream Playa are not hydrologically connected due to their spatial separation within the endorheic basin, the behaviors observed at each site remain valid. The absence of an instrumented watershed hydrologically connected to the Downstream Playa is a limitation of this study. However, if the study were to be replicated, utilizing both the Upland Watershed and a hydrologically connected ephemeral playa subject to similar hydrological forcings, it is anticipated that the Upland Watershed would maintain its continuous hydrological behavior. Conversely, the hydrologically connected ephemeral playa would likely transition from infrequent hydrological pulses to a more continuous pressing system, similar to that observed at the Upland Watershed. This outcome is contingent upon the maintenance of the same soil clay type and perennial grass found at the Downstream Playa, despite the potential for excess leakage.

Future Work

The findings of this study emphasize the critical need for detailed, site-specific data collection approaches that account for the hydrologic variability within endorheic basins. This study has the ability to replicated in other semiarid environments or endorheic basins to further try to understand the hydrological connectivity between upland and lowland regions. The applicability of the Cosmic-Ray Neutron Sensing method has the advantage of being able to be applied in several environments, without any significant obstacles due to its low maintenance soil moisture measurements. Additionally, the three methods of calculating leakage within study are easily reproducible in other locations. However, the one obstacle for the reproducibility of this study is the implementation of sensor networks to be able to capture a weighted spatial footprint in the same manner as a CRNS. Thus, a spatially distributed weighted sensor network at various depths would need to be incorporated for new sites. Hydrologic models that incorporate the unique characteristics of upland and lowland regions can enhance the accuracy of our understanding of soil moisture dynamics within internally draining basins. Future research should focus on improving the resolution and precision of these models to better capture the complex interactions between precipitation (P), evapotranspiration (ET), and discharge in diverse environments. Furthermore, the use of spatially averaged Cosmic-Ray Neutron Sensing (CRNS) soil moisture measurements can improve our ability to downscale remotely sensed soil moisture data, which often have too coarse a resolution. This is particularly relevant in areas like the Jornada Basin, which features topographic elements such as ephemeral playas and channels. By

advancing these models and measurement techniques, our understanding of hydrological processes in semiarid environments can be significantly enhanced.

REFERENCES

Andreasen, M., Jensen, K. H., Desilets, D., Franz, T. E., Zreda, M., Bogena, H. R., & Looms, M. C. (2017). Status and Perspectives on the Cosmic-Ray Neutron Method for Soil Moisture Estimation and Other Environmental Science Applications. *Vadose Zone Journal*, *16*(8), 1–11. https://doi.org/10.2136/vzj2017.04.0086

Armesto, J. J., & Martinez, J. A. (1978). Relations Between Vegetation Structure and Slope Aspect in the Mediterranean Region of Chile. *The Journal of Ecology*, *66*(3), 881. https://doi.org/10.2307/2259301

Babaeian, E., & Tuller, M. (2023). Proximal sensing of evapotranspiration. In *Encyclopedia of Soils in the Environment* (pp. 610–617). Elsevier. https://doi.org/10.1016/B978-0-12-822974-3.00156-7

Bernhardt, E. S., Blaszczak, J. R., Ficken, C. D., Fork, M. L., Kaiser, K. E., & Seybold, E. C. (2017). Control Points in Ecosystems: Moving Beyond the Hot Spot Hot Moment Concept. *Ecosystems*, *20*(4), 665–682. https://doi.org/10.1007/s10021-016-0103-y

Chrisman, B., & Zreda, M. (2013a). Quantifying mesoscale soil moisture with the cosmic-ray rover. *Hydrology and Earth System Sciences*, *17*(12), 5097–5108. https://doi.org/10.5194/hess-17-5097-2013

Daniel, D. W., Smith, L. M., McMurry, S. T., Tangen, B. A., Dahl, C. F., Euliss Jr., N. H., & LaGrange, T. (2019). Effects of Land Use on Greenhouse Gas Flux in Playa Wetlands and Associated Watersheds in the High Plains, USA. *Agricultural Sciences*, *10*(02), 181–201. https://doi.org/10.4236/as.2019.102016

Delworth, T. L., & Manabe, S. (1988). The Influence of Potential Evaporation on the Variabilities of Simulated Soil Wetness and Climate. *Journal of Climate*, *1*(5), 523–547. https://doi.org/10.1175/1520-0442(1988)001<0523:TIOPEO>2.0.CO;2

Desilets, D., & Zreda, M. (2013). Footprint diameter for a cosmic-ray soil moisture probe: Theory and Monte Carlo simulations. *Water Resources Research*, *49*(6), 3566–3575. https://doi.org/10.1002/wrcr.20187

Desilets, D., Zreda, M., & Ferré, T. P. A. (2010). Nature's neutron probe: Land surface hydrology at an elusive scale with cosmic rays. *Water Resources Research*, *46*(11). https://doi.org/10.1029/2009WR008726

Dong, J., Ochsner, T. E., Zreda, M., Cosh, M. H., & Zou, C. B. (2014). Calibration and Validation of the COSMOS Rover for Surface Soil Moisture Measurement. *Vadose Zone Journal*, *13*(4), 1–8. https://doi.org/10.2136/vzj2013.08.0148

Dorsaz, J., Gironás, J., Escauriaza, C., & Rinaldo, A. (2013). The geomorphometry of endorheic drainage basins: implications for interpreting and modelling their evolution. *Earth Surface Processes and Landforms*, *38*(15), 1881–1896. https://doi.org/10.1002/esp.3475

Duffy, C. J., & Al-Hassan, S. (1988a). Groundwater circulation in a closed desert basin: Topographic scaling and climatic forcing. *Water Resources Research*, *24*(10), 1675–1688. https://doi.org/10.1029/WR024i010p01675

Dugas, W. A., Hicks, R. A., & Gibbens, R. P. (1996). Structure and function of C3and C4Chihuahuan Desert plant communities. Energy balance components. *Journal of Arid Environments*, *34*(1), 63–79. https://doi.org/10.1006/jare.1996.0093

Duniway, M. C., Petrie, M. D., Peters, D. P. C., Anderson, J. P., Crossland, K., & Herrick, J. E. (2018). Soil water dynamics at 15 locations distributed across a desert landscape: insights from a 27-yr dataset. *Ecosphere*, *9*(7). https://doi.org/10.1002/ecs2.2335

Entin, J. K., Robock, A., Vinnikov, K. Y., Hollinger, S. E., Liu, S., & Namkhai, A. (2000). Temporal and spatial scales of observed soil moisture variations in the extratropics. *Journal of Geophysical Research: Atmospheres*, *105*(D9), 11865–11877. https://doi.org/10.1029/2000JD900051

Famiglietti, J. S., Ryu, D., Berg, A. A., Rodell, M., & Jackson, T. J. (2008). Field observations of soil moisture variability across scales. *Water Resources Research*, *44*(1). https://doi.org/10.1029/2006WR005804

Francke, T., Heistermann, M., Köhli, M., Budach, C., Schrön, M., & Oswald, S. E. (2022). Assessing the feasibility of a directional cosmic-ray neutron sensing sensor for estimating soil moisture. *Geoscientific Instrumentation, Methods and Data Systems*, *11*(1), 75–92. https://doi.org/10.5194/gi-11-75-2022

Franz, T. E., Wahbi, A., Vreugdenhil, M., Weltin, G., Heng, L., Oismueller, M., Strauss, P., Dercon, G., & Desilets, D. (2016). Using Cosmic-Ray Neutron Probes to Monitor Landscape Scale Soil Water Content in Mixed Land Use Agricultural Systems. *Applied and Environmental Soil Science*, *2016*, 1–11. https://doi.org/10.1155/2016/4323742

Franz, T. E., Zreda, M., Rosolem, R., & Ferre, T. P. A. (2012). Field Validation of a Cosmic-Ray Neutron Sensor Using a Distributed Sensor Network. *Vadose Zone Journal*, *11*(4). https://doi.org/10.2136/vzj2012.0046

Franz, T. E., Zreda, M., Rosolem, R., Hornbuckle, B. K., Irvin, S. L., Adams, H., Kolb, T. E., Zweck, C., & Shuttleworth, W. J. (2013). Ecosystem-scale measurements of biomass water using cosmic ray neutrons. *Geophysical Research Letters*, *40*(15), 3929–3933. https://doi.org/10.1002/grl.50791

Gao, Q., & Reynolds, J. F. (2003). Historical shrub–grass transitions in the northern Chihuahuan Desert: modeling the effects of shifting rainfall seasonality and event size over a landscape gradient. *Global Change Biology*, *9*(10), 1475–1493. https://doi.org/10.1046/j.1365-2486.2003.00676.x

Gibbens, R. P., & Lenz, J. M. (2001). Root systems of some Chihuahuan Desert plants. *Journal of Arid Environments*, *49*(2), 221–263. https://doi.org/10.1006/jare.2000.0784

Gibbens, R. P., McNeely, R. P., Havstad, K. M., Beck, R. F., & Nolen, B. (2005). Vegetation changes in the Jornada Basin from 1858 to 1998. *Journal of Arid Environments*, *61*(4), 651–668. https://doi.org/10.1016/j.jaridenv.2004.10.001

GOULDEN, M. L., MUNGER, J. W., FAN, S., DAUBE, B. C., & WOFSY, S. C. (1996). Measurements of carbon sequestration by long-term eddy covariance: methods and a critical evaluation of accuracy. *Global Change Biology*, *2*(3), 169–182. https://doi.org/10.1111/j.1365-2486.1996.tb00070.x

Guswa, A. J., Celia, M. A., & Rodriguez-Iturbe, I. (2002). Models of soil moisture dynamics in ecohydrology: A comparative study. *Water Resources Research*, *38*(9). https://doi.org/10.1029/2001WR000826

Gutiérrez-Jurado, H. A., Vivoni, E. R., Cikoski, C., Harrison, J. B. J., Bras, R. L., & Istanbulluoglu, E. (2013). On the observed ecohydrologic dynamics of a semiarid basin with aspect-delimited ecosystems. *Water Resources Research*, *49*(12), 8263–8284. https://doi.org/10.1002/2013WR014364

Gutiérrez-Jurado, H. A., Vivoni, E. R., Istanbulluoglu, E., & Bras, R. L. (2007). Ecohydrological response to a geomorphically significant flood event in a semiarid catchment with contrasting ecosystems. *Geophysical Research Letters*, *34*(24). https://doi.org/10.1029/2007GL030994

Holah, J. C., & Alexander, H. M. (1999). Soil pathogenic fungi have the potential to affect the co-existence of two tallgrass prairie species. *Journal of Ecology*, *87*(4), 598–608. https://doi.org/10.1046/j.1365-2745.1999.00383.x

Howes, D. A., & Abrahams, A. D. (2003). Modeling runoff and runon in a desert shrubland ecosystem, Jornada Basin, New Mexico. *Geomorphology*, *53*(1–2), 45–73. https://doi.org/10.1016/S0169-555X(02)00347-1

Huenneke, L. F., Anderson, J. P., Remmenga, M., & Schlesinger, W. H. (2002). Desertification alters patterns of aboveground net primary production in Chihuahuan ecosystems. *Global Change Biology*, *8*(3), 247–264. https://doi.org/10.1046/j.1365-2486.2002.00473.x

Ingersoll, R. v. (2001). Structural and Stratigraphic Evolution of the Rio Grande Rift, Northern New Mexico and Southern Colorado. *International Geology Review*, *43*(10), 867–891. https://doi.org/10.1080/00206810109465053

Iwema, J., Rosolem, R., Baatz, R., Wagener, T., & Bogena, H. (2015). Investigating temporal field sampling strategies for site-specific calibration of three soil moisture–neutron intensity parameterisation methods. *Hydrology and Earth System Sciences*, 19(7), 3203-3215. https://doi.org/10.5194/HESS-19-3203-2015

Ivanov, V. Y., Bras, R. L., & Vivoni, E. R. (2008). Vegetation-hydrology dynamics in complex terrain of semiarid areas: 2. Energy-water controls of vegetation spatiotemporal dynamics and topographic niches of favorability. *Water Resources Research*, *44*(3). https://doi.org/10.1029/2006WR005595

Jayawardena, R., Ranasinghe, P., Ranawaka, H., Gamage, N., Dissanayake, D., & Misra, A. (2020). Exploring the therapeutic benefits of Pranayama (yogic breathing): A systematic review. *International Journal of Yoga*, *13*(2), 99. https://doi.org/10.4103/ijoy.IJOY_37_19

Jiménez-Bonilla, A., Díaz-Azpiroz, M., & Rodríguez, M. R. (2023). Tectonics may affect closed watersheds used to monitor climate change and human activity effects. *Terra Nova*, *35*(1), 58–65. https://doi.org/10.1111/ter.12629

Kimsal, C. R. (2023). *Hydrologic dynamics of dryland playas and their catchments in the Chihuahuan Desert* (Master's thesis). Arizona State University.

Kizito, F., Dragila, M. I., Senè, M., Brooks, J. R., Meinzer, F. C., Diedhiou, I., Diouf, M., Lufafa, A., Dick, R. P., Selker, J., & Cuenca, R. (2012). Hydraulic redistribution by two semi-arid shrub species: Implications for Sahelian agro-ecosystems. *Journal of Arid Environments*, *83*, 69–77. https://doi.org/10.1016/j.jaridenv.2012.03.010

Köhli, M., Schrön, M., Zreda, M., Schmidt, U., Dietrich, P., & Zacharias, S. (2015). Footprint characteristics revised for field-scale soil moisture monitoring with cosmic-ray neutrons. *Water Resources Research*, *51*(7), 5772–5790. https://doi.org/10.1002/2015WR017169

Kurc, S. A., & Small, E. E. (2004). Dynamics of evapotranspiration in semiarid grassland and shrubland ecosystems during the summer monsoon season, central New Mexico. *Water Resources Research*, *40*(9). https://doi.org/10.1029/2004WR003068

Lv, L., Franz, T. E., Robinson, D. A., & Jones, S. B. (2014). Measured and Modeled Soil Moisture Compared with Cosmic-Ray Neutron Probe Estimates in a Mixed Forest. *Vadose Zone Journal*, *13*(12), 1–13. https://doi.org/10.2136/vzj2014.06.0077

Malek, E., Bingham, G. E., & McCurdy, G. D. (1990). Evapotranspiration from the margin and moist playa of a closed desert valley. *Journal of Hydrology*, *120*(1–4), 15–34. https://doi.org/10.1016/0022-1694(90)90139-O

McColl, K. A., Alemohammad, S. H., Akbar, R., Konings, A. G., Yueh, S., & Entekhabi, D. (2017). The global distribution and dynamics of surface soil moisture. *Nature Geoscience*, *10*(2), 100–104. https://doi.org/10.1038/ngeo2868

McJannet, D., Franz, T., Hawdon, A., Boadle, D., Baker, B., Almeida, A., Silberstein, R., Lambert, T., & Desilets, D. (2014). Field testing of the universal calibration function for determination of soil moisture with cosmic-ray neutrons. *Water Resources Research*, *50*(6), 5235–5248. https://doi.org/10.1002/2014WR015513

McJannet, D. L., & Desilets, D. (2023). Incoming neutron flux corrections for cosmic-ray soil and snow sensors using the global neutron monitor network. *Water Resources Research, 59*(4), Article e2022WR033889. https://doi.org/10.1029/2022WR033889

McKenna, O. P., & Sala, O. E. (2018). Playa-Wetlands Effects on Dryland Biogeochemistry: Space and Time Interactions. *Journal of Geophysical Research: Biogeosciences*, *123*(6), 1879–1887. https://doi.org/10.1029/2017JG004176

Menking, K. M., Anderson, R. Y., Brunsell, N. A., Allen, B. D., Ellwein, A. L., Loveland, T. A., & Hostetler, S. W. (2000). Evaporation from groundwater discharge playas, Estancia Basin, central New Mexico. *Global and Planetary Change*, *25*(1–2), 133–147. https://doi.org/10.1016/S0921-8181(00)00025-4

Mueller, E. N., Wainwright, J., & Parsons, A. J. (2008). Spatial variability of soil and nutrient characteristics of semi-arid grasslands and shrublands, Jornada Basin, New Mexico. *Ecohydrology*, *1*(1), 3–12. https://doi.org/10.1002/eco.1

Muldavin, E. H., Moore, D. I., Collins, S. L., Wetherill, K. R., & Lightfoot, D. C. (2008). Aboveground net primary production dynamics in a northern Chihuahuan Desert ecosystem. *Oecologia*, *155*(1), 123–132. https://doi.org/10.1007/s00442-007-0880-2

Nguyen, H. H., Kim, H., & Choi, M. (2017). Evaluation of the soil water content using cosmic-ray neutron probe in a heterogeneous monsoon climate-dominated region. *Advances in Water Resources*, *108*, 125–138. https://doi.org/10.1016/j.advwatres.2017.07.020

Nichols, G. (2011). Endorheic Basins. In *Tectonics of Sedimentary Basins* (pp. 621–632). Wiley. https://doi.org/10.1002/9781444347166.ch31

Pérez-Ruiz, E. R., Vivoni, E. R., & Sala, O. E. (2022). Seasonal carryover of water and effects on carbon dynamics in a dryland ecosystem. *Ecosphere*, *13*(7). https://doi.org/10.1002/ecs2.4189

Peters, D. P. C., Yao, J., Sala, O. E., & Anderson, J. P. (2012). Directional climate change and potential reversal of desertification in arid and semiarid ecosystems. *Global Change Biology*, *18*(1), 151–163. https://doi.org/10.1111/j.1365-2486.2011.02498.x

Prein, A. F., Towler, E., Ge, M., Llewellyn, D., Baker, S., Tighi, S., & Barrett, L. (2022). Sub-Seasonal Predictability of North American Monsoon Precipitation. *Geophysical Research Letters*, *49*(9). https://doi.org/10.1029/2021GL095602

Rivera Villarreyes, C. A., Baroni, G., & Oswald, S. E. (2013). Calibration approaches of cosmic-ray neutron sensing for soil moisture measurement in cropped fields. *Hydrology and Earth System Sciences Discussions*, 10(4), 4237-4275. https://doi.org/10.5194/HESSD-10-4237-2013

Rodriguez-Iturbe, I. (2000). Ecohydrology: A hydrologic perspective of climate-soil-vegetation dynamics. In *Ecohydrological Perspectives of the Earth System* (pp. 23-41). Cambridge University Press. https://doi.org/10.1017/CBO9780511535727

Rosen, M. R. (1994). The importance of groundwater in playas: A review of playa classifications and the sedimentology and hydrology of playas. In M. R. Rosen (Ed.), Paleoclimate and Basin Evolution of Playa Systems (pp. 1-18). Geological Society of America. https://doi.org/10.1130/SPE289-p1

Rosolem, R., Shuttleworth, W. J., Zreda, M., Franz, T. E., Zeng, X., & Kurc, S. A. (2013). The Effect of Atmospheric Water Vapor on Neutron Count in the Cosmic-Ray Soil Moisture Observing System. *Journal of Hydrometeorology*, *14*(5), 1659–1671. https://doi.org/10.1175/JHM-D-12-0120.1

Schreiner-McGraw, A. P., Vivoni, E. R., Mascaro, G., & Franz, T. E. (2016). Closing the water balance with cosmic-ray soil moisture measurements and assessing their relation to evapotranspiration in two semiarid watersheds. *Hydrology and Earth System Sciences*, *20*(1), 329–345. https://doi.org/10.5194/hess-20-329-2016

Schreiner-McGraw, A. P. (2017). *Deep percolation in arid piedmont watersheds and its sensitivity to ecosystem change* (Doctoral dissertation). Arizona State University.

Schrön, M., Köhli, M., Scheiffele, L., Iwema, J., Bogena, H. R., Lv, L., Martini, E., Baroni, G., Rosolem, R., Weimar, J., Mai, J., Cuntz, M., Rebmann, C., Oswald, S. E., Dietrich, P., Schmidt, U., & Zacharias, S. (2017). Improving calibration and validation of cosmic-ray neutron sensors in the light of spatial sensitivity. *Hydrology and Earth System Sciences*, *21*(10), 5009–5030. https://doi.org/10.5194/hess-21-5009-2017

Schrön, M., Oswald, S. E., Zacharias, S., Kasner, M., Dietrich, P., & Attinger, S. (2021). Neutrons on Rails: Transregional Monitoring of Soil Moisture and Snow Water Equivalent. *Geophysical Research Letters*, *48*(24). https://doi.org/10.1029/2021GL093924

Smith, L.M. (2003). *Playas of the Great Plains*. Austin, TX: University of Texas Press.

Snyder, K. A., Mitchell, K. A., & Herrick, J. E. (2006). Patterns and controls of soil water in the Jornada Basin. In K. M. Havstad, L. F. Huenneke, & W. H. Schlesinger (Eds.), *Structure and function of Chihuahuan Desert ecosystem: The Jornada Basin long-term ecological research site* (pp. 107-132). Oxford University Press

Templeton, R. (2011). *Insights on seasonal fluxes in a desert shrubland watershed* (master's thesis). Arizona State University.

Vivoni, E. R., Moreno, H. A., Mascaro, G., Rodriguez, J. C., Watts, C. J., Garatuza-Payan, J., & Scott, R. L. (2008). Observed relation between evapotranspiration and soil moisture in the North American monsoon region. *Geophysical Research Letters*, *35*(22). https://doi.org/10.1029/2008GL036001

Wang, J., Song, C., Reager, J. T., Yao, F., Famiglietti, J. S., Sheng, Y., MacDonald, G. M., Brun, F., Schmied, H. M., Marston, R. A., & Wada, Y. (2018). Recent global decline in endorheic basin water storages. *Nature Geoscience*, *11*(12), 926–932. https://doi.org/10.1038/s41561-018-0265-7

Wang, K., & Dickinson, R. E. (2012). A review of global terrestrial evapotranspiration: Observation, modeling, climatology, and climatic variability. In *Reviews of Geophysics* (Vol. 50, Issue 2). Blackwell Publishing Ltd. https://doi.org/10.1029/2011RG000373

Vieira Lima, B., Caldeira, A. G., Ferreira de Souza, A. E., Mendes, R. M., & others. (2023). Reply on RC2. *Peer Review*. https://typeset.io/papers/reply-on-rc2-n98k042d

Xie, Z., & Rosolem, R. (2017). Impact of multi-day field calibration of novel cosmic-ray soil moisture sensors. *Proceedings of IEEE Sensors*, 2017, 8234232. https://doi.org/10.1109/ICSENS.2017.8234232

Zreda, M., Desilets, D., Ferré, T. P. A., & Scott, R. L. (2008). Measuring soil moisture content non-invasively at intermediate spatial scale using cosmic-ray neutrons. *Geophysical Research Letters*, *35*(21), L21402. https://doi.org/10.1029/2008GL035655

Zreda, M., Shuttleworth, W. J., Zeng, X., Zweck, C., Desilets, D., Franz, T., & Rosolem, R. (2012). COSMOS: the COsmic-ray Soil Moisture Observing System. *Hydrology and Earth System Sciences*, *16*(11), 4079–4099. https://doi.org/10.5194/hess-16-4079-2012

APPENDIX A

WATER BALANCE TABLES

WATER BALANCE TABLES

This appendix describes a digital repository of the WATER BALANCE TABLES for the Upland Watershed and Downstream Playa. The datasets are organized within the digital folder "RubyYHurtado_Thesis Data/APPENDIX_A"

- The following Excel files contains the water balance variables: precipitation (P), evapotranspiration (ET), Streamflow (Q), leakage (L), and CRNS fluxes (f_{CRNS}) all on a daily time scale.

File Name	File Description
Appendix_A_UplandWatershed.xlsx	Daily: soil moisture, precipitation, evapotranspiration, streamflow, leakage, CRNS flux
Appendix_A_DownstreamPlaya.xlsx	Daily: soil moisture, precipitation, evapotranspiration, streamflow, leakage, CRNS flux

APPENDIX B

GIS DATASETS

GIS DATASETS

This appendix describes a digital repository of the GIS datasets for the Upland Watershed and Downstream Playa. The datasets are organized within the digital folder "RubyYHurtado_Thesis Data/APPENDIX_B"

- The following GIS shapefiles contains the information used in all of the maps, as well as the soil sample locations for both the Upland Watershed and Downstream Playa.

File Name	File Description
TrombleWeir_CRNS (GIS file extensions)	Upland Watershed CRNS locatoin
UW_CRNSFootprint (GIS file extensions)	Upland Watershed CRNS footprint location
UW_TransectSoilSensor (GIS file extensions)	Upland Watershed transect soil sensor locations (transect 1, transect 2, transect 3)
UW_WatershedOutline (GIS file extensions)	Upland Watershed boundary outline
UW_RunoffPlots (GIS file extensions)	Upland Watershed runoff plots 1 - 4
UW_RainGauges (GIS file extensions)	Upland Watershed rain gauges 1 - 3
UW_ET_Tower (GIS file extensions)	Upland Watershed ET tower location
ChannelSoilSensors (GIS file extensions)	Channel 2 soil sensors at the Upland Watershed
UW_OutletFlume (GIS file extensions)	Upland Watershed outlet flume location

PSMAL_CRNS (GIS file extensions)	Downstream Playa CRNS location
PSMAL_CRNSFootprint (GIS file extensions)	Downstream Playa CRNS footprint
Playa_Outline (GIS file extensions)	Downstream Playa outline
Restricted_Area (GIS file extensions)	Downstream Playa restricted area within the playa.
PSMAL_SoilTransect (GIS file extensions)	Downstream Playa soil transects (<5m, center of playa and outside of playa).
DP_RainGauge (GIS file extensions)	Downstream Playa rain gauge
DP_ET_Tower (GIS file extensions)	Downstream Playa ET tower location
JLTERBoundaries (GIS file extensions)	Jornada Experimental Range boundary line and Chihuahuan Desert Rangeland Research Center
UW_SoilSampleLocations (GIS file extensions)	Upland Watershed soil sample locations for gravimetric sampling
UW_RadialSensitivityLocations (GIS file extensions)	Upland Watershed radial sensitivity locations
DP_SoilSampleLocations (GIS file extensions)	Downstream Playa soil sample locations for gravimetric sampling
DP_RadialSensitivityLocations (GIS file extensions)	Downstream Playa radial sensitivity locations

APPENDIX C

MATLAB SCRIPTS

MATLAB SCRIPTS

This appendix describes a digital repository of the MATLAB scripts for the Upland Watershed and Downstream Playa. The datasets are organized within the digital folder "RubyYHurtado_Thesis Data/APPENDIX_C"

- The following MATLAB scripts calculate the various variables water balance variables used in this study.
- The MATLAB script included below the table include the **CRNS calibration** for the Upland Watershed and Downstream Playa labeled: "Upland Watershed CRNS Calibration" and "Downstream Playa CRNS Calibration".
- Additional MATLAB scripts include the "Upland Watershed – Weighted Sensor Network" and "Downstream Playa – Weighted Sensor Network" which calculates the vertical and horizontal weighting formulas applied.

File Name	File Description
Calibration_TW.mat	Upland Watershed CRNS calibration contains the Equation 1 – Equation 8 needed to convert raw neutron counts to **CRNS soil moisture values.** (1- hour and 30-minute temporal scale)
Calibration_FinalPS.mat	Downstream Playa CRNS calibration contains the Equation 1 – Equation 8 needed to convert raw neutron counts to **CRNS soil moisture values**. (1- hour and 30-minute temporal scale)
DepthWeightedAverages_TW.mat	Upland Watershed weighted sensor network script to combine all soil sensors into the vertically and horizontally weighted **Sensor Network soil moisture values.** (1- hour and 30-minute temporal scale)
DepthWeightedAverages_PS.mat	Downstream Playa weighted sensor network script to combine all soil sensors into the vertically and horizontally

	weighted **Sensor Network soil moisture values.** (1- hour and 30-minute temporal scale)
TW_PrecipCalculation.mat	Upland Watershed precipitation script to convert the three rain gauges into spatially averaged **Precipitation (*P*)** total values in mm. (1- hour and 30-minute temporal scale).
PSMAL_PrecipCalculation.mat	Downstream Playa precipitation script to convert the one rain gauge into **Precipitation (*P*)** total values in mm. (1- hour and 30-minute temporal scale)
TW_RainfallDuration_SMPulse.mat	Upland Watershed script to calculate rainfall duration and soil moisture pulse duration.
PS_RainfallDuration_SMPulse.mat	Downstream Playa script to calculate rainfall duration and soil moisture pulse duration.
WaterBalanceCalculation.mat	Script to calculate daily and monthly **leakage, monthly sum storage, soil and water loss ratios** for the Upland Watershed and Downstream Playa.
Cleaned_SchreinerFluxCRNS.mat	**CRNS flux calculation** script for the Upland Watershed and Downstream Playa.
ConfidenceBounds.mat	Prediction intervals and confidence bounds calculation script for the Upland Watershed and Downstream Playa.
ET_SoilMoisture.mat	Calculate **hourly and daily CRNS and weighted Sensor Network** statistic metrics for the Upland Watershed and Downstream Playa.

Upland Watershed – CRNS Calibration

% % % % Trenton Franz

```
% % % % 03/10/2022
% % % %
% % % % Main program to read in CRNS from Las Cruces, New Mexico. Based off of
% % % other codes so a bit of piecemeal code.
%%% Collaborators: Trenton Franz, Ruby Hurtado
%%%%Tromble Weir Watershed
clear all;
close all;
clc;

%Field name: Tromble Weir Watershed

%%%%Excel file input converted to a txt for ease of use, Excel file
%%%%provided by Ruby Hurtado

%%% Year     Month, Day,    Day_Fraction, N1Cts, T1_C,  P4_mb,          RH1
%%% Date Range of Calibration: 06/27/22 to 07/11/22
data_calib= readmatrix('updated_watershed01312024.csv'); %Updated from 06/2022 to
06/2023
%data = dataMatrix; %long term data series from 2013 to 2023

%%%%% Year, Month, Day,Day_Fraction
tdat=datenum(data_calib(:,1),data_calib(:,2),data_calib(:,3)+data_calib(:,4));
%check_date = datetime(tdat,'ConvertFrom','datenum');
%jday=data(:,5);


n1=data_calib(:,5);  %%epithermal counts
t7=data_calib(:,6);   %external temp. (deg C)
p4=data_calib(:,7);   %external pressure (mb)
h7=data_calib(:,8);   %external RH (%)


%%%%%REMOVE BAD COUNTS: from min and max bounds
n1(find(n1>8000|n1<100))=nan; %epithermal counts
t7(find(t7>80|t7<-50))=nan; %external temp
p4(find(p4>1100|p4<400))=nan; %externall pressure (mb)
h7(find(h7>105|h7<0))=nan; %external RH


%%%%%%%Probe location in field you can use google
%%%%earth to find in units of WGS84 and MASL
csx=-106.606028;  %%%Longitude
csy= 32.585458;  %%%Lattitude
elev=1458;       %%%Elevation
```

```
%%%Location Specific Parameters
pref=849;       %%%Reference air pressure (mb, hpa), scaling factor from COSMOS
online calculator using center pivot lat, long and elev.
(http://cosmos.hwr.arizona.edu/Util/calculator.php)
CSF=3.131;      %%%Scaling factor from COSMOS online calculator using lat, long,
elev. Not cutoff rigidity factor!!!!!!!!

%%Atmosphere
tref=25;          %%%Reference air temperature (Deg. C)
rhref=0;          %%%Reference air relative humidity (%) Roselem 2013
gama=6.7;         %%%Temperature lapse-rate (monthly climatology): Source Zweck et
al. 2011
lambda=130;       %%%Attenuation rate for North America

%%
% % % % % % Soil Site Average from guesses or chemistry sampling!!!!!
lw=0.003;             %%%Lattice water, (g/g)   (Primary & Supple Characterization NPP
Reports)  (0.0027)
soc=0.001;          %%%Soil organic carbon water equivalent (g/g)
bda=1.3;           %%%Soil bulk density (g/cm3) from first sampling jan/30/2021
%bda2=1.087;            %%%Soil bulk density (g/cm3) from second sampling oct/22/2021
%bda3=1.332;            %%%Soil bulk density (g/cm3) from third sampling may/23/2022
%bda=(bda1+bda2+bda3)/3;
tao=lw+soc;           %%%%Soil water sum(g/g)

%%Set upper bound to porosity
%por=((1-bda1/2.65)+(1-bda2/2.65))/2; %Necessary for multiple soil bulk to
%porosity correlations
por=((1-bda/2.65));

%%%%%%%%%%%%%%%%%%%%%%%%%%%%%%%%%%%%%%%%%%%%%%%%%%%%%%%%%%%%%%%%%%%%%%%%

%%%Calibration Data
swc1=0.03958;  %%%%(in g/g)  %%%calibration data
cd1=datenum(2022,07,11,13,0,0);  %%%Start of calibration, add 6 hours for average
tw1=(swc1+tao);    %%%%Total water for calibration (g/g)
%tw1=(swc1);    %%%%Total water for calibration (g/g)
%DECEMBER CALIBRATION

%%summary of calibration
cds=[cd1]';
swcs=[swc1*bda]'; %%% cm3/cm3

% cds=[cd1 cd2 cd3 cd4 cd5 cd6 cd7 cd8]';
```

```
% swcs=[swc1*bda swc2*bda swc3*bda swc4*bda swc5*bda swc6*bda swc7*bda
swc8*bda]'; %%% cm3/cm3
%%


%%%%%%%%%%%%%%%%%%%%%%%%%%%%%%%%%%%%%%%%%%%%%%%%%%%%%%%%%%%%%%%%%%%%
Pipe in data to find CI from Nearfield database and Jung. NMB
%%%%%%%%%%%%%%%%%%%%%%%%%%%%%%%%%%%%%%%%%%%%%%%%%%%%%%%%%%%%%%%%%%%%

url = 'https://nearfld.com/reguser/unl_2/data.php?tz=-
0:00&vw=`tb_UNL9`&IM=300234062531270&fn=IMEI_1270&pn=';
% % % c1, n1, n2, p1, b1, h7, h8, p3, p4, t7, t9, NMcounts, fbar, fhum, fsol, SMv

options = weboptions('Timeout',500,'CertificateFileName','');
fullfile(matlabroot,'sys','certificates','ca','rootcerts.pem');
data_calib = webread(url,options);
data1 = data_calib(149:(length(data_calib)-15));
data2 = textscan(data1,'%s %u %u %f %f %f %f %f %f %f %f %f %f %f
%f<br>','Delimiter',',','EmptyValue', Inf);
date = flipud(data2{1});
fsol = flipud(data2{15});


clearvars data data1 data2;

tdat2=datenum(date); %%%%Convert to matlab days
INTEN = 1./fsol;     %%%%%%%Intensity Correction Factor, inverse from fsol from
HydroInnova database !!!!!!
Level2.TIME=tdat2;
Level2.INTEN=INTEN;

for i = 1:length(tdat)
   dum = abs(tdat(i) - Level2.TIME);
   mind= min(dum);
   ind = find(mind == dum);

   if ~isempty(ind)
      CI(i,1) = Level2.INTEN(ind(1)); %%% Intensity Correction Factor
   else
      CI(i,1) = NaN; % Set CI(i,1) to NaN if ind is empty
   end

   clear dum mind ind
end
```

```
CI(find(CI>1.5)) = NaN;



%%%%%%%%%%%%%%%%%%%%%%%%%%%%%%%%%%%%%%%%%%%%%%%%%%%%%%%%%%%%%%%%%%%%%%%%

%%Variations in water vapor, See Rosolem 2013 J. Hydromet
rhovref=calculate_watervapor(tref,pref,rhref,gama); %%%Temp(C), Press(hPa/mb),
RH(%)

Text=t7;
Pext=p4;
RHext=h7;
Mod=n1;

[rhov,iwv]=calculate_watervapor(Text,Pext,RHext,gama); %%%Temp(C),
Press(hPa/mb), RH(%), gama
CWV=1.0+0.0054*(rhov-rhovref)*1000;  %%%%correction in g/m3!!!!
mean_CWV= mean(CWV);

%mean_rhov=mean(rhov);

%%Pressure variations against the specified average, See Zreda 2012 HESS
Cp=exp((Pext-pref)/lambda);
mean_cp=mean(Cp);

%%%Corrected Counts to reference atmospheric pressure
Nc=Mod.*CWV./CI.*Cp./CSF;

%Nc = (Mod .* CWV ./ CI) .* (Cp ./ CSF);

%%Find counts for calibration
ind21=find(tdat>cd1-8/24 & tdat<=(cd1+8/24));
Ncal1=nanmean(Nc(ind21));
%%%Summary stats
SumN(1,:)=[nanmean(Nc(ind21)) nanmedian(Nc(ind21)) length(ind21)
(nansum(Nc(ind21))^0.5)/nansum(Nc(ind21))
nanmean(Nc(ind21))*((nansum(Nc(ind21)))^0.5)/nansum(Nc(ind21))];

%%%Calculate N0 values
N0i(1,:)=Ncal1/(0.0808/(tw1+0.115)+0.372);   %%%%N0 (cph)

N0d=mean(N0i);
% N0std=std(N0i);
```

```
%%%Average Values over certain time period
%%%Starting and ending date of cosmos data rounding to closest hour value
st=datenum(2022, 07, 01, 0, 0, 0);    %%Starting date   Ajustar a fechas
en=datenum(2024, 01, 31, 0, 0, 0);    %%%Ending date
% en=ceil(now);    %%%Ending date

int=1/24;  %%%interval in days
ti=[st:int:en]';


% %%%Standing Wet Biomass Values, Biomass Water Content Values, Dates
%TIME AVERAGING
int=1/24;  %%%interval in days for time averaging
tii=[st:int:en]';

N0=N0d;

%%%Compute time average data
for i=1:length(tii)-1
   %%%Neutron Count in Time Interval
   ind1=find(tdat>=tii(i) & tdat<tii(i+1));

   Ncdum=nanmean(Nc(ind1));
%      Baredum=nanmean(Bare(ind1));
      %N0dum=nanmean(N0(ind1));
      %bwedum=nanmean(bwe(ind1));
%      TFRdum=nanmean(TFR(ind1));

    Textdum=nanmean(Text(ind1));
    Pextdum=nanmean(Pext(ind1));
    RHextdum=nanmean(RHext(ind1));


    SWC=((0.0808/(Ncdum/N0-.372)-0.115)-tao)*bda;  %(lattice water + organic carbon)
    %SWC=((0.0808/(Ncdum/N0-.372)-0.115))*bda;  %%%%

    if SWC>por
       SWC=por;
    end

    if ~isempty(ind1)
%         sswc(i,:)=[(tii(i)+tii(i+1))/2 Ncdum N0dum Baredum TFRdum Textdum
Pextdum RHextdum SWC];
       sswc_tw(i,:)=[(tii(i)+tii(i+1))/2 Ncdum N0 Textdum Pextdum RHextdum SWC];
    else
```

```
        sswc_tw(i,:)=[(tii(i)+tii(i+1))/2 nan nan nan nan nan nan ];
    end

    clear ind1 Ncdum N0dum SWC

end

%% Gap-filling: Linear interpolation if tgap <= 3 hours, and interpolation based on
previous/next 15 days if tgap > 3 hours
% forcing is the data matrix forcing(time,variables)
npoints = 24; % 24 data points per day
nshortmax = 3; % short gap size
ndayslong = 3; % long-gap analysis window

forcing=sswc_tw(:,2:7);

[Xforc,IDXforc] = GapFill(forcing',npoints,nshortmax,ndayslong,-
999999,999999,'forcing');
Xforc = Xforc'; % forcing matrix
IDXforc = IDXforc'; % matrix with gap fill indices


%%%%%Hourly Gap Filled Data
sswc_tw(:,2:7)=Xforc;

%%%%Remove bad counts
ncf=sswc_tw(:,2);
ncf(find(ncf>3000|ncf<100))=NaN;
sswc_tw(:,2)=ncf;

%% 30 minute interpolation
%Existing hourly timesteps
check_date_hourly = datetime(sswc_tw(:,1),'ConvertFrom','datenum'); % hourly soil
moisture from sswc.

%% Generating new 30-minute interval timesteps
start_date=check_date_hourly(1);
end_date=check_date_hourly(end);
check_date_30min=(start_date:minutes(30):end_date)';

%% Initialize the new array for 30 minutes interval data
sswc_30min_tw=nan(length(check_date_30min), size(sswc_tw,2));
sswc_30min_tw(:,1) = datenum(check_date_30min);

% Loop over columns to interpolate other columns
```

```
for col = 2:size(sswc_tw,2)
   % Choose interpolation method based on the nature of the column
   method = 'linear';

   sswc_30min_tw(:, col) = interp1(sswc_tw(:,1), sswc_tw(:,col), sswc_30min_tw(:,1),
method);
end

%% sgf = sgolayfilt(sswc(:,2),3,11);   % Smoothing filter
sgf = sgolayfilt(sswc_tw(:,2),3,11);   % SG filter for hourly interval data
sgf_30min=sgolayfilt(sswc_30min_tw(:,2),3,11); %SG filter for 30 minute interval data

SWC1_tw=((0.0808./(sgf./sswc_tw(:,3)-.372)-0.115)-tao).*bda;  %hourly interval data
SWC1_30min_tw=((0.0808./(sgf_30min./sswc_30min_tw(:,3)-.372)-0.115)-tao).*bda;
%30 minute interval data

%% Correct SWC for values greater than porosity (hourly interval
SWC1_tw(find(SWC1_tw>por))=por;  %%%Correct SWC for values greater than
porosity (hourly interval)
SWC1_30min_tw(find(SWC1_30min_tw>por))=por;  %%%Correct SWC for values
greater than porosity (30 min interval)

%% %Summarize data for analyses (hourly intervals)
[yy mm dd hh min sec]=datevec(sswc_tw(:,1));
dsum=[yy mm dd hh min sswc_tw sgf SWC1_tw];

%%%Summarize data for analyses (30 minute intervals)
[yy mm dd hh min sec]=datevec(sswc_30min_tw(:,1));
dsum=[yy mm dd hh min sswc_30min_tw sgf_30min SWC1_30min_tw];

%% %%%%%%%%%%%%%%% Penetration Depth
z_depth_tw= 5.8./((bda.*tao)+SWC1_tw+0.0829); % Franz 2012, Zreda 2020, Peterson
2016 (hourly intervals)
z_30mindepth_tw=5.8./((bda.*tao)+SWC1_30min_tw+0.0829);

check_date_z= datetime(sswc_tw(:,1),'ConvertFrom','datenum');


%% %%%%%%%%%%%%%%%% FIGURES
%%%%%%%%%%%%%%%%%%%%%%%%%%%%%%%%%%%%
fs = 20; % Font size
ms = 5; % Marker size
wd = 1;  % Line width

st = datenum(2022, 07, 01, 0, 0, 0);    % Starting date
```

```
en = datenum(2024, 01, 31, 0, 0, 0);    % Ending date

% Defining tick marks to be monthly
tick = (st:31:en);
xl = st - 1;
xu = en + 1;

figure(1000)
subplot(2,1,1,'Fontsize',fs,'XTick',tick)
hold on
plot(sswc_tw(:,1),sswc_tw(:,2),'k.','markersize',ms)
plot(sswc_tw(:,1),sgf,'b.-','markersize',ms)
hold off
ylabel('Moderated Neutron Counts (cph)','fontsize',fs)
title('Tromble Weir: Moderated Neutron Count & Soil Water Content
(SWC)','fontsize',fs)
datetick('x','mm/dd/yy','keepticks')
xlim([xl xu])
grid on
box on
legend('Hourly Raw','Filtered')

subplot(2,1,2,'Fontsize',fs,'XTick',tick)
hold on
plot(sswc_tw(:,1),sswc_tw(:,7),'k.','markersize',ms)
plot(sswc_tw(:,1),SWC1_tw,'b.-','markersize',ms)
plot(datenum(2022,07,11,6,0,0), 0.0515, 'rs','MarkerSize',10,'MarkerFaceColor','r')
hold off
ylabel('SWC (m^3/m^3)','fontsize',fs)
datetick('x','mm/dd/yy','keepticks')
xlim([xl xu])
ylim([0.05 0.45])
grid on
box on

%% %%%%SWC - Soil Water Content Figure %%%%%
%%%%%Marker Added%%%%%
figure(1002)
subplot(1,1,1,'Fontsize',fs,'XTick',tick)
hold on
%plot(sswc_tw(:,1),sswc_tw(:,7),'k.','markersize',ms)
plot(sswc_tw(:,1),SWC1_tw,'k','markersize',ms)
plot(datenum(2022,07,11,6,0,0), 0.0515, 'rs','MarkerSize',10,'MarkerFaceColor','r')
hold off
ylabel('SWC (m^3/m^3)','fontsize',fs)
```

```
title('Long Term CRNS Soil Water Content (SWC) Values from Tromble
Weir','fontsize',fs)
datetick('x','mm/dd/yy','keepticks');
xlim([xl xu])
legend('Soil Water Content (m^3/m^3)','Soil Sample - 07/11/2022 - 0.0515 m^3/m^3')
ylim([0.05 0.45])
grid on
box on

%% %%%%%%%%%%  EXPORT DATA TABLES
%Tromble Weir sswc Table
folder_path='./Data_Outputs/';
filename1 = fullfile(folder_path,'TW_sswc.mat'); %sswc (hourly interval)
save(filename1,'sswc_tw'); %sswc

%Tromble Weir SWC1 Table
filename2=fullfile(folder_path,'TW_SWC1.mat'); %SWC1 (hourly interval)
save(filename2,'SWC1_tw'); %SWC1

%Tromble Weir z_depth Table
filename3=fullfile(folder_path,'TW_z_depth.mat'); %z depth (hourly interval)
save(filename3,'z_depth_tw'); %z_depth

%30 minute intervals linearly interpolated
%sswc 30min
filename4=fullfile(folder_path,'TW_30min_sswc'); %sswc (30 minute interval)
save(filename4,'sswc_30min_tw');

%SWC1 30min
filename5=fullfile(folder_path,'TW_30min_SWC1'); %SWC1 (30minute interval)
save(filename5,'SWC1_30min_tw');

%z depth 30 min
filename6=fullfile(folder_path,'TW_30min_zdepth'); %z depth (30 minute interval)
save(filename6,'z_30mindepth_tw');
```

Downstream Playa – CRNS Calibration

```
% % % % Trenton Franz
% % % % 03/10/2022
```

```
% % % %
% % % % Main program to read in CRNS from Las Cruces, New Mexico. Based off of
% % % other codes so a bit of piecemeal code.
% %%% Collaborators: Ruby Hurtado
% % %%
clear all;
close all;
clc

%Field name: P-SMAL


%%% Year     Month, Day,    Day_Fraction, N1Cts, T1_C,  P4_mb, RH1
%%% Date Range of Calibration: Based on December gravimetric collection
%input file from "Concateneate_RawFiles" creates an updated file from CRNS
data= readmatrix('updated_playa01312024.csv');


%%%% Year, Month, Day,Day_Fraction to datenumber format
tdat=datenum(data(:,1),data(:,2),data(:,3)+data(:,4));
%check_date = datetime(sswc(:,1),'ConvertFrom','datenum');
%jday=data(:,5);


% Extract the data columns
n1 = data(:, 5);  % epithermal counts
t7 = data(:, 6);  % external temp. (deg C)
p4 = data(:, 7);  % external pressure (mb)
h7 = data(:, 8);  % external RH (%)

%%%%%remove bad data from min and max bounds
t7(find(t7>80|t7<-50))=nan;
h7(find(h7>105|h7<0))=nan;
n1(find(n1>8000|n1<100))=nan;
p4(find(p4>1100|p4<400))=nan;

%%%%%%%Probe location in field you can use google
%%%%earth to find in units of WGS84 and MASL
csx=-106.861340;  %%%Longitude
csy=32.540189;  %%%Lattitude
elev=1325;       %%%Elevation

%%%Location Specific Parameters
```

```
pref=863;       %%%Reference air pressure (mb, hpa), scaling factor from COSMOS
online calculator using center pivot lat, long and elev.
(http://cosmos.hwr.arizona.edu/Util/calculator.php)
CSF=3.19;       %%%Scaling factor from COSMOS online calculator using lat, long,
elev. Not cutoff rigidity factor!!!!!!!!

%%Atmosphere
tref=25;          %%%Reference air temperature (Deg. C)
rhref=0;          %%%Reference air relative humidity (%) Roselem 2013
gama=6.7;         %%%Temperature lapse-rate (monthly climatology): Source Zweck et
al. 2011
lambda=130;       %%%Attenuation rate for North America

% % % % % % Soil Site Average from guesses or chemistry sampling!!!!!
lw=0.059;             %%%Lattice water, (g/g)
soc=0.0042;           %%%Soil organic carbon water equivalent (g/g)
bda=1.23;           %%%Soil bulk density (g/cm3) from first sampling
%bda2=1.087;            %%%Soil bulk density (g/cm3) from second sampling oct/22/2021
%bda3=1.332;            %%%Soil bulk density (g/cm3) from third sampling may/23/2022
%bda=(bda1+bda2+bda3)/3;
tao=lw+soc;           %%%%Soil water sum(g/g)
%%Set upper bound to porosity
%por=((1-bda1/2.65)+(1-bda2/2.65))/2; %Necessary for multiple soil bulk to
%porosity correlations
por=((1-bda/2.65));


%%%Calibration Data
swc1=0.1149;  %%%%(in g/g) December (0.1149) & July (0.11702)
cd1=datenum(2022,12,05,13,0,0);  %%%Start of calibration, add 6 hours for average
tw1=(swc1+tao);    %%%%Total water for calibration (g/g)
%tw1=(swc1);    %%%%Total water for calibration (g/g)
%DECEMBER CALIBRATION
%
%%summary of calibration
cds=[cd1]';
swcs=[swc1*bda]'; %%% cm3/cm3

% cds=[cd1 cd2 cd3 cd4 cd5 cd6 cd7 cd8]';
% swcs=[swc1*bda swc2*bda swc3*bda swc4*bda swc5*bda swc6*bda swc7*bda
swc8*bda]'; %%% cm3/cm3
%%


%%%%%%%%%%%%%%%%%%%%%%%%%%%%%%%%%%%%%%%%%%%%%%%%%%%%%%%%%%%%%%%%%%%%%%%%
```

Pipe in data to find CI from Nearfield database and Jung. NMB

```
%%%%%%%%%%%%%%%%%%%%%%%%%%%%%%%%%%%%%%%%%%

url = 'https://nearfld.com/reguser/unl_2/data.php?tz=-
0:00&vw=`tb_UNL9`&IM=300234062531270&fn=IMEI_1270&pn=';
% % % c1, n1, n2, p1, b1, h7, h8, p3, p4, t7, t9, NMcounts, fbar, fhum, fsol, SMv

options = weboptions('Timeout',500,'CertificateFileName','');
fullfile(matlabroot,'sys','certificates','ca','rootcerts.pem');
data = webread(url,options);
data1 = data(149:(length(data)-15));
data2 = textscan(data1,'%s %u %u %f %f %f %f %f %f %f %f %f %f %f %f
%f<br>','Delimiter',',','EmptyValue', Inf);
date = flipud(data2{1});
fsol = flipud(data2{15});


clearvars data data1 data2;

tdat2=datenum(date); %%%%Convert to matlab days
INTEN = 1./fsol;     %%%%%%%Intensity Correction Factor, inverse from fsol from
HydroInnova database !!!!!!
Level2.TIME=tdat2;
Level2.INTEN=INTEN;

for i = 1:length(tdat)
   dum = abs(tdat(i) - Level2.TIME);
   mind = min(dum);
   ind = find(mind == dum);

   if ~isempty(ind)
      CI(i,1) = Level2.INTEN(ind(1)); %%% Intensity Correction Factor
   else
      CI(i,1) = NaN; % Set CI(i,1) to NaN if ind is empty
   end

   clear dum mind ind
end

CI(find(CI>1.5)) = NaN;

%%Variations in water vapor, See Rosolem 2013 J. Hydromet
rhovref=calculate_watervapor(tref,pref,rhref,gama); %%%Temp(C), Press(hPa/mb),
RH(%)
```

```
Text=t7;
Pext=p4;
RHext=h7;
Mod=n1;

[rhov,iwv]=calculate_watervapor(Text,Pext,RHext,gama); %%%Temp(C),
Press(hPa/mb), RH(%), gama
CWV=1.0+0.0054*(rhov-rhovref)*1000;  %%%%correction in g/m3!!!!
mean_CWV=mean(CWV);

%mean_CWV= mean(CWV);
%mean_rhov=mean(rhov);

%%Pressure variations against the specified average, See Zreda 2012 HESS
Cp=exp((Pext-pref)/lambda);
mean_Cp=mean(Cp);

%%%Corrected Counts
Nc=Mod.*CWV./CI.*Cp./CSF;

%Mean_NC= mean(rmmissing(Nc));

%%Find counts for calibration
ind21=find(tdat>cd1-8/24 & tdat<=(cd1+8/24));
Ncal1=nanmean(Nc(ind21));
%%%Summary stats
SumN(1,:)=[nanmean(Nc(ind21)) nanmedian(Nc(ind21)) length(ind21)
(nansum(Nc(ind21))^0.5)/nansum(Nc(ind21))
nanmean(Nc(ind21))*((nansum(Nc(ind21)))^0.5)/nansum(Nc(ind21))];

%Calculate N0 values
N0i(1,:)=Ncal1/(0.0808/(tw1+0.115)+0.372);   %%%%N0 (cph)
N0d=mean(N0i);
% N0std=std(N0i);

%%%Average Values over certain time period (entire period)
%%%Starting and ending date of cosmos data rounding to closest hour value
st=datenum(2022, 07, 01, 0, 0, 0);    %%Starting date
en=datenum(2024, 01, 31, 0, 0, 0);    %%%Ending date
% en=ceil(now);    %%%Ending date

int=1/24;  %%%interval in days
ti=[st:int:en]';
%TIME AVERAGING
int=1/24;  %%%interval in days for time averaging
```

```
tii=[st:int:en]';

N0=N0d;

%%Compute time average data
for i=1:length(tii)-1
   %%%Neutron Count in Time Interval
   ind1=find(tdat>=tii(i) & tdat<tii(i+1));

   Ncdum=nanmean(Nc(ind1));
%     Baredum=nanmean(Bare(ind1));
      %N0dum=nanmean(N0(ind1));
      %bwedum=nanmean(bwe(ind1));
%     TFRdum=nanmean(TFR(ind1));

    Textdum=nanmean(Text(ind1));
    Pextdum=nanmean(Pext(ind1));
    RHextdum=nanmean(RHext(ind1));


    SWC=((0.0808/(Ncdum/N0-.372)-0.115)-tao)*bda;  %(lattce water + organic carbon)
    %SWC=((0.0808/(Ncdum/N0-.372)-0.115))*bda;  %%%%
    if SWC>por
       SWC=por;
    end

    if ~isempty(ind1)
%         sswc(i,:)=[(tii(i)+tii(i+1))/2 Ncdum N0dum Baredum TFRdum Textdum
Pextdum RHextdum SWC];
       sswc_ps(i,:)=[(tii(i)+tii(i+1))/2 Ncdum N0 Textdum Pextdum RHextdum SWC];
    else
       sswc_ps(i,:)=[(tii(i)+tii(i+1))/2 nan nan nan nan nan nan ];
    end

    clear ind1 Ncdum N0dum SWC

end

% Gap-filling: Linear interpolation if tgap <= 3 hours, and interpolation based on
previous/next 15 days if tgap > 3 hours
% forcing is the data matrix forcing(time,variables)
npoints = 24; % 24 data points per day
nshortmax = 3; % short gap size
ndayslong = 3; % long-gap analysis window
```

```
forcing=sswc_ps(:,2:7);

[Xforc,IDXforc] = GapFill(forcing',npoints,nshortmax,ndayslong,-
999999,999999,'forcing');
Xforc = Xforc'; % forcing matrix
IDXforc = IDXforc'; % matrix with gap fill indices


%%%%%Hourly Gap Filled Data
sswc_ps(:,2:7)=Xforc;

%%%%Remove bad counts
ncf=sswc_ps(:,2);
ncf(find(ncf>3000|ncf<100))=NaN;
sswc_ps(:,2)=ncf;

%% Filtering sswc to SWC1
check_date_hourly = datetime(sswc_ps(:,1),'ConvertFrom','datenum'); % hourly soil
moisture from sswc.
sgf = sgolayfilt(sswc_ps(:,2),3,11);   % SG filter
SWC1_ps=((0.0808./(sgf./sswc_ps(:,3)-.372)-0.115)-tao).*bda;  %%%%
SWC1_ps(find(SWC1_ps>por))=por;  %%%Correct SWC for values greater than
porosity

%% Gap Filling from sswc to SWC1 (hourly)
non_soil = sswc_ps(:,7); %soil values I will use to base gap filling on
indices = find(~isnan(non_soil)); %identify any small gaps in the base soil values

%Using 'pchip' interpolation fill in tiny gaps in the base soil values
for k = 1:(length(indices) - 1)
   gap = indices(k + 1) - indices(k);
   if gap <= 23
      non_soil1(indices(k):indices(k + 1)) = interp1([indices(k), indices(k + 1)], ...
         [non_soil(indices(k)), non_soil(indices(k + 1))], ...
         indices(k):indices(k + 1), 'spline');
   end
end

non_soil1=non_soil1'; %transpose the interpolated base soil values
non_soil2=sgolayfilt(non_soil1,3,11); %smooth base soil values
non_soil3=non_soil2; %this is the section I will use from the interpolated, smoothed base
soil values


SWC = SWC1_ps; %soil values that need to be gap filled based on non_soil3
```

```
relationship =fitlm(non_soil3,SWC); %Run a linear regression between non_soil3 and
swc to calculate an equation to better fill the gaps in swc
predicted_swc = predict(relationship,non_soil3);

SWC1_filled = SWC;
for i = 1:length(SWC)
   if isnan(SWC(i))
      SWC1_filled(i) = predicted_swc(i);
   end
end

%% Convert hourly soil moisture values to 30 minute soil moisture values
start_date=check_date_hourly(1);
end_date=check_date_hourly(end);
check_date_30min=(start_date:minutes(30):end_date)';

sswc_30min_ps=nan(length(check_date_30min), size(sswc_ps,2));
sswc_30min_ps(:,1) = datenum(check_date_30min);

% Loop over columns to interpolate other columns
for col = 2:size(sswc_ps,2)
   % Choose interpolation method based on the nature of the column
   method = 'linear'; % You might choose 'nearest', 'spline', etc., based on the column.

   sswc_30min_ps(:, col) = interp1(sswc_ps(:,1), sswc_ps(:,col), sswc_30min_ps(:,1),
method);
end

sgf_30min=sgolayfilt(sswc_30min_ps(:,2),3,11); %SG filter for 30 minute interval data
SWC1_30min_ps=((0.0808./(sgf_30min./sswc_30min_ps(:,3)-.372)-0.115)-tao).*bda;
%30 minute interval data
SWC1_30min_ps(find(SWC1_30min_ps>por))=por;  %%%Correct SWC for values
greater than porosity (30 min interval)

%% Gap Filling from sswc to SWC1 (30 minutes)
non_soil30min = sswc_30min_ps(:,7); %30 minute values
indices30min = find(~isnan(non_soil30min)); %identify any small gaps in the base soil
values

%Using 'pchip' interpolation fill in tiny gaps in the base soil values
for k = 1:(length(indices30min) - 1)
   gap = indices30min(k + 1) - indices30min(k);
   if gap <= 46
```

```
      non_soil130min(indices30min(k):indices30min(k + 1)) = interp1([indices30min(k),
indices30min(k + 1)], ...
          [non_soil30min(indices30min(k)), non_soil30min(indices30min(k + 1))], ...
          indices30min(k):indices30min(k + 1), 'spline');
   end
end
non_soil130min=non_soil130min'; %transpose the interpolated base soil values
non_soil230min=sgolayfilt(non_soil130min,3,11); %smooth base soil values
non_soil330min=non_soil230min; %this is the section I will use from the interpolated,
smoothed base soil values


SWC_30min = SWC1_30min_ps; %soil values that need to be gap filled based on
non_soil3

relationship_30min =fitlm(non_soil330min,SWC_30min); %Run a linear regression
between non_soil3 and swc to calculate an equation to better fill the gaps in swc
predicted_swc30min = predict(relationship_30min,non_soil330min);

SWC1_filled30min = SWC_30min;
for i = 1:length(SWC_30min)
   if isnan(SWC_30min(i))
      SWC1_filled30min(i) = predicted_swc30min(i);
   end
end

%% Calculate z depth
z_depth_ps= 5.8./((bda.*tao)+SWC1_filled+0.0829); % Franz 2012, Zreda 2020,
Peterson 2016
z_depth30min_ps = 5.8./((bda.*tao)+SWC1_filled30min+0.0829);


%% FIGURES
%%%Summarize data for analyses
[yy mm dd hh min sec]=datevec(sswc_ps(:,1));
dsum=[yy mm dd hh min sswc_ps sgf SWC1_ps];

check_date = datetime(sswc_ps(:,1),'ConvertFrom','datenum');

%%%%Plot and figure settings
% fs = 18;
% ms = 12;
% wd = 2;
%
% st = datenum(2022, 07, 01, 0, 0, 0);    % Starting date
```

```
% en = datenum(2023, 06, 11, 0, 0, 0);    % Ending date
%
% xl = st - 1;
% xu = en + 1;
%
% tick = xl:10:xu;

% Plot and figure settings
fs = 18; % Font size
ms = 5; % Marker size
wd = 0.75;  % Line width

st = datenum(2022, 07, 01, 0, 0, 0);    % Starting date
en = datenum(2024, 01, 31, 0, 0, 0);    % Ending date

% Defining tick marks to be monthly
tick = (st:30:en);

xl = st - 1;
xu = en + 1;

%%%Neutron Count (Level 3) with SWC Figure %%%
figure(1000)
subplot(2,1,1,'Fontsize',fs,'XTick',tick)
hold on
plot(sswc_ps(:,1),sswc_ps(:,2),'k-','markersize',ms) %corrected neutron count
plot(sswc_ps(:,1),sgf,'k-','markersize',ms)
hold off
ylabel('Moderated Neutron Counts (cph)','fontsize',fs)
title('P-SMAL: Moderated Neutron Count & Soil Water Content (SWC)','fontsize',fs)
datetick('x','mmmm','keepticks')
xlim([xl xu])
grid on
box on
legend('Hourly Raw','Filtered')
subplot(2,1,2,'Fontsize',fs,'XTick',tick)
hold on
plot(sswc_ps(:,1),sswc_ps(:,7),'k','markersize',ms) %swc
hold on
plot(sswc_ps(:,1),SWC1_filled,'b','markersize',ms) %filtered swc
plot(datenum(2022,07,01,15,0,0), 0.14391, 'rs','MarkerSize',10,'MarkerFaceColor','r')
plot(datenum(2022,12,04,14,0,0), 0.1427, 'rs','MarkerSize',10,'MarkerFaceColor','r')
hold off
ylabel('SWC (m^3/m^3)','fontsize',fs)
datetick('x','mmmm','keepticks')
```

```
xlim([xl xu])
ylim([0.05 0.45])
grid on
box on


% %%%%%Marker Added - From Gravimetric Collection%%%%%
figure(1002)
hold on
subplot(1,1,1,'Fontsize',fs,'XTick',tick, 'LineWidth', wd)

plot(sswc_30min_ps(:,1),sswc_30min_ps(:,7),'k','MarkerSize',ms, 'LineWidth', wd)
plot(sswc_30min_ps(:,1),SWC1_filled30min,'b.-','MarkerSize',ms, 'LineWidth', wd)
plot(datenum(2022,07,01,11,0,0), 0.14391, 'rs','MarkerSize',ms,'MarkerFaceColor','r',
'LineWidth', wd)
plot(datenum(2022,12,04,14,0,0), 0.1427, 'rs','MarkerSize',ms,'MarkerFaceColor','r',
'LineWidth', wd)

hold off
ylabel('Soil Water Content - SWC (m^3/m^3)','Fontsize',fs)
title('P-SMAL: Summer & Winter Gravimetric Collections','Fontsize',fs)
datetick('x','mmmm','keepticks')  % Updated to show month and year
xlim([xl xu])

labels = {'Hourly Raw', 'Filtered', 'July Collection - 0.14391 m^3/m^3', 'December
Collection - 0.1427 m^3/m^3'};
legend(labels, 'Location', 'best', 'FontSize', fs)

ylim([0.05 0.45])

% Change the grid line style
set(gca,'GridLineStyle',':', 'MinorGridLineStyle',':')
grid on

% Adjust the linewidth of the axes
set(gca, 'LineWidth', wd)

box on


% Change the grid line style
set(gca,'GridLineStyle',':', 'MinorGridLineStyle',':')
grid on

% Adjust the linewidth of the axes
```

```
set(gca, 'LineWidth', wd)

box on

%%%%%%%%%%%%  EXPORT DATA TABLES
%%%%%%%%%%%%%%%%%%%%%%%%%%%%%
%P-SMAL sswc Table
folder_path='./Data_Outputs/';
filename1 = fullfile(folder_path,'P_SMAL_sswc.mat'); %sswc
save(filename1,'sswc_ps');

filename2 = fullfile(folder_path,'P_SMAL_30min_sswc.mat'); %sswc
save(filename2,'sswc_30min_ps');

%P-SMAL SWC1 Table
filename3=fullfile(folder_path,'P_SMAL_SWC1.mat');
save(filename3,'SWC1_ps'); %SWC1

%P-SMAL SWC1_filled Table
filename4=fullfile(folder_path,'P_SMAL_SWC1_filled.mat');
save(filename4,'SWC1_filled'); %SWC1 filled

%P-SMAL SWC1_filled Table
filename5=fullfile(folder_path,'P_SMAL_SWC1_30min_filled.mat');
save(filename5,'SWC1_filled30min'); %SWC1 30 min filled

%P-SMAL z_depth Table
filename6=fullfile(folder_path,'PS_SMAL_z_depth.mat');
save(filename6,'z_depth_ps'); %z_depth

%P-SMAL z_depth Table
filename8=fullfile(folder_path,'PS_SMAL_z_depth_30min.mat');
save(filename8,'z_depth30min_ps'); %z_depth
```

Upland Watershed – Weighted Sensor Network

```
%%%%%%%% IMPORT FILES FROM SOIL PROFILE TRANSECTS %%%%%%%%
%%%depth weighted averages from depth (Z*) - CRNS (09/30/23 7:30)
file1 = 'Transect1.csv';
file2= 'Transect2.csv';
file3 = 'Transect3.csv'; %Not Updated :(
file4 = 'TW_Chanel2_SM.csv'; %Last data row 6/11/23 10:53
file5 = 'Plot1_2SM.xlsx'; %plots next to TW-CRNS
file6 = 'Plot3_4SM.xlsx'; %plots across the stream from TW-CRNS

data1 =readmatrix(file1); %transect 1
data2 = readmatrix(file2); %transect 2
data3 = readmatrix(file3); %transect 3
data4= readmatrix(file4); %Chanel 2
data5 = readmatrix(file5); %Plot 1 & 2
data6 = readmatrix(file6); %Plot 3 & 4

%%%%% Year, Month, Day,Day_Fraction = converts to date/number
tdat_1=datenum(data1(:,2),data1(:,3),data1(:,4)+data1(:,5)); %transect 1
tdat_2=datenum(data2(:,2),data2(:,3),data2(:,4)+data2(:,5)); %transect 2
tdat_3=datenum(data3(:,2),data3(:,3),data3(:,4)+data3(:,5)); %transect 3
tdat_4=datenum(data4(:,2),data4(:,3),data4(:,4)+data4(:,5)); %Channel 2
tdat_5=datenum(data5(:,2),data5(:,3),data5(:,4)+data5(:,5)); %Plot 1 & 2
tdat_6=datenum(data6(:,2),data6(:,3),data6(:,4)+data6(:,5)); %Plot 3 & 4


%%Extract columns transect 1-3 (5-30cm), chanel 2 & plots 1-4 (5-100cm)
data1_5_30cm = data1(:,[7 9 11 13 15 17 19 21 23]); %(5, 15, 30 x 3) transect 1 (9)
data2_5_30cm = data2(:,[7 9 11 13 15 17 19 21 23 25 27 29 31 33 35]); %(5,15,30 x5)
transect 2
data3_530 = data3(:,[7 9 11 13 15 17 19 21 23]); %(5,15,30 x3) transect 3
data4_5_100cm = data4(:,[7 10 13 16 19 ]); %(5,15, 30, 50, 100) Chanel 2
data5_5_100cm = data5(:,[6 9 12 15 18 21]) ;%( 5, 15, 30, 5, 15, 30) Plot 1 & 2
data6_5_100cm = data6(:,[6 9 12 15 18 21]) ;%( 5, 15, 30, 5, 15, 30) Plot 3 & 4



%% %%%%%  CALCULATE HOURLY SOIL MOISTURE VALUES  %%%
% % Calculate hourly average of soil moisture for each depth column
%TRANSECT 1
hourly_data1 = [];
for i = 1:floor(length(tdat_1)/2)
   idx = ((i-1)*2+1):(i*2);
   hourly_data1(i,:) = [tdat_1(idx(1)), nanmean(data1_5_30cm(idx,:), 1)];
end
%TRANSECT 2
```

```
hourly_data2 = [];
for i = 1:floor(length(tdat_2)/2)
   idx = ((i-1)*2+1):(i*2);
   hourly_data2(i,:) = [tdat_2(idx(1)), nanmean(data2_5_30cm(idx,:), 1)];
end

%TRANSECT 3
hourly_data3 = [];
for i = 1:floor(length(tdat_3)/2)
   idx = ((i-1)*2+1):(i*2);
   hourly_data3(i,:) = [tdat_3(idx(1)), nanmean(data3_530(idx,:), 1)];
end


%CHANNEL 2 (MINUTELY TO HOURLY DATA)
hourly_data4 = [];
for i = 1:floor(length(tdat_4)/60)
   idx = ((i-1)*60+1):(i*60);
   hourly_data4(i,:) = [tdat_4(idx(1)), nanmean(data4_5_100cm(idx,:), 1)];
end

%Plot 1 & 2 (30 minute intervals to hourly data)
hourly_data5 = [];
for i = 1:floor(length(tdat_5)/2)
   idx = ((i-1)*2+1):(i*2);
   hourly_data5(i,:) = [tdat_5(idx(1)), nanmean(data5_5_100cm(idx,:), 1)];
end

%Plot 3 & 4 (30 minute intervals to hourly data)
hourly_data6 = [];
for i = 1:floor(length(tdat_6)/2)
   idx = ((i-1)*2+1):(i*2);
   hourly_data6(i,:) = [tdat_6(idx(1)), nanmean(data6_5_100cm(idx,:), 1)];
end


%% %%%%%%%%%% SPATIAL AVERAGE OF SOIL TRANSECTS %%%%
% Convert matrices to tables
t1= array2table(hourly_data1, 'VariableNames', {'Date', '5cm1', '15cm1', '30cm1', '5cm2',
'15cm2','30cm2','5cm3','15cm3','30cm3'}); %Transect 1
t2 = array2table(hourly_data2, 'VariableNames', {'Date', '5cm1', '15cm1', '30cm1', '5cm2',
'15cm2',
'30cm2','5cm3','15cm3','30cm3','5cm4','15cm4','30cm4','5cm5','15cm5','30cm5'}); %
Transect 2
```

```
t3= array2table(hourly_data3, 'VariableNames', {'Date', '5cm1', '15cm1', '30cm1', '5cm2',
'15cm2', '30cm2','5cm3','15cm3','30cm3'}); % Transect 3
t4 = array2table(hourly_data4, 'VariableNames', {'Date', '5cm', '15cm', '30cm', '50cm',
'100cm'}); %Chanel 2
t5 = array2table(hourly_data5, 'VariableNames', {'Date', '5cm1', '15cm1', '30cm1', '5cm2',
'15cm2', '30cm2'}); % Plot 1&2
t6 = array2table(hourly_data6, 'VariableNames', {'Date', '5cm3', '15cm3', '30cm3', '5cm4',
'15cm4', '30cm4'}); % Plot 3&4


% Convert datenumbers to datetime
t1.Date = datetime(t1.Date, 'ConvertFrom', 'datenum'); %Transect 1
t2.Date = datetime(t2.Date, 'ConvertFrom', 'datenum'); %Transect 2
t3.Date = datetime(t3.Date, 'ConvertFrom', 'datenum'); %Transect 3
t4.Date = datetime(t4.Date, 'ConvertFrom', 'datenum'); %Chanel 2
t5.Date = datetime(t5.Date, 'ConvertFrom', 'datenum'); %Plot 1&2
t6.Date = datetime(t6.Date, 'ConvertFrom', 'datenum'); %Plot 3&4

% Convert tables to timetables
tt1 = table2timetable(t1); %Transect 1
tt2 = table2timetable(t2); %Transect 2
tt3 = table2timetable(t3); %Transect 3
tt4 = table2timetable(t4); %Chanel 2
tt5 = table2timetable(t5); %Plot 1&2
tt6 = table2timetable(t6); %Plot 3&4

%Resample timetables to have regular hourly intervals
tt1 = retime(tt1,'hourly','nearest'); %Transect 1
tt2 = retime(tt2,'hourly','nearest'); %Transect 2
tt3 = retime(tt3,'hourly','nearest'); %Transect 3
tt4 = retime(tt4,'hourly','nearest'); %Chanel 2
tt5 = retime(tt5,'hourly','nearest'); %Plot 1&2
tt6 = retime(tt6,'hourly','nearest'); %Plot 3&4

%% Daily Soil Moisture Values %%%%%%%%%%%%%%%%%%
transect1_daily=retime(tt1,'daily','mean');
transect2_daily=retime(tt2,'daily','mean');
transect3_daily=retime(tt3,'daily','mean');
channel2_daily=retime(tt4,'daily','mean');
plot12_daily=retime(tt5,'daily','mean');
plot34_daily=retime(tt6,'daily','mean');

Daily_tt1_5cm = mean(transect1_daily{:, {'5cm1', '5cm2', '5cm3'}}, 2); %Transect 1
Daily_tt1_15cm = mean(transect1_daily{:, {'15cm1', '15cm2', '15cm3'}}, 2);
Daily_tt1_30cm = mean(transect1_daily{:, {'30cm1', '30cm2', '30cm3'}}, 2);
```

```
Daily_tt2_5cm = mean(transect2_daily{:, {'5cm1', '5cm2', '5cm3'}}, 2); %Transect 2
Daily_tt2_15cm = mean(transect2_daily{:, {'15cm1', '15cm2', '15cm3'}}, 2);
Daily_tt2_30cm = mean(transect2_daily{:, {'30cm1', '30cm2', '30cm3'}}, 2);

Daily_tt3_5cm = mean(transect3_daily{:, {'5cm1', '5cm2', '5cm3'}}, 2); %Transect 3
Daily_tt3_15cm = mean(transect3_daily{:, {'15cm1', '15cm2', '15cm3'}}, 2);
Daily_tt3_30cm = mean(transect3_daily{:, {'30cm1', '30cm2', '30cm3'}}, 2);

Daily_tt5_5cm = mean(plot12_daily{:, {'5cm1', '5cm2'}}, 2); %Plot 1 & 2
Daily_tt5_15cm = mean(plot12_daily{:, {'15cm1', '15cm2'}}, 2);
Daily_tt5_30cm = mean(plot12_daily{:, {'30cm1', '30cm2'}}, 2);

Daily_tt6_5cm = mean(plot34_daily{:, {'5cm3', '5cm4'}}, 2); %Plot 1 & 2
Daily_tt6_15cm = mean(plot34_daily{:, {'15cm3', '15cm4'}}, 2);
Daily_tt6_30cm = mean(plot34_daily{:, {'30cm3', '30cm4'}}, 2);

%% Daily Soil Moisture Values %%%%%%%%%%%%%%%%%

% Synchronize timetables based on hourly interval
st_tw = synchronize(tt1, tt2, tt3, tt4,tt5, tt6,'union');

% Re place negative numbers with NaN
st_tw{:,:}(st_tw{:,:}<0) = NaN;


%% Check
%
% % Define tables array
% tables = {t1, t2, t3, t4, t5, t6};
%
% % Plot only 15cm and 30cm columns
% figure;
% for i = 1:length(tables)
%     tbl = tables{i};
%     subplot(2, length(tables), i); % Arrange plots in a 2xN grid
%     plot(tbl.Date, tbl{:, contains(tbl.Properties.VariableNames, '15cm')});
%     title(['Table ' num2str(i) ' - 15cm']);
%     xlabel('Date');
%     ylabel('Value');
%     grid on;
%
%     subplot(2, length(tables), i + length(tables)); % Arrange plots in a 2xN grid
%     plot(tbl.Date, tbl{:, contains(tbl.Properties.VariableNames, '30cm')});
%     title(['Table ' num2str(i) ' - 30cm']);
```

```
%     xlabel('Date');
%     ylabel('Value');
%     grid on;
% end

%% %%%%%%%%%%% Horizontal weighted function %%%%%%%%%%%
%Radial weights calculated from Shron exponential decay graph: 5, 25, 75m
%Transect 1: Radial weights
weight_1tran1 =0.000234464; % 118.58m
weight_1tran2 = 0.00022386; %125.02m
weight_1tran3 = 0.000219154;%128.77m

%Transect 2: Radial weights
weight_2tran1= 0.000346152; %65.67m
weight_2tran2=0.00035549; %62.17m
weight_2tran3=0.000355219; %62.27m
weight_2tran4=0.000357119; %61.54m
weight_2tran5=0.000336332;%69.47m

%Transect 3: Radial weights (Problem Transect 3 : Remove it for now)
weight_3tran1=0.000287525; %90.45m
weight_3tran2=0.000266607; %100.74m
weight_3tran3=0.000243716; %113.16m

%Chanel 2: Radial weights
weight_2chan1= 0.000455845; %42.67m

%Plot 1
weight_plot1=0.000578; %14.5m


%Plot 2
weight_plot2=0.000548; %22.09m

%Plot 3
weight_plot3=0.000388877; %50.39m

%Plot 4
weight_plot4=0.000383218; %52.31

%% %%%%%%%%%%%% Horizontal Weights Applied
%%%%%%%%%%%%%%%%%%
% Calculate total weighted sum for each depth (treat missing data as nan values)
```

```
sum_5cm = nansum([weight_1tran1*st_tw.('5cm1_tt1'),
weight_1tran2*st_tw.('5cm2_tt1'),
weight_1tran3*st_tw.('5cm3_tt1'),weight_2tran1*st_tw.('5cm1_tt2') ...

,weight_2tran2*st_tw.('5cm2_tt2'),weight_2tran3*st_tw.('5cm3_tt2'),weight_2tran4*st_t
w.('5cm4_tt2'),weight_2tran5*st_tw.('5cm5'),weight_2chan1*st_tw.('5cm'),weight_plot1
*st_tw.('5cm1_tt5'),weight_plot2*st_tw.('5cm2_tt5'),weight_plot3*st_tw.('5cm3_tt6'),wei
ght_plot4*st_tw.('5cm4_tt6'),], 2);

sum_15cm = nansum([weight_1tran1*st_tw.('15cm1_tt1'),
weight_1tran2*st_tw.('15cm2_tt1'),
weight_1tran3*st_tw.('15cm3_tt1'),weight_2tran1*st_tw.('15cm1_tt2') ...

,weight_2tran2*st_tw.('15cm2_tt2'),weight_2tran3*st_tw.('15cm3_tt2'),weight_2tran4*st
_tw.('15cm4_tt2'),weight_2tran5*st_tw.('15cm5'),weight_2chan1*st_tw.('15cm'),weight_
plot1*st_tw.('15cm1_tt5'),weight_plot2*st_tw.('15cm2_tt5'),weight_plot3*st_tw.('15cm3
_tt6'),weight_plot4*st_tw.('15cm4_tt6')], 2);

sum_30cm = nansum([weight_1tran1*st_tw.('30cm1_tt1'),
weight_1tran2*st_tw.('30cm2_tt1'),
weight_1tran3*st_tw.('30cm3_tt1'),weight_2tran1*st_tw.('30cm1_tt2') ...

,weight_2tran2*st_tw.('30cm2_tt2'),weight_2tran3*st_tw.('30cm3_tt2'),weight_2tran4*st
_tw.('30cm4_tt2'),weight_2tran5*st_tw.('30cm5'),weight_2chan1*st_tw.('30cm'),weight_
plot1*st_tw.('30cm1_tt5'),weight_plot2*st_tw.('30cm2_tt5'),weight_plot3*st_tw.('30cm3
_tt6'),weight_plot4*st_tw.('30cm4_tt6')], 2);

sum_50cm = nansum([weight_2chan1*st_tw.('50cm')], 2);

sum_100cm = nansum([weight_2chan1*st_tw.('100cm')], 2);

%% %%%%%%%%%%%%%% No Horizontal Weights Applied
%%%%%%%%%%%%%
% sum_5cm = nanmean([st_tw.('5cm1_tt1'),st_tw.('5cm2_tt1'),
st_tw.('5cm3_tt1'),st_tw.('5cm1_tt2')
,st_tw.('5cm2_tt2'),st_tw.('5cm3_tt2'),st_tw.('5cm4_tt2'),st_tw.('5cm5'),st_tw.('5cm'),st_t
w.('5cm1_tt5'),st_tw.('5cm2_tt5'),st_tw.('5cm3_tt6'),st_tw.('5cm4_tt6'),], 2);
%
% sum_15cm = nanmean([st_tw.('15cm1_tt1'), st_tw.('15cm2_tt1'),
st_tw.('15cm3_tt1'),st_tw.('15cm1_tt2'),st_tw.('15cm2_tt2'),st_tw.('15cm3_tt2'),st_tw.('15
cm4_tt2'),st_tw.('15cm5'),st_tw.('15cm'),st_tw.('15cm1_tt5'),st_tw.('15cm2_tt5'),st_tw.('1
5cm3_tt6'),st_tw.('15cm4_tt6')], 2);
%
% sum_30cm =
nanmean([st_tw.('30cm1_tt1'),st_tw.('30cm2_tt1'),st_tw.('30cm3_tt1'),st_tw.('30cm1_tt2')
```

```
,st_tw.('30cm2_tt2'),st_tw.('30cm3_tt2'),st_tw.('30cm4_tt2'),st_tw.('30cm5'),st_tw.('30cm'
),st_tw.('30cm1_tt5'),st_tw.('30cm2_tt5'),st_tw.('30cm3_tt6'),st_tw.('30cm4_tt6')], 2);
%
% sum_50cm = nanmean([st_tw.('50cm')], 2);
%
% sum_100cm = nanmean([st_tw.('100cm')], 2);

%% %%%%%%%%%%%%%%%%%%%%%%%% Apply Horizontal Weights %%%
% Total weights for each depth
total_weights = weight_1tran1 + weight_1tran2
+weight_1tran3+weight_2tran1+weight_2tran2+weight_2tran3+weight_2tran4+weight_2
tran5+...
+weight_2chan1+weight_plot1+weight_plot2+weight_plot3+weight_plot4;


% Calculate weighted averages
avg_5cm = sum_5cm / total_weights;
avg_15cm = sum_15cm / total_weights;
avg_30cm = sum_30cm / total_weights;
avg_50cm = sum_50cm / total_weights;
avg_100cm = sum_100cm / total_weights;


% %No Horizontal weight
% avg_5cm = sum_5cm;
% avg_15cm = sum_15cm;
% avg_30cm = sum_30cm;
% avg_50cm = sum_50cm;
% avg_100cm = sum_100cm;

% Create the numeric matrix with the averages
averageMatrix_tw = [avg_5cm,avg_15cm,avg_30cm,avg_50cm, avg_100cm];
%averageMatrix_tw = [avg_5cm,avg_50cm, avg_100cm];


%% %%%%%%%%%%%% WEIGHTED SOIL DEPTH %%%%%%%%%%%%
% Assuming z_star is a matlab double table
z_star = z_depth_tw; %replace with z_depth from calibration output

% Define the soil depths
soil_depths = [5, 15,30,50, 100];
%soil_depths = [5,50, 100];

% Number of time steps
num_timesteps = height(z_star);
```

```
% Initialize a matrix to store the weights for each soil depth at each time step
weights = zeros(num_timesteps, length(soil_depths));

% Calculate the weights at each time step for each soil depth
for i = 1:num_timesteps
   % Calculate the constant 'a' for this time step
   b = 1; % assuming b is 1 for a linear relationship
   a = 1 / (z_star(i) - (z_star(i)^(b+1)) / ((z_star(i)^b) * (b+1)));

   for j = 1:length(soil_depths)
      % Calculate the weight for this soil depth at this time step
      if soil_depths(j) <= z_star(i)
         weights(i, j) = a * (1 - (soil_depths(j) / z_star(i))^b);
      else
         weights(i, j) = 0;
      end
   end
end

% Convert the weights matrix to a table
weights_table = array2table(weights, 'VariableNames', strcat('Depth_',
string(soil_depths)));


SN_Table = averageMatrix_tw(1:13896,:);

% Multiply each soil moisture column by its corresponding weight
weighted_soil_moisture = SN_Table .* weights;

% Compute the weighted average at each time step
weighted_average_tw = sum(weighted_soil_moisture, 2) ./ sum(weights, 2); %final
product

WA_sgf_tw = sgolayfilt(weighted_average_tw,3,11); %filtered product
% Replace values larger than 0.32 with NaN
WA_sgf_tw(WA_sgf_tw > 0.32) = NaN;

% Replace values below 0 with NaN
WA_sgf_tw(WA_sgf_tw < 0) = NaN;

% Extract hourly timestamps from your table (Assuming it is a timetable)
hourly_intervals = st_tw.Date; % Change to the actual variable name representing time in
your table.
hourly_intervals=hourly_intervals(1:13896,:);
```

```
%Generate new 30 minute interval timestamps
start_time = hourly_intervals(1);
end_time = hourly_intervals(end);
weightaverage_30= (start_time:minutes(30):end_time)';

% Initialize the new array for 30 minutes interval data
wa_30min = nan(length(weightaverage_30), 2); % Second column will hold the
interpolated values.
wa_30min(:, 1) = datenum(weightaverage_30);

% Perform linear interpolation to get 30-minute interval data.
wa_30min(:, 2) = interp1(datenum(hourly_intervals), WA_sgf_tw, wa_30min(:, 1),
'linear');

WA_30minsgf_tw = sgolayfilt(wa_30min,3,11); %filtered product
% Replace values larger than 0.32 with NaN
WA_30minsgf_tw(WA_30minsgf_tw > 0.32) = NaN;

% Replace values below 0 with NaN
WA_30minsgf_tw(WA_30minsgf_tw < 0) = NaN;



check_date_30min= datetime(sswc_30min_tw (:,1),'ConvertFrom','datenum');

%% Test Different sections of soil sensors at UW

num_days1 = floor(length(avg_100cm)/24);
Depth_100cm = zeros(num_days1,1); % Only in the channel
for i = 1:num_days1
   day_sum = 0;
   for j = 1:24
      day_sum = day_sum + avg_100cm((i-1)*24+j);
   end
   Depth_100cm(i) = day_sum / 24; % Daily Channel soil moisture
end

Depth_50cm = zeros(num_days1,1); %Only in the channel
for i = 1:num_days1
   day_sum = 0;
   for j = 1:24
      day_sum = day_sum + avg_50cm((i-1)*24+j);
   end
   Depth_50cm(i) = day_sum / 24; % Daily Channel soil moisture
```

```
end

Depth_30cm = zeros(num_days1,1); %Only in the channel
for i = 1:num_days1
   day_sum = 0;
   for j = 1:24
      day_sum = day_sum + avg_30cm((i-1)*24+j);
   end
   Depth_30cm(i) = day_sum / 24; % Daily Channel soil moisture
end

Depth_15cm = zeros(num_days1,1); %Only in the channel
for i = 1:num_days1
   day_sum = 0;
   for j = 1:24
      day_sum = day_sum + avg_15cm((i-1)*24+j);
   end
   Depth_15cm(i) = day_sum / 24; % Daily Channel soil moisture
end

Depth_5cm = zeros(num_days1,1); %Only in the channel
for i = 1:num_days1
   day_sum = 0;
   for j = 1:24
      day_sum = day_sum + avg_5cm((i-1)*24+j);
   end
   Depth_5cm(i) = day_sum / 24; % Daily Channel soil moisture
end
% PLOT TDT WEIGHTED - Neutron Data with TDT -Weighted
figure(1002)
clf % clear figure
subplot(1,1,1,'Fontsize',fs,'XTick',tick)
hold on
plot(sswc_tw(:,1),sswc_tw(:,7),'k.','markersize',ms) %Mod Count
plot(sswc_tw(:,1),SWC1_tw,'b.-','markersize',ms) %Mod Count filtered
plot(sswc_tw(:,1),WA_sgf_tw,'r.-','markersize',ms)
hold off
ylabel('SWC (m^3/m^3)','fontsize',fs)
title('Tromble Weir CRNS - Weighted Sensor Network','fontsize',fs)
datetick('x','mmmm','keepticks')
xlim([xl xu])
legend('CRNS - SWC','CRNS - SWC Filtered','TDT- Weighted','Location', 'NorthWest')
ylim([0.05 0.45])
grid on
box on
```

```
figure(1002)
clf % clear figure

% Create the top axes for the SWC data
ax1 = subplot(2,1,1);
plot(ax1, sswc_30min_tw(:,1), sswc_30min_tw(:,7), 'k.','markersize',ms); %Mod Count
hold on;
plot(sswc_30min_tw(:,1), SWC1_30min_tw, 'b.-','markersize',ms); %Mod Count filtered
hold on
plot(sswc_30min_tw(:,1), WA_30minsgf_tw(:,2), 'r.-','markersize',ms); %Depth weighted
SN
ylabel(ax1, 'SWC (m^3/m^3)', 'fontsize', fs);
title(ax1, 'Tromble Weir CRNS - Weighted Sensor Network', 'fontsize', fs);
datetick('x','mmmm','keepticks');
xlim([xl xu]);
legend('CRNS - SWC', 'CRNS - SWC Filtered', 'TDT- Weighted', 'Location',
'NorthWest');
ylim([0.05 0.45]);
grid on;
ax1.XAxisLocation = 'origin';

% Create the bottom axes for the penetration depth data
ax2 = subplot(2,1,2);
plot(ax2, sswc_30min_tw(:,1), -z_30mindepth_tw, 'b.-', 'markersize',ms); % Negative
depth data
ylabel(ax2, 'Depth (cm)', 'fontsize', fs);
datetick('x','mmmm','keepticks');
xlim([xl xu]);
ax2.YDir = 'reverse';
grid on;
ax2.XAxisLocation = 'origin';

% Link the x-axes to synchronize when zooming or panning
linkaxes([ax1, ax2], 'x');

% % Create the bottom axes for the penetration depth data
% ax2 = subplot(2,1,2);
plot(sswc_tw(:,1), -z_depth_tw, 'LineWidth', 2, 'Marker', '.','markersize',ms); % Negative
depth data
ylabel(ax2, 'Depth (cm)', 'fontsize', fs);
datetick('x','mmmm','keepticks');
xlim([xl xu]);
ax2.YDir = 'reverse';
grid on;
```

```
ax2.XAxisLocation = 'origin';

% Link the x-axes to synchronize when zooming or panning
linkaxes([ax1, ax2], 'x');

%% Sensor Comparison
st =tromble_daily.Timestamp(1);    % Starting date
en = tromble_daily.Timestamp(580);    % Ending date
fs = 30; %font size
plotwidth = 2800; % Adjust width as needed
plotheight = 2800; % Adjust height as needed

startDate= tromble_daily.Timestamp(50);
endDate = tromble_daily.Timestamp(53);

tick=(st:en);
tick = tick(day(tick)==1);

xl=st-1;
xu=en+1;
figure1 = figure('position', [0, 0, plotwidth, plotheight]);
yyaxis left
ax1=subplot(2,1,1);
plot(tromble_daily.Timestamp, tromble_daily.CRNS);
hold on
plot(tromble_daily.Timestamp, tromble_daily.Network);
plot(tromble_daily.Timestamp, Depth_5cm);
plot(tromble_daily.Timestamp, Depth_15cm);
plot(tromble_daily.Timestamp, Depth_30cm);
plot(tromble_daily.Timestamp, Depth_50cm);
plot(tromble_daily.Timestamp, Depth_100cm);
set(ax1,'XTick',tick);
datetick('x','mm/dd/yy','keepticks')
xlim([xl xu])
ylim([0 0.4])
set(ax1, 'YTick', [0 0.05 0.10 0.15 0.20 0.25 0.30 0.35 0.40],'YTickLabel',
{'0','0.05','0.10','0.15','0.20','0.25','0.30','0.35','0.40'});
set(ax1, 'XTickLabel',{});
legend ('','CRNS','Sensor Network','5cm','15cm','30cm','50cm','100cm','','');

plot(tromble_daily.Timestamp(11), 0.0515, "diamond", 'MarkerSize', 15,
'MarkerEdgeColor', 'k','LineWidth',3);
yLimits = ([0.001 0.3990]);
shadedArea = fill([startDate, startDate, endDate, endDate], [yLimits(1), yLimits(2),
yLimits(2), yLimits(1)], [0.9, 0.9, 0.9], 'EdgeColor', 'none');
```

```
uistack(shadedArea, 'bottom');
ylabel('{\itθ_{CRNS}} [m^3/m^3]', 'Interpreter', 'tex');

yyaxis right;
invertedPrecipitation = -tw_JRain_day; % Inverting precipitation data
bar(tromble_daily.Timestamp, invertedPrecipitation, 'BarWidth', 2, 'FaceColor', [0 0 0]);
ylabel('Precipitation [mm/day]');
ax1=gca;
set(ax1,'Ycolor','k', 'YLim', [-150 0], 'YTick', -[75 50 25 0], 'YTickLabel', [75 50 25 0]);
legend('August Event','CRNS','Sensor
Network','5cm','15cm','30cm','50cm','100cm','Gravimetric Samples','');

%%
figure2 = figure('position', [0, 0, plotwidth, plotheight]);
yyaxis left
ax1=subplot(2,2,1); %Plot 1 & 2
plot(tromble_daily.Timestamp, Daily_tt5_5cm);
hold on
plot(tromble_daily.Timestamp, Daily_tt5_15cm);
plot(tromble_daily.Timestamp, Daily_tt5_30cm);
set(ax1,'XTick',tick);
datetick('x','mm/dd/yy','keepticks')
xlim([xl xu])
ylim([0 0.4])
set(ax1, 'YTick', [0 0.05 0.10 0.15 0.20 0.25 0.30 0.35 0.40],'YTickLabel',
{'0','0.05','0.10','0.15','0.20','0.25','0.30','0.35','0.40'});
set(ax1, 'XTickLabel',{});
plot(tromble_daily.Timestamp(11), 0.0515, "diamond", 'MarkerSize', 15,
'MarkerEdgeColor', 'k','LineWidth',3);
yyaxis right;
invertedPrecipitation = -tw_JRain_day; % Inverting precipitation data
bar(tromble_daily.Timestamp, invertedPrecipitation, 'BarWidth', 2, 'FaceColor', [0 0 0]);
ylabel('Precipitation [mm/day]');
ax1=gca;
set(ax1,'Ycolor','k', 'YLim', [-150 0], 'YTick', -[75 50 25 0], 'YTickLabel', [75 50 25 0]);

ax2=subplot(2,2,2); %Plot 3 & 4
plot(tromble_daily.Timestamp, Daily_tt6_5cm);
hold on
plot(tromble_daily.Timestamp, Daily_tt6_15cm);
plot(tromble_daily.Timestamp, Daily_tt6_30cm);
set(ax2,'XTick',tick);
datetick('x','mm/dd/yy','keepticks')
xlim([xl xu])
ylim([0 0.4])
```

```
set(ax2, 'YTick', [0 0.05 0.10 0.15 0.20 0.25 0.30 0.35 0.40],'YTickLabel',
{'0','0.05','0.10','0.15','0.20','0.25','0.30','0.35','0.40'});
set(ax2, 'XTickLabel',{});
plot(tromble_daily.Timestamp(11), 0.0515, "diamond", 'MarkerSize', 15,
'MarkerEdgeColor', 'k','LineWidth',3);
yyaxis right;
invertedPrecipitation = -tw_JRain_day; % Inverting precipitation data
bar(tromble_daily.Timestamp, invertedPrecipitation, 'BarWidth', 2, 'FaceColor', [0 0 0]);
ylabel('Precipitation [mm/day]');
ax2=gca;
set(ax2,'Ycolor','k', 'YLim', [-150 0], 'YTick', -[75 50 25 0], 'YTickLabel', [75 50 25 0]);

ax3=subplot(2,2,3); %Plot 3 & 4
plot(tromble_daily.Timestamp, channel2_daily.('5cm'));
hold on
plot(tromble_daily.Timestamp, channel2_daily.('15cm'));
plot(tromble_daily.Timestamp, channel2_daily.('30cm'));
plot(tromble_daily.Timestamp, channel2_daily.('50cm'));
plot(tromble_daily.Timestamp, channel2_daily.('100cm'));
set(ax3,'XTick',tick);
datetick('x','mm/dd/yy','keepticks')
xlim([xl xu])
ylim([0 0.4])
set(ax3, 'YTick', [0 0.05 0.10 0.15 0.20 0.25 0.30 0.35 0.40],'YTickLabel',
{'0','0.05','0.10','0.15','0.20','0.25','0.30','0.35','0.40'});
set(ax3, 'XTickLabel',{});
plot(tromble_daily.Timestamp(11), 0.0515, "diamond", 'MarkerSize', 15,
'MarkerEdgeColor', 'k','LineWidth',3);

yyaxis right;
invertedPrecipitation = -tw_JRain_day; % Inverting precipitation data
bar(tromble_daily.Timestamp, invertedPrecipitation, 'BarWidth', 2, 'FaceColor', [0 0 0]);
ylabel('Precipitation [mm/day]');
ax3=gca;
set(ax3,'Ycolor','k', 'YLim', [-150 0], 'YTick', -[75 50 25 0], 'YTickLabel', [75 50 25 0]);

ax4=subplot(2,2,4); %Plot 3 & 4
plot(tromble_daily.Timestamp, tromble_daily.CRNS);
hold on
plot(tromble_daily.Timestamp, tromble_daily.Network);
set(ax4,'XTick',tick);
datetick('x','mm/dd/yy','keepticks')
xlim([xl xu])
ylim([0 0.4])
```

```
set(ax4, 'YTick', [0 0.05 0.10 0.15 0.20 0.25 0.30 0.35 0.40],'YTickLabel',
{'0','0.05','0.10','0.15','0.20','0.25','0.30','0.35','0.40'});
set(ax4, 'XTickLabel',{});
plot(tromble_daily.Timestamp(11), 0.0515, "diamond", 'MarkerSize', 15,
'MarkerEdgeColor', 'k','LineWidth',3);

yyaxis right;
invertedPrecipitation = -tw_JRain_day; % Inverting precipitation data
bar(tromble_daily.Timestamp, invertedPrecipitation, 'BarWidth', 2, 'FaceColor', [0 0 0]);
ylabel('Precipitation [mm/day]');
ax4=gca;
set(ax4,'Ycolor','k', 'YLim', [-150 0], 'YTick', -[75 50 25 0], 'YTickLabel', [75 50 25 0]);
```

Downstream Playa – Weighted Sensor Network

```
%%%%%%%% IMPORTANT FILES FROM SOIL PROFILE TRANSECTS
%%%%%%%%
% Read in csv files
file1 = 'HPS1.csv';
file2 = 'HPS2.csv';
file3 = 'HPS3.csv';


% ... read in more files and concatenate them
data1 =readmatrix(file1); %HPS1 (Next to CRNS)
data2 = readmatrix(file2); %HPS2 (Middle of Playa)
data3 = readmatrix(file3); %HPS3 (Outside of Playa)

% ... read in more files and concatenate them

%%% Year, Month, Day,       Day_Fraction
tdat_SM1=datenum(data1(:,2),data1(:,3),data1(:,4)+data1(:,5));
tdat_SM2=datenum(data2(:,2),data2(:,3),data2(:,4)+data2(:,5));
tdat_SM3=datenum(data3(:,2),data3(:,3),data3(:,4)+data3(:,5));


%%Extract columns from HPS1, HPS2, HPS3
data1_5_100cm = data1(:,[6 8 10 12 14 16]);%( 5, 15, 30, 50, 75, 100) HPS1
data2_5_100cm = data2(:,[6 8 10 12 14 16]) ;%( 5, 15, 30, 50, 75, 100) HPS2
data3_5_100cm = data3(:,[6 8 10 12 14 16]) ;%( 5, 15, 30, 50, 75, 100) HPS3


%%%%%%%  CALCULATE HOURLY SOIL MOISTURE VALUES  %%%%%%%%
%HPS1
hourly_dataHP1 = [];
for i = 1:floor(length(tdat_SM1)/2)
   idx = ((i-1)*2+1):(i*2);
   hourly_dataHP1(i,:) = [tdat_SM1(idx(1)), nanmean(data1_5_100cm(idx,:), 1)];
end
hourly_dataHP1(hourly_dataHP1 == 0) = NaN; % Replace zeros with NaN

%HPS2
hourly_dataHP2= [];
for i = 1:floor(length(tdat_SM2)/2)
   idx = ((i-1)*2+1):(i*2);
   hourly_dataHP2(i,:) = [tdat_SM2(idx(1)), nanmean(data2_5_100cm(idx,:), 1)];
end
hourly_dataHP2(hourly_dataHP2 == 0) = NaN; % Replace zeros with NaN
```

```
%HPS3
hourly_dataHP3 = [];
for i = 1:floor(length(tdat_SM3)/2)
   idx = ((i-1)*2+1):(i*2);
   hourly_dataHP3(i,:) = [tdat_SM3(idx(1)), nanmean(data3_5_100cm(idx,:), 1)];
end
hourly_dataHP3(hourly_dataHP3 == 0) = NaN; % Replace zeros with NaN

%%%%%%%%%% Synchronize HPS1, HPS2, HPS3 %%%%%%%%
%HPS1 = Next to CRNS,  HPS2 = Center of Playa, HPS3 = Outside of Playa
% Convert matrices to tables
% Apply function to replace '0' with 'nan' in tables
% Apply function to replace '0' with 'nan' in tables
t1_hp1 = array2table(hourly_dataHP1, 'VariableNames', {'Date', '5cm', '15cm', '30cm',
'50cm','75cm','100cm'});
t2_hp2= array2table(hourly_dataHP2, 'VariableNames', {'Date', '5cm', '15cm', '30cm',
'50cm', '75cm', '100cm'});
t3_hp3 = array2table(hourly_dataHP3, 'VariableNames', {'Date', '5cm', '15cm', '30cm',
'50cm', '75cm', '100cm'});


% Convert datenumbers to datetime
t1_hp1.Date = datetime(t1_hp1.Date, 'ConvertFrom', 'datenum');
t2_hp2.Date = datetime(t2_hp2.Date, 'ConvertFrom', 'datenum');
t3_hp3.Date = datetime(t3_hp3.Date, 'ConvertFrom', 'datenum');


% Convert tables to timetables
tt1_hp1 = table2timetable(t1_hp1);
tt2_hp2 = table2timetable(t2_hp2);
tt3_hp3 = table2timetable(t3_hp3);

% Resample timetables to have regular hourly intervals
tt1_hp1 = retime(tt1_hp1, 'hourly', 'pchip');
tt2_hp2 = retime(tt2_hp2, 'hourly', 'pchip');
tt3_hp3 = retime(tt3_hp3, 'hourly', 'pchip');

%% Daily Soil Moisture Values %%%%%%%%%%%%%%%%%%
transect1_daily=retime(tt1_hp1,'daily','mean'); %Close to the CRNS
transect2_daily=retime(tt2_hp2,'daily','mean'); %Middle of playa
transect3_daily=retime(tt3_hp3,'daily','mean'); %Outside Playa
```

```
%% Daily Soil Moisture Values %%%%%%%%%%%%%%%%%%

% Synchronize timetables based on hourly interval
st_tt = synchronize(tt1_hp1, tt2_hp2, tt3_hp3,  'union');

% Replace negative numbers with NaN
st_tt{:,:}(st_tt{:,:}<0) = NaN;

%% %%%%%%%%%% Horizontal weighted function
%%%%%%%%%%%%%%%%%%
%Radial weights calculated from Shron exponential decay graph: 5, 25, 75m
weight_hp1 =2.13E-03; %changed to 5m horizontal weight
% weight_hp1= 0.014809922;
% weight_hp2=0.000706353;
% weight_hp3= 0.000172111;
weight_hp2 = 5.87E-04; %25 m
weight_hp3 = 2.02E-04;%75 m
%weight_hp3 = 0.00019104188317194 6;%75 m

%% Calculate total weighted sum for each depth (treat missing data as nan values)
sum_5cm = nansum([weight_hp1*st_tt.('5cm_tt1_hp1'),
weight_hp2*st_tt.('5cm_tt2_hp2'), weight_hp3*st_tt.('5cm_tt3_hp3')], 2);
sum_15cm = nansum([weight_hp1*st_tt.('15cm_tt1_hp1'),
weight_hp2*st_tt.('15cm_tt2_hp2'), weight_hp3*st_tt.('15cm_tt3_hp3')], 2);
sum_30cm =
nansum([weight_hp1*st_tt.('30cm_tt1_hp1'),weight_hp2*st_tt.('30cm_tt2_hp2'),
weight_hp3*st_tt.('30cm_tt3_hp3')], 2);
sum_50cm = nansum([weight_hp1*st_tt.('50cm_tt1_hp1'),
weight_hp2*st_tt.('50cm_tt2_hp2'), weight_hp3*st_tt.('50cm_tt3_hp3')], 2);
sum_75cm = nansum([weight_hp1*st_tt.('75cm_tt1_hp1'),
weight_hp2*st_tt.('75cm_tt2_hp2'), weight_hp3*st_tt.('75cm_tt3_hp3')], 2);
sum_100cm = nansum([weight_hp1*st_tt.('100cm_tt1_hp1'),
weight_hp2*st_tt.('100cm_tt2_hp2'), weight_hp3*st_tt.('100cm_tt3_hp3')], 2);

%% %%%%%%%%%% Non Horizontal weighted function
%%%%%%%%%%%%%%%%%%
% sum_5cm = nanmean([st_tt.('5cm_tt1_hp1'), st_tt.('5cm_tt2_hp2'),
st_tt.('5cm_tt3_hp3')], 2);
% sum_15cm = nanmean([st_tt.('15cm_tt1_hp1'), st_tt.('15cm_tt2_hp2'),
st_tt.('15cm_tt3_hp3')], 2);
% sum_30cm = nanmean([st_tt.('30cm_tt1_hp1'),st_tt.('30cm_tt2_hp2'),
st_tt.('30cm_tt3_hp3')], 2);
% sum_50cm = nanmean([st_tt.('50cm_tt1_hp1'), st_tt.('50cm_tt2_hp2'),
st_tt.('50cm_tt3_hp3')], 2);
```

```
% sum_75cm = nanmean([st_tt.('75cm_tt1_hp1'), st_tt.('75cm_tt2_hp2'),
st_tt.('75cm_tt3_hp3')], 2);
% sum_100cm = nanmean([st_tt.('100cm_tt1_hp1'), st_tt.('100cm_tt2_hp2'),
st_tt.('100cm_tt3_hp3')], 2);

% % Total weights for each depth
total_weights = weight_hp1 + weight_hp2 + weight_hp3;

% Calculate weighted averages
avg_5cm = sum_5cm / total_weights;
avg_15cm = sum_15cm / total_weights;
avg_30cm = sum_30cm / total_weights;
avg_50cm = sum_50cm / total_weights;
avg_75cm = sum_75cm / total_weights;
avg_100cm = sum_100cm / total_weights;

% No Horizontal Weight
% avg_5cm = sum_5cm;
% avg_15cm = sum_15cm;
% avg_30cm = sum_30cm;
% avg_50cm = sum_50cm;
% avg_75cm = sum_75cm;
% avg_100cm = sum_100cm;

% Create the numeric matrix with the averages
averageMatrix_ps = [avg_5cm, avg_15cm, avg_30cm, avg_50cm, avg_75cm,
avg_100cm];

%%%%%%%%%%%%%% Vertical weighted function %%%%%%%%%%%
% Assuming z_star is a matlab double table
z_star = z_depth_ps; %changed to z_depth_filled_ps (12/20/23)

% Identify the indices of the non-missing values
zot_zan_indices = find(~isnan(z_star)); % Now zot_zan_indices contains the indices of
non-NaN elements

for k = 1:(length(zot_zan_indices) - 1)
   gap = zot_zan_indices(k + 1) - zot_zan_indices(k);
   if gap <= 23 % Including the starting point, so gap is 16 for 15 NaNs in between
      z_star(zot_zan_indices(k):zot_zan_indices(k + 1)) = interp1([zot_zan_indices(k),
zot_zan_indices(k + 1)], ...
         [z_star(zot_zan_indices(k)), z_star(zot_zan_indices(k + 1))],
zot_zan_indices(k):zot_zan_indices(k + 1));
   end
end
```

```
% Define the soil depths
soil_depths = [5, 15,30, 50,75,100];

% Number of time steps
num_timesteps = height(z_star);

% Initialize a matrix to store the weights for each soil depth at each time step
weights = zeros(num_timesteps, length(soil_depths));

% Calculate the weights at each time step for each soil depth
for i = 1:num_timesteps
    % Calculate the constant 'a' for this time step
    b = 1; % assuming b is 1 for a linear relationship
    a = 1 / (z_star(i) - (z_star(i)^(b+1)) / ((z_star(i)^b) * (b+1)));

    for j = 1:length(soil_depths)
        % Calculate the weight for this soil depth at this time step
        if soil_depths(j) <= z_star(i)
            weights(i, j) = a * (1 - (soil_depths(j) / z_star(i))^b);
        else
            weights(i, j) = 0;
        end
    end
end

% Convert the weights matrix to a table for easy viewing and manipulation
weights_table = array2table(weights, 'VariableNames', strcat('Depth_',
string(soil_depths)));

SN_Table = averageMatrix_ps(1:13896,:);


% Multiply each soil moisture column by its corresponding weight
weighted_soil_moisture = SN_Table.* weights;

% Compute the weighted average at each time step
weighted_average_ps = sum(weighted_soil_moisture, 2) ./ sum(weights, 2);

WA_sgf_ps = sgolayfilt(weighted_average_ps,2,3); %filtered product


% Extract hourly timestamps from your table (Assuming it is a timetable)
hourly_intervals = st_tt.Date(1:13896,:); % Change to the actual variable name
representing time in your table.
```

```
%Generate new 30 minute interval timestamps
start_time = hourly_intervals(1);
end_time = hourly_intervals(end);
weightaverage_30= (start_time:minutes(30):end_time)';

% Initialize the new array for 30 minutes interval data
wa_30min = nan(length(weightaverage_30), 2); % Second column will hold the
interpolated values.
wa_30min(:, 1) = datenum(weightaverage_30);

% Perform linear interpolation to get 30-minute interval data.
wa_30min(:, 2) = interp1(datenum(hourly_intervals), WA_sgf_ps, wa_30min(:, 1),
'linear');

WA_30minsgf_ps = sgolayfilt(wa_30min,3,11); %filtered product


% Replace values below 0 with NaN
WA_30minsgf_ps(WA_30minsgf_ps < 0) = NaN;

%% Test Different sections of soil sensors at DP %%%%%%%%%%%%%%%%%%

num_days1 = floor(length(avg_100cm)/24);
Depth_100cm = zeros(num_days1,1); %100cm
for i = 1:num_days1
   day_sum = 0;
   for j = 1:24
      day_sum = day_sum + avg_100cm((i-1)*24+j);
   end
   Depth_100cm(i) = day_sum / 24; %100cm
end

Depth_75cm = zeros(num_days1,1); %75cm
for i = 1:num_days1
   day_sum = 0;
   for j = 1:24
      day_sum = day_sum + avg_75cm((i-1)*24+j);
   end
   Depth_75cm(i) = day_sum / 24; %75cm
end

Depth_50cm = zeros(num_days1,1); %50cm
for i = 1:num_days1
   day_sum = 0;
```

```
   for j = 1:24
      day_sum = day_sum + avg_50cm((i-1)*24+j);
   end
   Depth_50cm(i) = day_sum / 24; %50cm
end

Depth_30cm = zeros(num_days1,1); %30cm
for i = 1:num_days1
   day_sum = 0;
   for j = 1:24
      day_sum = day_sum + avg_30cm((i-1)*24+j);
   end
   Depth_30cm(i) = day_sum / 24; %30cm
end

Depth_15cm = zeros(num_days1,1); %15cm
for i = 1:num_days1
   day_sum = 0;
   for j = 1:24
      day_sum = day_sum + avg_15cm((i-1)*24+j);
   end
   Depth_15cm(i) = day_sum / 24; %15cm
end

Depth_5cm = zeros(num_days1,1); %5cm
for i = 1:num_days1
   day_sum = 0;
   for j = 1:24
      day_sum = day_sum + avg_5cm((i-1)*24+j);
   end
   Depth_5cm(i) = day_sum / 24; %5cm
end

%%%%%%%%%%%%%%%%%  PLOTTING FIGURE  %%%%%%%%%%%
% PLOT TDT WEIGHTED - Neutron Data with TDT -Weighted
figure(1002)
clf % clear figure
subplot(1,1,1,'Fontsize',fs,'XTick',tick)
hold on
%plot(sswc(:,1),sswc(:,7),'k.','markersize',ms) %Mod Count
plot(sswc_30min_ps(:,1),SWC1_filled30min,'k-','markersize',ms,'LineWidth',1); %Mod
Count filtered
%plot(sswc(:,1),WA_sgf,'r.-','markersize',ms)
plot(sswc_30min_ps(:,1),WA_30minsgf_ps,'r-','markersize',ms,'LineWidth',1);
hold off
```

```
ylabel('SWC (m^3/m^3)','fontsize',fs)
title('PS-SMAL:  Weighted Sensor Network','fontsize',fs)
datetick('x','mmmm','keepticks')
xlim([xl xu])
legend('CRNS - SWC ','TDT- Weighted','Location', 'NorthWest')
ylim([0.05 0.45])
grid on
box on


figure(1003)
clf % clear figure

% Create the top axes for the SWC data
ax1 = subplot(2,1,1);
%plot(ax1, sswc(:,1), sswc(:,7), 'k.','markersize',ms); %Mod Count
hold on;
plot(sswc_30min_ps(:,1), SWC1_filled30min, 'b-','markersize',ms); %Mod Count filtered
hold on
plot(sswc_30min_ps(:,1), WA_30minsgf_ps(:,2), 'r-','markersize',ms);
ylabel(ax1, 'SWC (m^3/m^3)', 'fontsize', fs);
title(ax1, 'PS-SMAL CRNS: Weighted Sensor Network', 'fontsize', fs);
datetick('x','mmmm','keepticks');
xlim([xl xu]);
legend('CRNS - SWC', 'CRNS - SWC Filtered', 'TDT- Weighted', 'Location',
'NorthWest');
ylim([0.05 0.45]);
grid on;
ax1.XAxisLocation = 'origin';

% Link the x-axes to synchronize when zooming or panning
linkaxes([ax1, ax2], 'x');



%%%Exponential Decay of Sensors
%%%%%%%%%%%%%%%%%%%%%%%%%%%%%%%%%%
tw_distance = TWRadialWeights.DistanceRm;
tw_weight = TWRadialWeights.normalized;

ps_distance = PSSMALRadialWeights.DistanceRm;
ps_weight = PSSMALRadialWeights.normalized;

plot(tw_distance,tw_weight);
hold on
```

```
plot(SensorLocationsweights.Distance_tw(1:2),
SensorLocationsweights.weight_tw(1:2),'hexagram'); %Plot 1 &2
plot(SensorLocationsweights.Distance_tw(3:3),
SensorLocationsweights.weight_tw(3:3),'diamond'); %Channel 2
plot(SensorLocationsweights.Distance_tw(4:5),
SensorLocationsweights.weight_tw(4:5),'hexagram'); %Plot3&4
plot(SensorLocationsweights.Distance_tw(6:8),
SensorLocationsweights.weight_tw(6:8),'+'); %Transects
plot(SensorLocationsweights.Distance_tw(6:8),
SensorLocationsweights.weight_tw(6:8),'+'); %Transects
xlabel('Distance [m]');
ylabel('Horizontal Weight [-]');
legend('Footprint Behavior','Runoff Plots','Channel Soil Sensors','','','Transect Soil
Sensors');
title('Upland Watershed: Sensor Network Horizontal Weights');

plot(ps_distance,ps_weight);
hold on
plot(SensorLocationsweights.Distance_ps, SensorLocationsweights.weight_ps,'+');
plot(SensorLocationsweights.Distance_ps, SensorLocationsweights.weight_ps,'+');
xlabel('Distance [m]');
ylabel('Horizontal Weight [-]');
legend('Footprint Behavior','','Transect Soil Sensors');
title('Downstream Playa: Sensor Network Horizontal Weights');

%% Figures Depth and Location
%%%%%%%%%%%%%%%%%%%%%%%%%%%%%%%%%%%%%%%%%%%%%%%%%%%%%%%%%%%%%%%%%%%%%%%%%%%%%%%%
st =playa_daily.Timestamp(1);    % Starting date
en = playa_daily.Timestamp(580);    % Ending date
fs = 30; %font size
plotwidth = 2800; % Adjust width as needed
plotheight = 2800; % Adjust height as needed

startDate= playa_daily.Timestamp(50);
endDate = playa_daily.Timestamp(53);

tick=(st:en);
tick = tick(day(tick)==1);

xl=st-1;
xu=en+1;
figure1 = figure('position', [0, 0, plotwidth, plotheight]);
yyaxis left
ax1=subplot(2,1,1);
```

```
plot(playa_daily.Timestamp, playa_daily.CRNS);
hold on
plot(playa_daily.Timestamp, playa_daily.Network);
plot(playa_daily.Timestamp, Depth_5cm);
plot(playa_daily.Timestamp, Depth_15cm);
plot(playa_daily.Timestamp, Depth_30cm);
plot(playa_daily.Timestamp, Depth_50cm);
plot(playa_daily.Timestamp, Depth_75cm);
plot(playa_daily.Timestamp, Depth_100cm);
set(ax1,'XTick',tick);
datetick('x','mm/dd/yy','keepticks')
xlim([xl xu])
ylim([0 0.4])
set(ax1, 'YTick', [0 0.05 0.10 0.15 0.20 0.25 0.30 0.35 0.40],'YTickLabel',
{'0','0.05','0.10','0.15','0.20','0.25','0.30','0.35','0.40'});
set(ax1, 'XTickLabel',{});
legend ('','CRNS','Sensor Network','5cm','15cm','30cm','50cm','75cm','100cm','','');

plot(playa_daily.Timestamp(1), 0.12, "diamond",'MarkerSize', 15, 'MarkerEdgeColor',
'k','LineWidth',3); %Gravimetric Markers
plot(playa_daily.Timestamp(157), 0.1427, "diamond",'MarkerSize', 15,
'MarkerEdgeColor', 'k','LineWidth',3); %Gravimetric Markers
yLimits = ([0.001 0.3990]);
shadedArea = fill([startDate, startDate, endDate, endDate], [yLimits(1), yLimits(2),
yLimits(2), yLimits(1)], [0.9, 0.9, 0.9], 'EdgeColor', 'none');
uistack(shadedArea, 'bottom');
ylabel('{\itθ_{CRNS}} [m^3/m^3]', 'Interpreter', 'tex');

yyaxis right;
invertedPrecipitation = -ps_JRain_day; % Inverting precipitation data
bar(playa_daily.Timestamp, invertedPrecipitation, 'BarWidth', 2, 'FaceColor', [0 0 0]);
ylabel('Precipitation [mm/day]');
ax1=gca;
set(ax1,'Ycolor','k', 'YLim', [-150 0], 'YTick', -[75 50 25 0], 'YTickLabel', [75 50 25 0]);

%%
figure2 = figure('position', [0, 0, plotwidth, plotheight]);
yyaxis left
ax1=subplot(2,2,1); %HPS1
plot(playa_daily.Timestamp, transect1_daily.('5cm'));
hold on
plot(playa_daily.Timestamp, transect1_daily.('15cm'));
plot(playa_daily.Timestamp, transect1_daily.('30cm'));
plot(playa_daily.Timestamp, transect1_daily.('50cm'));
plot(playa_daily.Timestamp, transect1_daily.('75cm'));
```

```
plot(playa_daily.Timestamp, transect1_daily.('100cm'));
set(ax1,'XTick',tick);
datetick('x','mm/dd/yy','keepticks')
xlim([xl xu])
ylim([0 0.5])
set(ax1, 'YTick', [0 0.05 0.10 0.15 0.20 0.25 0.30 0.35 0.40 0.45 0.50],'YTickLabel',
{'0','0.05','0.10','0.15','0.20','0.25','0.30','0.35','0.40','0.45','0.50'});
set(ax1, 'XTickLabel',{});
plot(playa_daily.Timestamp(1), 0.12, "diamond",'MarkerSize', 15, 'MarkerEdgeColor',
'k','LineWidth',3); %Gravimetric Markers
plot(playa_daily.Timestamp(157), 0.135, "diamond",'MarkerSize', 15,
'MarkerEdgeColor', 'k','LineWidth',3); %Gravimetric Markers
ylabel('{\itθ} [m^3/m^3]', 'Interpreter', 'tex');
legend ('5cm','15cm','30cm','50cm','75cm','100cm');

yyaxis right;
invertedPrecipitation = -ps_JRain_day; % Inverting precipitation data
bar(playa_daily.Timestamp, invertedPrecipitation, 'BarWidth', 2, 'FaceColor', [0 0 0]);
ylabel('Precipitation [mm/day]');
ax1=gca;
set(ax1,'Ycolor','k', 'YLim', [-150 0], 'YTick', -[75 50 25 0], 'YTickLabel', [75 50 25 0]);

ax2=subplot(2,2,2); %HPS2
plot(playa_daily.Timestamp, transect2_daily.('5cm'));
hold on
plot(playa_daily.Timestamp, transect2_daily.('15cm'));
plot(playa_daily.Timestamp, transect2_daily.('30cm'));
plot(playa_daily.Timestamp, transect2_daily.('50cm'));
plot(playa_daily.Timestamp, transect2_daily.('75cm'));
%plot(playa_daily.Timestamp, transect2_daily.('100cm'));
set(ax2,'XTick',tick);
datetick('x','mm/dd/yy','keepticks')
xlim([xl xu])
ylim([0 0.5])
set(ax2, 'YTick', [0 0.05 0.10 0.15 0.20 0.25 0.30 0.35 0.40 0.45 0.50],'YTickLabel',
{'0','0.05','0.10','0.15','0.20','0.25','0.30','0.35','0.40','0.45','0.50'});
set(ax2, 'XTickLabel',{});
plot(playa_daily.Timestamp(1), 0.12, "diamond",'MarkerSize', 15, 'MarkerEdgeColor',
'k','LineWidth',3); %Gravimetric Markers
plot(playa_daily.Timestamp(157), 0.135, "diamond",'MarkerSize', 15,
'MarkerEdgeColor', 'k','LineWidth',3); %Gravimetric Markers
ylabel('{\itθ} [m^3/m^3]', 'Interpreter', 'tex');
legend('5cm','15cm','30cm','50cm','75cm');

yyaxis right;
```

```
invertedPrecipitation = -ps_JRain_day; % Inverting precipitation data
bar(playa_daily.Timestamp, invertedPrecipitation, 'BarWidth', 2, 'FaceColor', [0 0 0]);
ylabel('Precipitation [mm/day]');
ax2=gca;
set(ax2,'Ycolor','k', 'YLim', [-150 0], 'YTick', -[75 50 25 0], 'YTickLabel', [75 50 25 0]);


ax3=subplot(2,2,3); %HPS3
plot(playa_daily.Timestamp, transect3_daily.('5cm'));
hold on
plot(playa_daily.Timestamp, transect3_daily.('15cm'));
%plot(playa_daily.Timestamp, transect3_daily.('30cm'));
plot(playa_daily.Timestamp, transect3_daily.('50cm'));
plot(playa_daily.Timestamp, transect3_daily.('75cm'));
plot(playa_daily.Timestamp, transect3_daily.('100cm'));
set(ax3,'XTick',tick);
datetick('x','mm/dd/yy','keepticks')
xlim([xl xu])
ylim([0 0.5])
set(ax3, 'YTick', [0 0.05 0.10 0.15 0.20 0.25 0.30 0.35 0.40 0.45 0.50],'YTickLabel',
{'0','0.05','0.10','0.15','0.20','0.25','0.30','0.35','0.40','0.45','0.50'});
set(ax3, 'XTickLabel',{});
plot(playa_daily.Timestamp(1), 0.12, "diamond",'MarkerSize', 15, 'MarkerEdgeColor',
'k','LineWidth',3); %Gravimetric Markers
plot(playa_daily.Timestamp(157), 0.135, "diamond",'MarkerSize', 15,
'MarkerEdgeColor', 'k','LineWidth',3); %Gravimetric Markers
ylabel('{\itθ} [m^3/m^3]', 'Interpreter', 'tex');
legend('5cm','15cm','50cm','75cm','100cm');

yyaxis right;
invertedPrecipitation = -ps_JRain_day; % Inverting precipitation data
bar(playa_daily.Timestamp, invertedPrecipitation, 'BarWidth', 2, 'FaceColor', [0 0 0]);
ylabel('Precipitation [mm/day]');
ax3=gca;
set(ax3,'Ycolor','k', 'YLim', [-150 0], 'YTick', -[75 50 25 0], 'YTickLabel', [75 50 25 0]);


ax4=subplot(2,2,4); %CRNS & Sensor Network
plot(playa_daily.Timestamp, playa_daily.CRNS);
hold on
plot(playa_daily.Timestamp, playa_daily.Network);
set(ax4,'XTick',tick);
datetick('x','mm/dd/yy','keepticks')
xlim([xl xu])
ylim([0 0.5])
```

```
set(ax4, 'YTick', [0 0.05 0.10 0.15 0.20 0.25 0.30 0.35 0.40 0.45 0.50],'YTickLabel',
{'0','0.05','0.10','0.15','0.20','0.25','0.30','0.35','0.40','0.45','0.50'});
set(ax4, 'XTickLabel',{});
plot(playa_daily.Timestamp(1), 0.12, "diamond",'MarkerSize', 15, 'MarkerEdgeColor',
'k','LineWidth',3); %Gravimetric Markers
plot(playa_daily.Timestamp(157), 0.135, "diamond",'MarkerSize', 15,
'MarkerEdgeColor', 'k','LineWidth',3); %Gravimetric Markers
ylabel('{\itθ} [m^3/m^3]', 'Interpreter', 'tex');
legend('CRNS','Sensor Network');

yyaxis right;
invertedPrecipitation = -ps_JRain_day; % Inverting precipitation data
bar(playa_daily.Timestamp, invertedPrecipitation, 'BarWidth', 2, 'FaceColor', [0 0 0]);
ylabel('Precipitation [mm/day]');
ax4=gca;
set(ax4,'Ycolor','k', 'YLim', [-150 0], 'YTick', -[75 50 25 0], 'YTickLabel', [75 50 25 0]);
```

APPENDIX D

SOIL SAMPLES

SOIL SAMPLES

This appendix describes a digital repository of the SOIL SAMPLES for the Upland Watershed and Downstream Playa. The datasets are organized within the digital folder "RubyYHurtado_Thesis Data/APPENDIX_D"

- The following Excel files contain the gravimetric results of each soil sample collection, and the following variables derived from the soil samples: soil bulk density, gravimetric water content, porosity, and the raw data from soil sample tins.

File Name	File Description
SoilChemistryResults.xlsx	**Upland Watershed and Downstream Playa soil chemistry results including** lattice water and soil organic carbon**.**
UplandWatershed_July_GravimetricSamples.xlsx	**Upland Watershed July 11th, 2022, gravimetric soil collections.** Soil bulk density**,** gravimetric water content**.**
DownstreamPlaya_December_GravimetricSamples.xlsx	**Downstream Playa December 5th, 2022, gravimetric soil**

	collections. Soil bulk density, gravimetric water content**.**
DownstreamPlaya_July_GravimetricSamples.xlsx	**Downstream Playa July 1st, 2022.** Soil bulk density, gravimetric water content**.**

148

APPENDIX E

ADDITIONAL DATASETS

ADDITIONAL DATASETS

This appendix describes a digital repository of the ADDITIONAL DATSETS for the Upland Watershed and Downstream Playa. The datasets are organized within the digital folder "RubyYHurtado_Thesis Data/APPENDIX_E"150

File Name	File Description
CRNS_Rover_FieldDescription.pdf	Field description and instructions of CRNS and Rover sensors summer campaign deployment.
CRNS_RovingFieldCampaign.mat	MATLAB script to calculate relationship between RV1 (Roving Sensor 1), RV2 (Roving Sensor 2), and the CRNS at the Downstream Playa.
CRNS_RovingFieldCampaign_PartB.mat	MATLAB script plot the exponential behavior of the CRNS and roving sensors at the Downstream Playa.
CRS/1000-B Manual Guide	Instructional manual for the CRS-1000/B Hydroinnova sensor model type used at the Upland Watershed and Downstream Playa.

Upland Watershed Soil Sample Collections

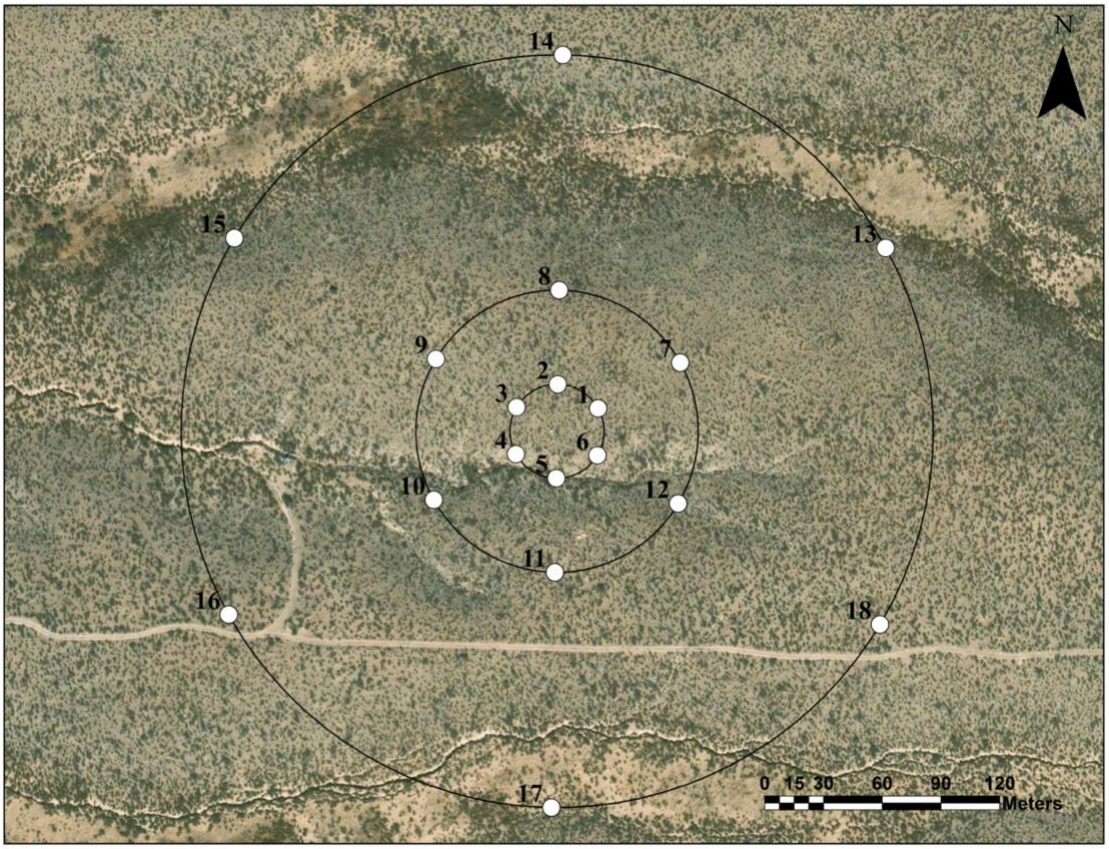

- Gravimetric soil sample collections for the July 11th, 2022, field campaign. Coordinates for each location can be found with the Excel "UplandWatershed_July_GravimetricSamples.xlsx" file

Downstream Playa Soil Sample Collections

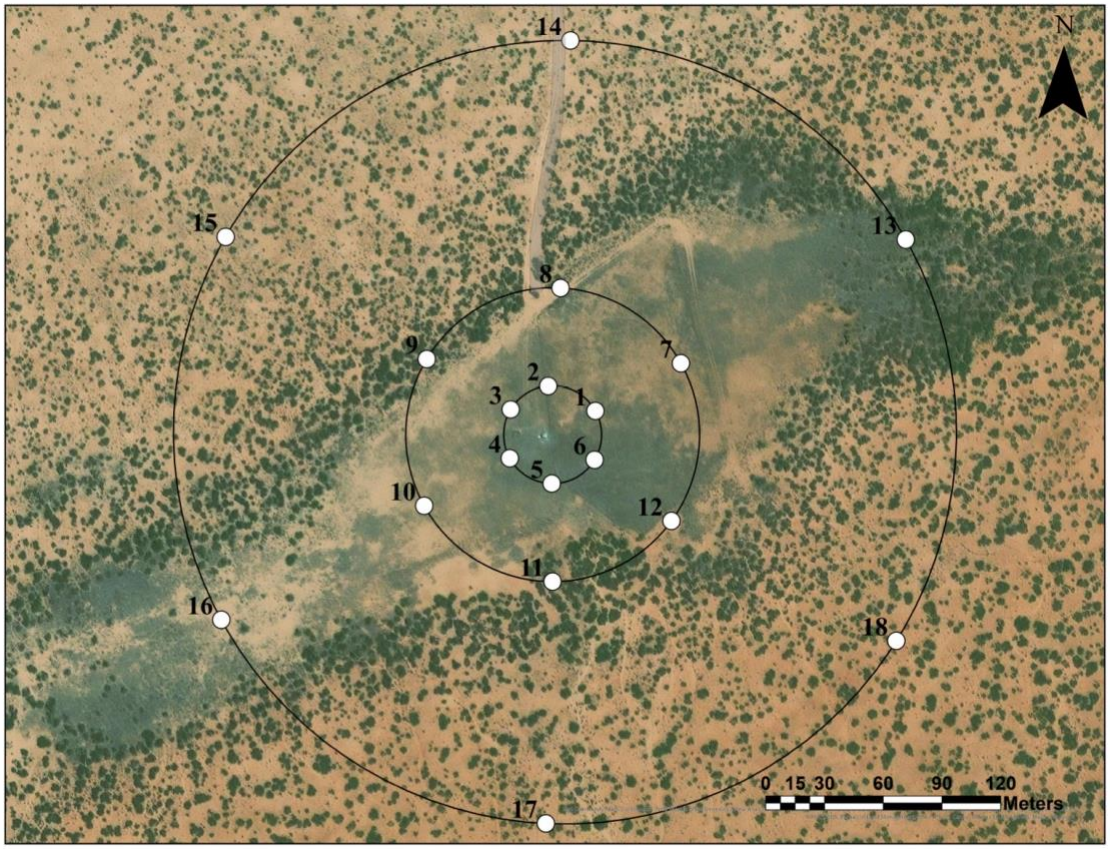

- Gravimetric soil sample collections for the July 1st, 2022, and December 5th, 2022, field campaign. Coordinates for each location can be found with the Excel "DownstreamPlaya_December_GravimetricSamples.xlsx" file

Soil Sample Collection Procedure

Equipment Needed
- Soil auger
- Tins with lids
- Electrical tape
- Marker
- Scale
- Oven
- Plastic bags (optional for transporting samples)

Procedure

Preparation
1. Ensure you have all necessary equipment ready, including a soil auger, tins with lids, electrical tape, a marker, a scale, an oven, and plastic bags for sample transport if needed.
2. Label each tin and lid with the corresponding depth (5cm, 10cm, 15cm, 20cm, 25cm, and 30cm) and sample number (1-108) for one site.

Sample Collection

3. Identify and mark the specific locations where you will collect the samples. Ensure you have a total of 18 locations.
4. At the first location, use the soil auger to extract soil down to the first depth (5cm).

5. Carefully remove the soil from the auger and place it into the appropriately labeled tin for the 5cm depth. Fill the tin to about three-quarters full.

6. Place the lid on the tin and wrap it with electrical tape to ensure it is sealed to prevent moisture loss.

7. Repeat the augering and soil collection process for the depths of 10cm, 15cm, 20cm, 25cm, and 30cm at the same location, placing each depth's sample in its corresponding tin and sealing it with electrical tape.

8. Move to the next location and repeat steps 4-7. Continue this process until you have collected samples from all 18 locations at the six depths (108 samples).

Post-Collection

9. If necessary, place the sealed tins in plastic bags for transportation to the lab.

10. Wet Samples: In the lab, weigh each tin with its wet soil sample and record the weights.

11. Dry Samples: Place the tins with soil samples in an oven set to 105°C and dry them for at least 24 hours to remove all moisture.

12. Weigh Dry Samples: After drying, weigh each tin again with the dry soil and record the weights.

Calculations

13. Calculate the gravimetric water content for each sample using the formula: (weight of wet soil – weight of dry soil) / (weight of dry soil) X 100, also found in the Excel files for the Upland Watershed and Downstream Playa.

APPENDIX F

SITE PHOTOS

SITE PHOTOS

This appendix describes a digital repository of SITE PHOTOS for the Upland Watershed and Downstream Playa. The datasets are organized within the digital folder "RubyYHurtado_Thesis Data/APPENDIX_F"156

Figure F1. Downstream Playa Site Instrumentation: ~ July 1st, 2022

Figure F2. Downstream Playa Site Instrumentation, ~ September 15th, 2022

Figure F3. Upland Watershed Roving Sensors During Summer Field Campaign

Figure F4. Downstream Playa – Soil Sample Procedure During December 5th, 2022 Collection

APPENDIX G

THESIS MANUSCRIPTS

THESIS MANUSCRIPTS

This appendix describes a digital repository of the THESIS MANUSCRIPTS for the Upland Watershed and Downstream Playa. The datasets are organized within the digital folder "RubyYHurtado_Thesis Data/APPENDIX_G"160

- The following MATLAB script plots the "Manuscript Grade" final figures used in this study:

```
%% Load Data
load('TW_30min_SWC1.mat') %30minute resolution
load('TW_SWC1.mat')%hour resolution
load('TW_30min_sswc.mat')
load('TW_sswc.mat')%hour resolution
load('TW_30min_precip.mat')
load('TW_30min_rounded.mat')%rounded time
load('TW30minfiltered_wa.mat')%weighted filter sensor
load('TW_30min_zdepth.mat') %z depth
% load('TW_NoHorizontalSN_30min.mat'); %No Horizontal Weighting
%
load('P_SMAL_SWC1_30min_filled.mat') %soil water content
load('P_SMAL_SWC1_filled.mat') %soil water content filled
load('P_SMAL_sswc.mat')
load('P_SMAL_30min_precip.mat')
load('P_SMAL_rounded_30min_time.mat')
load('PS_SMAL_z_depth_30min.mat')
load('P_SMAL_WA_30minsgf.mat'); %weighted Sensor Network
load('PS_NonHorizontalSN_30min.mat');

%
%
tromble=table(rounded_sswc_datetime_tw,SWC1_30min_tw,WA_30minsgf_tw(:,2),z_3
0mindepth_tw,tw_NonHori_SN(:,2) ...
%     ,'VariableNames', {'Timestamp', 'CRNS', 'Network', 'Depth','NonHorizontalNet'});
%
% tromble_tt=table2timetable(tromble);
% tromble_daily =retime(tromble_tt,'daily','mean');
% tromble_hour=retime(tromble_tt,'hour','mean');
%
rain_tw=retime(TW30min_raintable,'daily','sum');
rain_twyr=retime(TW30min_raintable,'yearly','sum');
```

```
rain_ps=retime(PSrain_timetable,'daily','sum');
rain_psyr=retime(PSrain_timetable,'yearly','sum');
%
negatives = SWC1_filled30min <=0;
SWC1_filled30min(negatives, :) = NaN;

playa=table(rounded_sswc_datetime_ps,SWC1_filled30min,WA_30minsgf_ps(:,2),z_de
pth30min_ps,ps_NonHori_SN(:,2) ...
,'VariableNames', {'Timestamp', 'CRNS', 'Network', 'Depth','NonHorizontalNet'});

playa_tt=table2timetable(playa);
playa_daily=retime(playa_tt,'daily','mean');
playa_hour=retime(playa_tt,'hour','mean');

daily=playa_daily.CRNS;
hour=playa_hour.CRNS;

%%  Figure 2. CRNS Soil Calibration (Font Size 30, Box Line Width 30, Times New
Roman) %%%%%%%%%%%%%%%%%%%%%%%%%%%%%%%%%%%%%%%%%%%%%%%%%%%%%%%%
st =tromble_daily.Timestamp(1);    % Starting date
en = tromble_daily.Timestamp(580);    % Ending date
fs = 30; %font size
plotwidth = 2800; % Adjust width as needed
plotheight = 2800; % Adjust height as needed

startDate= tromble_daily.Timestamp(50);
endDate = tromble_daily.Timestamp(53);

tick=(st:en);
tick = tick(day(tick)==1);

xl=st-1;
xu=en+1;
%% Main ^^ Plot Components
figure1 = figure('position', [0, 0, plotwidth, plotheight]);
% Subplot for the watershed
yyaxis left
ax1=subplot(2,1,1);
plot(tromble_daily.Timestamp, tromble_daily.CRNS, 'k-','LineWidth',2); % Soil moisture
at the watershed
set(ax1,'XTick',tick);
datetick('x','mm/dd/yy','keepticks')
xlim([xl xu])
ylim([0 0.4])
```

```
set(ax1, 'YTick', [0 0.05 0.10 0.15 0.20 0.25 0.30 0.35 0.40],'YTickLabel',
{'0','0.05','0.10','0.15','0.20','0.25','0.30','0.35','0.40'});
set(ax1, 'XTickLabel',{});
hold on;
plot(tromble_daily.Timestamp(11), 0.0515, "diamond", 'MarkerSize', 15,
'MarkerEdgeColor', 'k','LineWidth',3);
yLimits = ([0.001 0.3990]);
shadedArea = fill([startDate, startDate, endDate, endDate], [yLimits(1), yLimits(2),
yLimits(2), yLimits(1)], [0.9, 0.9, 0.9], 'EdgeColor', 'none');
uistack(shadedArea, 'bottom');
ylabel('{\itθ_{CRNS}} [m^3/m^3]', 'Interpreter', 'tex');

yyaxis right;
invertedPrecipitation = -rain_tw.SumRain; % Inverting precipitation data
bar(tromble_daily.Timestamp, invertedPrecipitation, 'BarWidth', 2, 'FaceColor', [0 0 0]);
ylabel('Precipitation [mm/day]');
ax1=gca;
set(ax1,'Ycolor','k', 'YLim', [-150 0], 'YTick', -[75 50 25 0], 'YTickLabel', [75 50 25 0]);


hold off
set(gca,'FontSize',fs);
title('Upland Watershed (UW)')

% Subplot for the playa
yyaxis left %Soil Moisture
ax2=subplot(2,1,2);
plot(playa_daily.Timestamp, playa_daily.CRNS,'k-','LineWidth',2); % Soil moisture at
the playa
set(ax2,'XTick',tick);
datetick('x','mm/dd/yy','keepticks')
xlim([xl xu])
ylim([0 0.40])
ylim([0 0.40])
set(ax2, 'YTick', [0, 0.05, 0.10, 0.15, 0.20, 0.25, 0.30, 0.35, 0.40],'YTickLabel',
{'0','0.05','0.10','0.15','0.20','0.25','0.30','0.35','0.40'});
hold on;
plot(playa_daily.Timestamp(1), 0.12, "diamond",'MarkerSize', 15, 'MarkerEdgeColor',
'k','LineWidth',3); %Gravimetric Markers
plot(playa_daily.Timestamp(157), 0.1427, "diamond",'MarkerSize', 15,
'MarkerEdgeColor', 'k','LineWidth',3); %Gravimetric Markers
yLimits1 =([0.001 0.3990]);
shadedArea1 = fill([startDate, startDate, endDate, endDate], [yLimits1(1), yLimits1(2),
yLimits1(2), yLimits1(1)], [0.9, 0.9, 0.9], 'EdgeColor', 'none');
uistack(shadedArea1, 'bottom'); %Shaded Area
```

```
ylabel('{\itθ_{CRNS}} [m^3/m^3]', 'Interpreter', 'tex');

yyaxis right; %Precipitation
invertedPrecipitation1 = -rain_ps.p_tip1;
bar(rain_ps.rounded_sswc_datetime_ps, invertedPrecipitation1, 'BarWidth', 2,
'FaceColor', [0 0 0]);
ylabel('Precipitation [mm]');
ax2=gca;
set(ax2, 'YColor','k','YLim', [-150 0], 'YTick', -[75 50 25 0], 'YTickLabel', [75 50 25 0]);

hold off;
set(gca,'FontSize',fs);
xlabel('Day');
ylabel('Precipitation [mm/day]');
title('Downstream Playa (DP)');

%% Figure 3. CRNS - Gravimetric Collection
%%%%%%%%%%%%%%%%%%%%%%%%%%%%%%%%%%%%%%%%%%%%%%%%%%%%%%%%%%%%%%%%

figure1 = figure('position', [0, 0, plotwidth, plotheight]);
%% Subplot for the WATERSHED
yyaxis left
ax1=subplot(2,1,1);
plot(tromble_daily.Timestamp, tromble_daily.CRNS, 'k-','LineWidth',2); % Soil moisture
at the watershed
set(ax1,'XTick',tick);
datetick('x','mm/dd/yy','keepticks')
xlim([xl xu])
ylim([0 0.4])
set(ax1, 'YTick', [0 0.05 0.1 0.15 0.2 0.25 0.3 0.35 0.4],'YTickLabel',
{'0','0.05','0.10','0.15','0.20','0.25','0.30','0.35','0.40'});
set(ax1, 'XTickLabel',{});
hold on;
plot(tromble_daily.Timestamp, tromble_daily.Network, 'b-','LineWidth',2);
plot(tromble_daily.Timestamp(11), 0.0515, "diamond", 'MarkerSize', 15,
'MarkerEdgeColor', 'k','LineWidth',3);
yLimits = ([0.001 0.3990]);
shadedArea = fill([startDate, startDate, endDate, endDate], [yLimits(1), yLimits(2),
yLimits(2), yLimits(1)], [0.9, 0.9, 0.9], 'EdgeColor', 'none');
uistack(shadedArea, 'bottom');
ylabel('{\itθ} [m^3/m^3]', 'Interpreter', 'tex');
yyaxis right;
invertedPrecipitation = -rain_tw.SumRain; % Inverting precipitation data
bar(rain_tw.rounded_sswc_datetime_tw, invertedPrecipitation, 'BarWidth', 2,
'FaceColor', [0 0 0]);
```

```
ylabel('Precipitation [mm/day]');
ax1=gca;
set(ax1,'Ycolor','k', 'YLim', [-150 0], 'YTick', -[75 50 25 0], 'YTickLabel', [75 50 25 0]);
hold off
set(gca,'FontSize',fs);
title('Upland Watershed (UW)')
legend('','CRNS','Sensor Network','Gravimetric Samples','','');

% Subplot for the pendetration Depth at the WATERSHED
%yyaxis left %Soil Moisture
ax2=subplot(2,1,2);
plot(tromble_daily.Timestamp, tromble_daily.Depth,'k-','LineWidth',2); % Soil moisture
at the playa
set(ax2,'XTick',tick);
datetick('x','mm/dd/yy','keepticks')
xlim([xl xu])
ylim([0 70])
set(ax2, 'YTick', [ 10 20 30 40 50 60]);
hold on;
ylabel('{\it{Z^*}} [cm]', 'Interpreter', 'tex');
xlabel('Day')
set(gca,'FontSize',fs);


%% Playa
figure1 = figure('position', [0, 0, plotwidth, plotheight]);
% Subplot for the Playa
yyaxis left
ax1=subplot(2,1,1);
plot(playa_daily.Timestamp, playa_daily.CRNS, 'k-','LineWidth',2); % Soil moisture at
the watershed
set(ax1,'XTick',tick);
datetick('x','mm/dd/yy','keepticks')
xlim([xl xu])
ylim([0 0.40])
set(ax1, 'YTick', [0 0.05 0.10 0.15 0.20 0.25 0.30 0.35 0.40],'YTickLabel',
{'0','0.05','0.10','0.15','0.20','0.25','0.30','0.35','0.40'});
set(ax1, 'XTickLabel',{});
hold on;
plot(playa_daily.Timestamp, playa_daily.Network, 'b-','LineWidth',2);
plot(playa_daily.Timestamp(1), 0.12, "diamond",'MarkerSize', 15, 'MarkerEdgeColor',
'k','LineWidth',3); %Gravimetric Markers
plot(playa_daily.Timestamp(157), 0.1427, "diamond",'MarkerSize', 15,
'MarkerEdgeColor', 'k','LineWidth',3); %Gravimetric Markers
yLimits = ([0.001 0.3990]);
```

```
shadedArea = fill([startDate, startDate, endDate, endDate], [yLimits(1), yLimits(2),
yLimits(2), yLimits(1)], [0.9, 0.9, 0.9], 'EdgeColor', 'none');
uistack(shadedArea, 'bottom');
ylabel('{\itθ_{CRNS}} [m^3/m^3]', 'Interpreter', 'tex');
yyaxis right;
invertedPrecipitation1 = -rain_ps.p_tip1;
bar(rain_ps.rounded_sswc_datetime_ps, invertedPrecipitation1, 'BarWidth', 2,
'FaceColor', [0 0 0]);
ylabel('Precipitation [mm]');
ax1=gca;
set(ax1,'Ycolor','k', 'YLim', [-150 0], 'YTick', -[75 50 25 0], 'YTickLabel', [75 50 25 0]);
hold off
set(gca,'FontSize',fs);
title('Downstream Playa (DP)')
legend('','CRNS','Sensor Network','Gravimetric Samples','','','');

% Subplot for the pendetration Depth at the PLAYA
%yyaxis left %Soil Moisture
ax2=subplot(2,1,2);
plot(playa_daily.Timestamp, playa_daily.Depth,'k-','LineWidth',2); % Soil moisture at
the playa
set(ax2,'XTick',tick);
datetick('x','mm/dd/yy','keepticks')
xlim([xl xu])
ylim([0 70])
set(ax2, 'YTick', [ 10 20 30 40 50 60]);
hold on;
ylabel('{\it{Z^*}} [cm]', 'Interpreter', 'tex');
set(gca,'FontSize',fs);


%% Four Subplot
%%%%%%%%%%%%%%%%%%%%%%%%%%%%%%%%%%%%%%%%%%%%%%%%%%%%%%%%%%%%%%%%%%%%%%%%%%%%%%%%
%%%%%%%%%%%%%%%%%%%%%

figure12 = figure('position', [0, 0, plotwidth, plotheight]);
yyaxis left
ax1=subplot(4,1,1);
plot(tromble_daily.Timestamp, tromble_daily.CRNS, 'k-','LineWidth',2); % Soil moisture
at the watershed
set(ax1,'XTick',tick);
datetick('x','mm/dd/yy','keepticks')
xlim([xl xu])
ylim([0 0.40])
```

```
set(ax1, 'YTick', [0 0.05 0.1 0.15 0.2 0.25 0.3 0.35 0.4],'YTickLabel',
{'0','0.05','0.10','0.15','0.20','0.25','0.30','0.35','0.40'});
set(ax1, 'XTickLabel',{});
hold on;
plot(tromble_daily.Timestamp, tromble_daily.Network, 'b-','LineWidth',2);
plot(tromble_daily.Timestamp(11), 0.0515, "diamond", 'MarkerSize', 15,
'MarkerEdgeColor', 'k','LineWidth',3);
yLimits = ([0.001 0.3990]);
shadedArea = fill([startDate, startDate, endDate, endDate], [yLimits(1), yLimits(2),
yLimits(2), yLimits(1)], [0.9, 0.9, 0.9], 'EdgeColor', 'none');
uistack(shadedArea, 'bottom');
ylabel('{\itθ_{CRNS}} [m^3/m^3]', 'Interpreter', 'tex');
yyaxis right;
invertedPrecipitation = -rain_tw.SumRain; % Inverting precipitation data
bar(rain_tw.rounded_sswc_datetime_tw, invertedPrecipitation, 'BarWidth', 2,
'FaceColor', [0 0 0]);
ylabel('Precipitation [mm/day]');
ax1=gca;
set(ax1,'Ycolor','k', 'YLim', [-150 0], 'YTick', -[75 50 25 0], 'YTickLabel', [75 50 25 0]);
hold off
set(gca,'FontSize',fs);
legend('','CRNS','Sensor Network','Gravimetric Samples','','','');

% Subplot for the pendetration Depth at the WATERSHED
yyaxis left %Soil Moisture
ax2=subplot(4,1,2);
plot(tromble_daily.Timestamp, tromble_daily.Depth,'k-','LineWidth',2); % Soil moisture
at the playa
set(ax2,'XTick',tick);
datetick('x','mm/dd/yy','keepticks')
set(ax2, 'XTickLabel',{});
xlim([xl xu])
ylim([0 70])
set(ax2, 'YTick', [ 10 20 30 40 50 60]);
hold on;
ylabel('{\it{Z_r}} [cm]', 'Interpreter', 'tex');
set(gca,'FontSize',fs);

yyaxis left
ax3=subplot(4,1,3);
plot(playa_daily.Timestamp, playa_daily.CRNS, 'k-','LineWidth',2); % Soil moisture at
the watershed
set(ax3,'XTick',tick);
datetick('x','mm/dd/yy','keepticks')
xlim([xl xu])
```

```
ylim([0 0.40])
set(ax3, 'YTick', [0 0.05 0.10 0.15 0.20 0.25 0.30 0.35 0.40],'YTickLabel',
{'0','0.05','0.10','0.15','0.20','0.25','0.30','0.35','0.40'});
set(ax3, 'XTickLabel',{});
hold on;
plot(playa_daily.Timestamp, playa_daily.Network, 'b-','LineWidth',2);
plot(playa_daily.Timestamp(1), 0.12, "diamond",'MarkerSize', 15, 'MarkerEdgeColor',
'k','LineWidth',3); %Gravimetric Markers
plot(playa_daily.Timestamp(157), 0.1427, "diamond",'MarkerSize', 15,
'MarkerEdgeColor', 'k','LineWidth',3); %Gravimetric Markers
yLimits = ([0.001 0.3990]);
shadedArea = fill([startDate, startDate, endDate, endDate], [yLimits(1), yLimits(2),
yLimits(2), yLimits(1)], [0.9, 0.9, 0.9], 'EdgeColor', 'none');
uistack(shadedArea, 'bottom');
ylabel('{\itθ_{CRNS}} [m^3/m^3]', 'Interpreter', 'tex');
yyaxis right;
invertedPrecipitation1 = -rain_ps.p_tip1;
bar(rain_ps.rounded_sswc_datetime_ps, invertedPrecipitation1, 'BarWidth', 2,
'FaceColor', [0 0 0]);
ylabel('Precipitation [mm/day]');
ax3=gca;
set(ax3,'Ycolor','k', 'YLim', [-150 0], 'YTick', -[75 50 25 0], 'YTickLabel', [75 50 25 0]);
hold off
set(gca,'FontSize',fs);


% Subplot for the pendetration Depth at the PLAYA
%yyaxis left %Soil Moisture
ax4=subplot(4,1,4);
plot(playa_daily.Timestamp, playa_daily.Depth,'k-','LineWidth',2); % Soil moisture at
the playa
set(ax4,'XTick',tick);
datetick('x','mm/dd/yy','keepticks')
xlim([xl xu])
ylim([0 70])
set(ax4, 'YTick', [ 10 20 30 40 50 60]);
hold on;
ylabel('{\it{Z_r}} [cm]', 'Interpreter', 'tex');
set(gca,'FontSize',fs);



%% Figure 4. Rainfall-Runoff Plot
%%%%%%%%%%%%%%%%%%%%%%%%%%%%%%%%%%%%%%%%%%%%%%%%%%%%%%%%%%%%%%%%%%%%%%%%%%%%%%%%
playa= playawaterlvlrain(35:120,:); % August Inundation Event at Playa
```

```
tromble=tromblewaterlvlrain(35:120,:); %August Inundation Event at Tromble

plotwidth=300;
plotheight=300;

st1 =tromble.Timestamp(1);    % Starting date
en1 = tromble.Timestamp(86);    % Ending date

tick1=(st1:en1);
tick1 = tick1(day(tick1)==1);

xl1=st1;
xu1=en1;
soil = smooth(playa.SoilMoisture);

%% Four subplot of August Raint Event
%%%%%%%%%%%%%%%%%%%%%%%%%%%%%%%%%%%%%%%%%%%%%%%%
%Upland Watershed
figure20 = figure('position', [0, 0, plotwidth, plotheight]);
ax1= subplot(4,1,1);
yyaxis left
plot(tromble.Timestamp, tromble.SoilMoisture, 'k-','LineWidth',3); %Soil Moisture
hold on
plot(tromble.Timestamp,tromble.SoilMoistureNetwork, 'g-','LineWidth',3);
ylim([0 0.80])
set(ax1, 'YTick', [0 0.20 0.40 0.60 0.80], 'YTickLabel', {'0','0.20','0.40','0.60','0.80'});
set(ax1,'Ycolor','k');
%set(ax1,'XTick',tick1);
xlim([xl1 xu1]);
ylabel('{\itθ} [m^3/m^3]', 'Interpreter', 'tex');
yyaxis right;
invertedPrecipitation2 = -tromble.Rain;
bar(tromble.Timestamp, invertedPrecipitation2, 'BarWidth', 2, 'FaceColor', [0 0 0]); %top
yyaxis right
set(ax1,'Ycolor','k', 'YLim', [-40 0], 'YTick', -[20 15 10 5 0], 'YTickLabel', [20 15 10 5
0]);
ylabel('Precipitation [mm/30min]');
title('Upland Watershed (UW)');
legend('CRNS','Sensor Network');
xlabel('Day');

ax2=subplot(4,1,2);
yyaxis left
set(ax2, 'YTickLabel',{});
set(ax2,'Ycolor','k');
```

```
yyaxis right
plot(tromble.Timestamp, tromble.Combined_Discharge, 'b-','LineWidth',3);
%set(ax2,'XTick',tick1);
xlim([xl1 xu1]);
set(ax2, 'XTickLabel',{});
set(ax2,'Ycolor','k', 'YLim', [0 .40], 'YTick', [0 0.05 0.10 0.15], 'YTickLabel', [0 0.05 0.10
0.15]);
legend('Discharge')
ylabel('Discharge [m^3/s]');

%Downstream Playa
yyaxis left
ax3= subplot(4,1,3);
plot(playa.Timestamp, soil, 'k-','LineWidth',3); %Soil Moisture
hold on
plot(playa.Timestamp,playa.SoillMoistureNetwork, 'g-','LineWidth',3);
ylim([0 0.80]);
xlim([xl1 xu1]);
set(ax3, 'YTick', [0 0.20 0.40 0.60 0.80], 'YTickLabel', {'0','0.20','0.40','0.60','0.80'});
set(ax3,'Ycolor','k');
ylabel('{\itθ} [m^3/m^3]', 'Interpreter', 'tex');
yyaxis right;
invertedPrecipitation1 = -playa.Rain;
bar(playa.Timestamp, invertedPrecipitation1, 'BarWidth', 2, 'FaceColor', [0 0 0]); %top
yyaxis right
set(ax3,'Ycolor','k', 'YLim', [-40 0], 'YTick', -[20 15 10 5 0], 'YTickLabel', [20 15 10 5
0]);
ylabel('Precipitation [mm/30min]');
title('Downstream Playa (DP)')
legend('CRNS','Sensor Network','');

ax4= subplot(4,1,4);
yyaxis left
set(ax4, 'YTickLabel',{});
set(ax4,'Ycolor','k');
yyaxis right
plot(playa.Timestamp, playa.Water_Level_cm, 'b-','LineWidth',3);
set(ax4,'Ycolor','k', 'YLim', [0 30], 'YTick', [0 5 10], 'YTickLabel', [0 5 10]);
xlim([xl1 xu1]);
set(ax4, 'XTickLabel',{});
ylabel('Water Level [cm]');
legend('Water Level');
```


169